Mapping Glacier Dynamics: A Flux-Gate Approach to Analysing Ice Discharge Variability and Sea Level Contributions in the Patagonian Icefields

Daniel James Turnbull

Submitted in accordance with the requirements for the degree of Master of Science by Research

The University of Leeds

The School of Geography

September 2023

I confirm that the work submitted is my own and that appropriate credit has been given where reference has been made to the work of others.

Acknowledgements

To begin with, this research and the motivation to develop my knowledge and understanding in the field of glaciology would not have been possible without the support and unwavering enthusiasm of my supervisors, Professor Jonathan Carrivick and Professor Duncan Quincey. I would like to thank them immensely for all the guidance and confidence they have given me in my own research but also pushing me to develop new skills academically and personally.

Finally, I also would like to thank my partner, friends and family for their continued support and encouragement that they have supplied throughout my studies.

Abstract

This study used a flux-gate methodology coupled with ice thickness and ice velocity grids equivalent to 2004 and 2017 to ascertain ice discharge (Gt yr^{-1}) and associated sea level equivalents (mm yr^{-1}) through 124 outlet glaciers spanning the different termini environments of the Patagonian Icefields. In addition, glaciers that experienced a terminus environment transition (i.e., from land-terminating to lake-terminating or vice versa) were identified and any associated changes in ice discharge were quantified. Overall, total ice discharge equalled 24.59 Gt yr^{-1} (0.068 mm yr^{-1}) in 2004 (Northern Patagonian Icefield = 7.07 Gt yr^{-1} or 0.019 mm yr^{-1}, Southern Patagonian Icefield = 17.52 Gt yr^{-1} or 0.049 mm yr^{-1}) and 23.94 ± 7.18 Gt yr^{-1} (0.066 mm yr^{-1}) in 2017 (Northern Patagonian Icefield = 5.02 ± 1.57 Gt yr^{-1} or 0.014 mm yr^{-1}, Southern Patagonian Icefield = 18.92 ± 5.98 Gt yr^{-1} or 0.052 mm yr^{-1}). In 2004 most of the ice was discharged through marine-terminating environments in the Western regions of the icefields. But, in 2017 there was a shift towards equilibrium whereby lake-terminating environments in the eastern regions matched the ice discharge of marine-terminating environments. This is attributed to the expansion of lake-terminating environments and an apparent acceleration of surface velocity. Although these trends do exist there were heterogeneous changes in ice discharge for all termini environments resulting from a complex array of dynamics at the calving front. A strong agreement was found between the ice discharge estimates in this study and geodetic mass loss estimates found in the literature, reinforcing the current knowledge around mass loss on the Patagonian Icefields. Future work should focus on the accuracy of ice thickness and ice velocity grids at the margins of icefields and using accurate frontal ablation estimates to constrain future sea level rise projections.

Table of Contents

List of Figures

List of Tables

Glossary

Marine-terminating: An ice mass which interacts with the ocean either along a grounded terminus, floating terminus or shelf.

Lake-terminating: An ice mass which interacts with a lake either along a grounded terminus or floating terminus.

Land-terminating: An ice mass where the terminus culminates on land which does not involve an active calving front.

Transitional environment: An environment in which a glacier shifts from calving to non-calving or vice versa e.g., a glacier retreats from a proglacial lake, changing the regime from lake-terminating to land-terminating.

Interaction margin: The point at which the termini of the glacial outlets on the icefield reach the external catalyst e.g., the point at which a marine-terminating glacier contacts the ocean.

Mass balance: The sum of inputs and outputs of ice from the glacier system.

Frontal ablation: A combination of calving processes and subaqueous melt emanating from the calving fronts of lake and marine-terminating glaciers.

Key

AAR – Accumulation Area Ratio

LIA – Little Ice Age

NPI – Northern Patagonian Icefield

PIF – Patagonian Icefield

SPI – Southern Patagonian Icefield

1.0 Introduction

1.1 Study Background

Glaciers on the Northern Patagonian Icefield (NPI) and Southern Patagonian Icefield (SPI) have the largest contribution to sea level rise per unit area in the world (Ivins and others, 2011; Jaber et al., 2013; Rignot et al., 2003). Many glaciers on the Patagonian Icefields (PIF) terminate into an aqueous environment; the icefield condition is therefore moulded by frontal ablation processes (Bravo et al., 2021; Minowa et al., 2021; Warren and Aniya, 1999). Frontal ablation is the sum of mass loss from calving and subaqueous melting, which are processes that are often deemed to be coupled with climatic forcing (Lopez et al., 2010). Complex glacial processes such as subaqueous melt and surface velocity changes can decouple glaciers from climate, fragmenting linear relationships between climate forcing and dynamic mass loss (Van der Veen, 2002). However, the spatial and temporal asynchronous behaviour of calving termini indicates that this widespread mass loss has extraneous patterns that need to be further investigated (Aniya et al., 1997). Therefore, the quantification of frontal ablation is an important factor in defining the future evolution of the Patagonian icefields and is increasingly important in estimating future sea level rise. In regions characterised by calving glaciers such as Patagonia, research needs to be focussed on processes which dominate glacier mass changes such as frontal ablation. By quantifying frontal ablation for interaction margins on the PIF, considering transitional termini environments, this study aims to further develop the understanding surrounding glacier mass loss in the region. Alongside assessing glacier behaviour through spatial and temporal variations in frontal ablation, important delineations can be made in terms of global sea level rise due to the connectivity of the icefields with the ocean.

1.2 Rationale

The PIF's position as a temperate ice mass comprising of diverse termini environments, where 90 % of the icefield terminates in a calving environment makes the region an area of important scientific interest (Minowa et al., 2021). Even though calving environments dominate the PIF, holistic frontal ablation estimates are yet to be made for the PIF. Minowa et al., (2021) provides frontal ablation estimates for 80 % of the calving area on the icefields but fails to consider smaller glaciers and transitional termini environments. Neglecting transitional changes from land-terminating to lake-terminating glaciers fails to quantify the frontal ablation of glaciers that were previously land-terminating. Loriaux and Casassa (2013) found a 65 % increase in lake

area and 174 % increase in lake frequency between 1945 and 2011 on the NPI, exemplifying the potential for transitional change in the region.

A recognised influence of proglacial lake presence constitutes of velocity increases, drawing down upstream ice and weakening the calving front (Trüssel et al., 2013; Tsutaki et al., 2011). Consequently, this effect needs to be characterised as it substantially alters the magnitude of frontal ablation evident at transitional termini. As inferred by Loriaux and Casassa (2013) the likelihood of potential ice-lake interactions on the PIF is increasing, highlighting the importance of including these in frontal ablation estimates. The direct quantification of frontal ablation transitioning through all interaction margins on the PIF will improve the understanding of mass change on the PIF, becoming increasingly important considering the heterogeneous spatial and temporal variations in calving glaciers observed on the PIF (Aniya et al., 1997; Sakakibara and Sugiyama, 2014). The complex interplay of ice dynamics on calving glaciers remains largely unconstrained, with estimations of frontal ablation change over time attempting to explore the relationships between dynamic thinning, calving front physics, ocean-ice interaction, and hypsometry (Benn et al., 2017; Furbish and Andrews, 1984; Motyka et al., 2013; Truffer and Motyka, 2016).

The current lack of holistic regional studies and incomplete understanding quantifying frontal ablation limits the ability to accurately predict cryospheric contributions to future eustatic sea level rise (Church et al., 2013). This presents a critical knowledge gap, as previous studies indicate frontal ablation in areas such as Patagonia, Greenland periphery and Alaska contribute significantly to global sea level rise (McNabb et al., 2015; Minowa et al., 2021; Recinos et al., 2023). The lack of knowledge related to patterns of frontal ablation is of great concern since small glaciers outside of the major ice sheets make up < 1 % of the global land ice volume yet contribute significantly to global sea level rise (Hock et al., 2019). Estimates suggest the Greenland ice sheet and Antarctica has 65.7 m of sea level equivalent stored in ice volume compared to 0.4 m in small glaciers which have the potential to contribute 0.1 to 0.25 m to eustatic sea level rise by 2100 (Meier et al., 2007; Vaughan et al., 2013). The PIF have contributed approximately 3 mm since 1961 to global sea level rise (Zemp et al., 2019). This accounts for some of the highest contribution to sea level rise per unit area globally, reinforcing the need to quantify mass change across the icefields. Therefore, given projections of global atmospheric and oceanic warming, delineating ocean and ice dynamic processes is a necessity to produce accurate sea level estimates (Slater et al., 2020).

1.3 Research Question, Aims and Objectives

This study set out to address the following research question: '(How) has the volume of ice discharged by Patagonian glaciers changed between 2004 and 2017?'.

1.3.1 Research Aims

- Quantify terminus-specific ice discharge through marine-terminating, lake-terminating, and land-terminating outlet glaciers in both the Northern and Southern Patagonian Icefields for the years 2004 and 2017.

- Identify transitions of terminus environments from land-terminating to lake-terminating or vice versa and quantify any associated changes in ice discharge.

- Characterise broad-scale spatial trends in ice discharge, comparing the patterns between the Northern Patagonian Icefield and the Southern Patagonian Icefield.

- Evaluate the extent to which ice discharge patterns have evolved over time by comparing 2004 and 2017.

- Calculate associated sea level rise estimates by utilising the ice discharge volume obtained from the Northern and Southern Patagonian Icefields for 2004 and 2017.

1.3.2 Research Objectives

- Quantify ice discharge from marine-terminating, lake-terminating, and land-terminating outlet glaciers in the Northern and Southern Patagonian Icefields for 2004 and 2017.

- Identify and document instances of terminus environment transitions from land-terminating to lake-terminating or vice versa within the Patagonian Icefields.

- Quantify the changes in ice discharge associated with terminus environment transitions.

- Analyse and compare spatial trends in ice discharge within the Northern and Southern Patagonian Icefields.

- Analyse and compare spatial trends in ice discharge between the Northern and Southern Patagonian Icefields.

- Evaluate and compare the ice discharge patterns in the Patagonian Icefields between the years 2004 and 2017.

- Calculate sea level rise equivalents based on the ice discharge volume estimates obtained from the Northern and Southern Patagonian Icefields for 2004 and 2017.

1.4 Study Area

The continent of South America hosts the NPI and SPI, collectively known as the Patagonian Icefields. Combined, the ice fields constitute the largest temperate ice mass in both hemispheres (Aniya, 2013; Meier et al., 2018). In total, the icefields span approximately 16,600 km^2, comprising ~ 3,600 km^2 for the NPI and ~ 13,000 km^2 for the SPI (Casassa et al., 2014; Dussaillant et al., 2018).

The climatic pattern across the PIF is defined by a strong east-west gradient. The austral Andes acts as an orographic barrier, impeding the eastward movement of atmospheric flow originating from the Pacific Ocean (Garreaud et al., 2013; Meier et al., 2018). This disturbance results in rising humid air masses, causing a severe precipitation gradient on the westerly side of the icefields (Smith and Evans, 2007). Carrasco et al., (2002) reports precipitation differences either side of the divide of up to 9,500 mm yr^{-1}. On the icefields, the disparity in precipitation dominates trends in accumulation (Bravo et al., 2019). Rosenblüth et al., (1997) attributes near-surface temperature increases to regional mass loss, elucidating the control of atmospheric conditions on the icefield. Lake-terminating environments dominate in the east, and marine-terminating environments are predominantly on the west (Sakakibara and Sugiyama, 2014; Figure 1). Low-lying marine-terminating glaciers are heavily influenced by calving processes, glacier geometry and small ablation areas leading to dynamic termini environments (Lenaerts et al., 2014; Minowa et al., 2021). Together, there exists a complex interplay of glacial characteristics and climatic conditions forcing glacial change on the PIF.

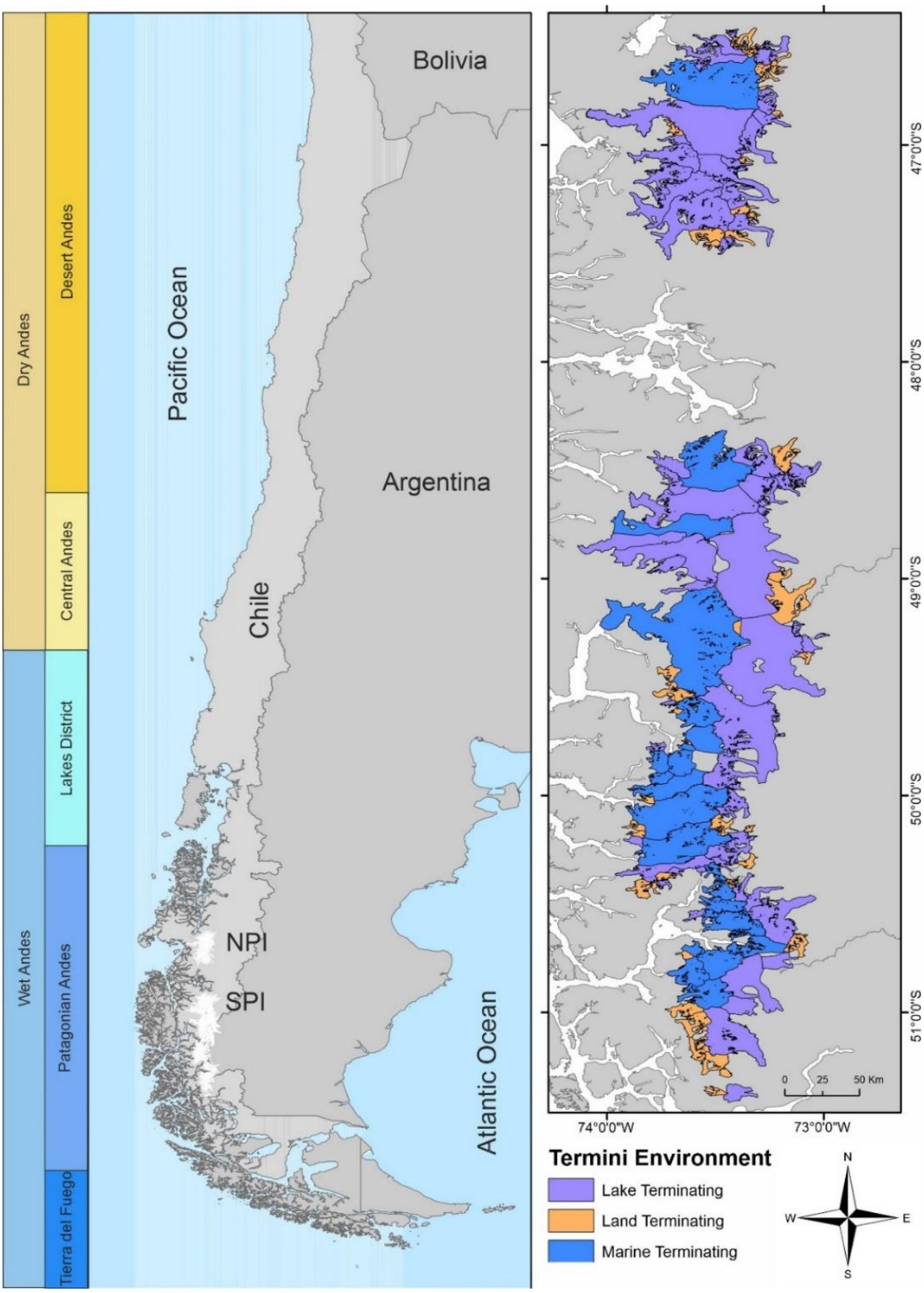

Figure 1 - Both the Northern and Southern Patagonian Icefields in context with the southern tip of South America and their associated glacier termini environments (equivalent to 2004).

2.0 Literature Review

2.1 Global Glacier Mass Loss

Globally, between 2000 and 2019, glaciers outside of the Greenland and Antarctic ice sheets have lost mass at rates between 199 ± 32 Gt yr^{-1} and 335 ± 144 Gt yr^{-1}, with some estimates indicating an increase in mass loss equivalent to 50 Gt yr^{-1} per decade (CiracÍ et al., 2020; Gardner et al., 2013; Hugonnet et al., 2021; Jakob and Gourmelen, 2023; Wouters et al., 2019; Zemp et al., 2019). The estimates of global glacier mass losses are equivalent to losses from both ice sheets for the same period with the Antarctic and Greenland ice sheets losing 298 ± 58 Gt yr^{-1} of mass between 2000 and 2011 (Shepherd et al., 2012). Consequently, smaller glacierised regions have been shown to have much greater prominence in global estimates of ice loss than previously realised. There is clear consensus in the literature that seven glacierised regions outside of the ice sheets dominated mass loss signals throughout the mid-20th century up until the present day (CiracÍ et al., 2020; Gardner et al., 2013; Hugonnet et al., 2021; Jakob and Gourmelen, 2023; Wouters et al., 2019; Zemp et al., 2019). These regions are Alaska, Northern Canadian Arctic, Southern Canadian Arctic, Southern Andes, High-mountain Asia, Greenland Periphery, and Iceland. Although there is general agreement globally, large uncertainties and disparity in regional spatial patterns still exist (Hock et al., 2019). The Arctic constitutes most of the mass loss globally, with Alaska being the largest net contributor (~ 70 Gt yr^{-1}) (Jakob and Gourmelen, 2023; Wouters et al., 2019). Outside of the Arctic region, High-mountain Asia (~ 30 Gt yr^{-1}) and the Southern Andes (~ 30 Gt yr^{-1}) are two glacierised regions which exhibit high estimates of mass loss in recent decades (CiracÍ et al., 2020; Hugonnet et al., 2021; Figure 2). The overarching global trend is therefore negative mass balance rates, with depleted glaciers becoming “icons of climate change” (Zemp et al., 2019).

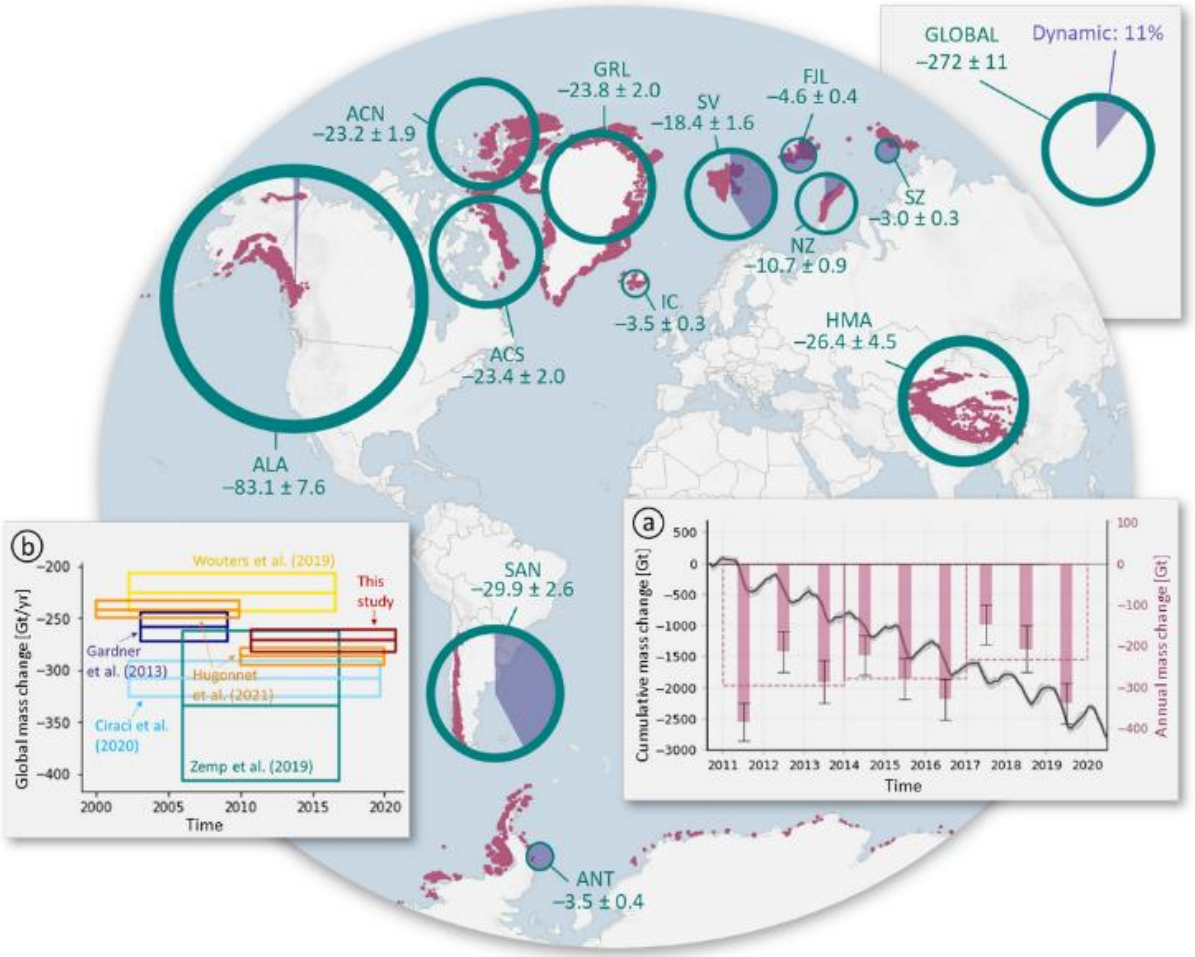

Figure 2 - Pie charts comparing mass loss via frontal ablation to total mass loss (between 2010 and 2020). (a) total cumulative monthly mass changes in Gigatonnes (Gt). (b) published global estimates of glacier mass changes and associated timeframes (figure taken from Jakob and Gourmelen, 2023).

A direct result of accelerating mass loss is eustatic sea level rise which is expedited by glacier meltwater flowing directly into the ocean (Wouters et al., 2019). The increase in glacier mass loss contributing to sea level rise is outlined by the IPCC report encompassing the Ocean and Cryosphere which identifies sea level rise since the mid-19th century to be larger than the “mean of the previous two millennia” (Church et al., 2013). Meier and others (2007) ascertain that sea level rise excluding ocean warming is attributable to glacial ice loss to the sea. They also indicate that 60 % of this ice loss comes from glaciers and ice caps, in contrast to the contribution from ice sheets (Meier and others, 2007). This notion is reinforced by the fact that global glaciers have a potential contribution to sea level rise equivalent to 324 ± 8 mm, an order of magnitude lower than that of the ice sheets yet glaciers have been the dominant contribution to sea level rise in recent decades (Church et al., 2013; Farinotti et al., 2019).

Rounce et al., (2023) predicts that by 2100 glaciers are set to lose 26 % to 41 % of their mass, with the potential for up to 83 % of glaciers to completely disappear depending on warming scenarios. Coinciding with these projections, glacier contribution to sea level rise could increase to 2.5 mm yr^{-1} by 2100 (Marzeion et al., 2020). This signposts the importance of attempting to quantify glacial discharge in high-mountain areas and areas such as Patagonia where there is significant ocean-ice interaction. Ocean-ice interactions are a critical part of the cryospheric system as they provide a direct route for meltwater to contribute to sea level rise as well as leading to feedbacks that can rapidly warm the ice terminus and cool the local oceanic waters (Chauce et al., 2014). This significant ocean-ice interaction is exemplified by ~ 25 % of the current PIF constituting of marine-terminating glaciers, directly discharging ice mass into the ocean (Gardner et al., 2013).

Between 1961 and 2016, the glacierised regions of the Southern Andes contributed 3.3 mm to eustatic sea level rise, while the PIF contributed at a higher rate than the rest of the South American ice masses (Braun et al., 2019; Dussaillant et al., 2019; Zemp et al., 2019). Glasser et al., (2011) indicate that 10 % of sea level rise in the past 50 years can be attributed to the PIF, exceeding per unit contributions of Alaskan glaciers (Rignot et al., 2003). Whilst contributions to sea level rise are the over-riding consequence of global glacier mass loss, water availability and glacier-related hazards are consequences which must be acknowledged as well (Rounce et al., 2023).

2.2 Patagonian Icefields: Current State of the Icefields

Direct glacial observations of the PIF are scarce due to inhospitable climates and inaccessibility (Mernild et al., 2015). Therefore, approximations of the processes which govern the state of the icefield rely on remote sensing observations and model-based studies. Here, we describe the findings of these studies and the inferences they make regarding the evolution of the PIF.

Studies focussing on changes in areal extent on the NPI indicate a steady recession, with ~ 5 % of total area lost between 1975 and 2000 and ~ 3 % being lost between 2000 and 2012 (Dussaillant et al., 2018; Rivera et al., 2007). Most of the recession can be attributed to the ablation areas of glaciers in the southwest of the icefield (Rivera et al., 2007). McDonnell et al., (2022) found lake-terminating glaciers as the key driver behind increasing mass loss and therefore area change from 1976 and 2000 to 2000 and 2020, likely due to the increase of proglacial lakes in the region (Wilson et al., 2018). The development of proglacial lakes at Exploradores Glacier is one of the best cited examples, transitioning the glacier from land-

terminating to lake-terminating (Aniya et al., 2007; Fernandez and Rivera, 2003). This transition has led to the continuing disintegration of the termini and sustained calving at the east marginal lake (Irarrazaval et al., 2020), thus highlighting the role transitional termini environments play in the dynamics of the NPI.

Surface and geodetic mass balance assessments of the NPI spanning the past 50 years agree in terms of direction, magnitude, and spatial pattern. Mass loss rates derived from geodetic assessments have accelerated in a negative direction. For example, the NPI thinned at a rate equivalent to 0.67 ± 0.14 Gt yr^{-1} from 1870 but since 1975 estimates have placed thinning between 2.88 Gt yr^{-1} and 5.13 Gt yr^{-1} (Abdel Jaber, 2016; Dussaillant et al., 2018; Glasser et al., 2011; Rignot et al., 2003; Rivera et al., 2007; Willis et al., 2012a; Table 1). These data indicate that mass loss estimates spanning the last 50 years are significantly higher than previous estimates (Glasser et al., 2011). Spatially, glaciers on the southwestern margin of the icefield thin at greater rates than elsewhere on the icefield, with termini margins also thinning substantially quicker than the main plateaus, coinciding with the areas undergoing the most substantial areal retreat (Abdel Jaber, 2016; Dussaillant, 2018; McDonell et al., 2022; Willis et al., 2012a).

However, the agreement between surface mass balance and geodetic mass balance estimates of widespread thinning on the NPI hides an important part of the icefield narrative. Since the 1970's, Schaefer et al., (2013) modelled an increase in accumulation over the NPI, where simulated values agreed with observed values from Nakajima (1985). Consequently, their data also suggested a marginal increasing trend in annual surface mass balance over the same time (Schaefer et al., 2013). The juxtaposition of modelled positive mass balances and geodetic negative mass balances is derived from the fact that ice dynamics, which includes calving, are not included in modelling studies. Bravo et al., (2021) and Schaefer et al., (2013) expect meltwater to force positive loss feedbacks at calving termini on the NPI in future scenarios. However, there exists feedback processes that can increase or decrease calving fluxes through various feedback mechanisms involving thinning, subglacial meltwater, basal friction and driving stresses (Schaefer et al., 2013).

Table 1 - Published estimates of Northern Patagonian icefield mass balance.

Region (coverage)	Mass Balance Estimate (Gt yr^{-1})	Time Period	Method	Reference
NPI (50 largest outlet glaciers)	- 0.67 ± 0.14	1870 - 2010	Geodetic (SRTM & field determinations e.g., Trimlines, Moraines)	Glasser et al., (2011)
NPI (63 largest outlet glaciers)	-2.88 ± 0.36	1968/1975 - 2000	Geodetic (SRTM & cartography)	Rignot et al., (2003)
NPI (70 largest outlet glaciers)	-5.13	1975 - 2001	Geodetic (ASTER & cartography)	Rivera et al., (2007)
NPI	-3.4 ± 0.07	2000 - 2011	Geodetic (ASTER & SRTM)	Willis et al., (2012a)
NPI (68%)	-4.1 ± 0.41	2000 - 2012	Geodetic (SRTM & SPOT5)	Dussaillant et al., (2018)
NPI (82%)	-4.25 ± 0.34	2000 - 2012	Geodetic (ASTER)	Dussaillant et al., (2018)
NPI (90%)	-3.83 ± 0.18	2000 - 2012	Geodetic (TanDEM-X & SRTM)	Abdel Jaber et al., (2019)
NPI (87%)	-3.96 ± 0.14	2000 - 2014	Geodetic (TanDEM-X & SRTM)	Abdel Jaber (2016)
NPI (95%)	-5.04 ± 0.67	2012 - 2016	Geodetic (TanDEM-X & SRTM)	Abdel Jaber et al., (2019)
NPI (45.7%)	-6.79 ± 1.16	2011 - 2017	Altimetry (Cryosat-2)	Foresta et al., (2018)
NPI	-6.17 ± 0.5	2000 - 2099	Surface Mass Balance model based	Schaefer et al., (2013)

Recent estimates of area changes on the SPI detect an overall area loss of ~ 4 % from 1986 to 2000, reinforcing the general retreat of the SPI previously reported in scientific studies (Aniya et al., 1997; Casassa et al., 2014; Davies and Glasser, 2012; Rignot et al., 2003). An estimate which sits within the range of values proposed by Dussaillant et al., (2018) and Rivera et al., (2007) for area loss % on the NPI, indicating that both icefields are receding at similar proportional rates. Whilst the NPI shows existential area losses, the SPI has had a more complex areal response to forcing via climatic or dynamical factors. Most calving glaciers on

the SPI have retreated over the past 60 years, with a mean retreat rate of 1.56 km between 1984 and 2011 (Aniya et al., 1997; Sakakibara and Sugiyama, 2014). Glaciers Jorge Montt, Upsala and HPS12 retreated by > 6 km in the observed period whilst both branches of Pio Xi advanced and thickened on different timescales (Sakakibara and Sugiyama, 2014). Hence these observations show that the SPI has been retreating in general but spatial and temporal differences do exist.

The overarching recessional trend is coupled with widespread thinning on the SPI (Malz et al., 2018). Foresta et al., (2018) attributes surface mass loss on the SPI to the northern section of the icefield. This area of the icefield imitates similar mass losses to the NPI due to an equivalent area-altitude spread (Foresta et al., 2018). The southern part of the icefield (~ 40 % of SPI area) sits above 1500 m reducing the impact of surface ablation, whilst the lower reaches at sea level are only subject to moderate thinning (Malz et al., 2018). This heterogeneous spatial pattern of surface mass loss on the SPI is epitomised by thinning propagating into accumulation areas of northern glaciers such as Occidental and Jorge Montt compared to the relative stability of Perito Moreno and Asia glaciers in the south of the icefield (Malz et al., 2018; Minowa et al., 2021; Willis et al., 2012b; Figure 3). These patterns are consistently observed across multiple time periods, making them a robust signal of mass loss on the icefield (Abdel Jaber, 2016; Malz et al., 2018; Willis et al., 2012b).

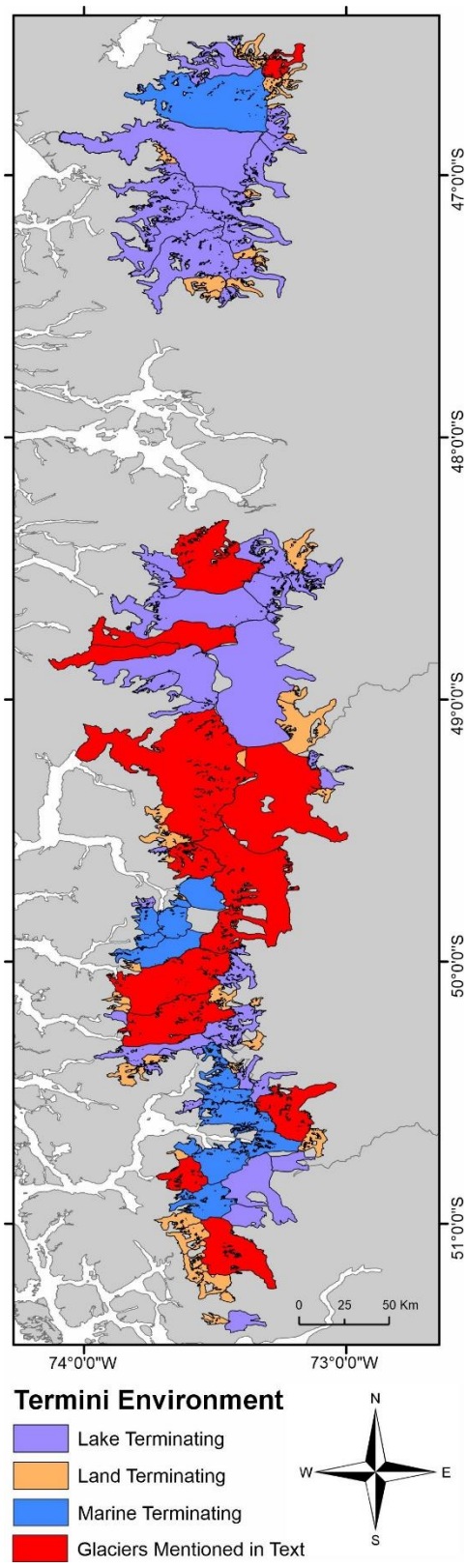

Figure 3 - Map of the PIF displaying the locations of each glacier mentioned within the literature review text.

Geodetic mass balance estimates of the SPI follow an analogous trend to those of the NPI, increasing in the order of magnitudes since the Little Ice Age (LIA) (Glasser et al., 2011). Negative mass balance estimates from 2000 up until 2016 range from 11.84 ± 3.3 Gt yr^{-1} to 20 ± 1.2 Gt yr^{-1} (Abdel Jaber et al., 2019; Braun et al., 2019; Dussaillant et al., 2019; Foresta et al., 2018; Malz et al., 2018; Rignot et al., 2003; Willis et al., 2012b; Table 2). Contrastingly, positive surface mass balance estimates of 2.7 ± 1.6 m.w.e yr^{-1}, 1.8 ± 0.4 m.w.e yr^{-1} and 2.3 ± 0.9 m.w.e yr^{-1} exist for the SPI for historical periods spanning 1976 to 2010 (Bravo et al., 2021; Mernild et al., 2017; Schaefer et al., 2015). This positive mass balance is set to continue (Bravo et al., 2021; Schaefer et al., 2015). Therefore, it is likely that if the SPI is driven solely by climate forcing the SPI will be in a net accumulative state. The polarity of surface and geodetic mass balance estimates promotes the strong contribution of mass loss via dynamic calving to the SPI.

Table 2 - Published estimates of Southern Patagonian icefield mass balance.

Region (coverage)	Mass Balance Estimate (Gt a^{-1})	Time Period	Method	Reference
SPI	-1.25 ± 0.25	1650 - 2000	Geodetic reconstruction	Glasser et al., (2011)
SPI	-15.2 ± 0.72	1968/1975 - 2000	Geodetic (SRTM & Cartography)	Jacob et al., (2012)
SPI	-12.15 ± 0.72	1995 - 2000	Geodetic (SRTM & Cartography)	Rignot et al., (2003)
SPI	-20 ± 1.2	2000 - 2011	Geodetic (ASTER & SRTM)	Willis et al., (2012b)
SPI (97%)	-13.38 ± 0.47	2000 - 2012	Geodetic (TanDEM-X & SRTM)	Abdel Jaber (2019)
SPI	-11.84 ± 3.3	2000 – 2015/2016	Geodetic (TanDEM-X & SRTM)	Malz et al., (2018)
SPI (70%)		2009 - 2018	Geodetic (ASTERIX)	Dussaillant et al., (2019)
SPI (70%)	-18.3 ± 5.7	2010 - 2016	Geodetic (ASTERIX)	Dussaillant et al., (2019)
SPI (49.9%)	-14.5 ± 1.6	2011 - 2017	Altimetry (Cryosat-2)	Foresta et al., (2018)
SPI (98%)	-10.67 ± 1.79	2012 - 2016	Geodetic (TanDEM-X & SRTM)	Abdel Jaber (2019)

To summarise, there is general agreement in surface and geodetic mass balance estimates for the NPI, where land and lake-terminating glaciers dominate (Bravo et al., 2021). This highlights the role that frontal characteristics play in determining the dynamics of the icefield, through the promotion or moderation of calving fluxes. The effect of frontal ablation is lower on the NPI, suggesting the NPI may be particularly sensitive to climate forcing (Bravo et al., 2021). In comparison, the deep lake and fjord terminating glaciers of the SPI promote frontal ablation as an ice loss mechanism, demonstrated by the disparity in surface and geodetic mass balance estimates (Malz et al., 2018; Schaefer et al., 2015; Willis et al., 2012b). In rapidly retreating marine-terminating glaciers such as Jorge Montt, mass balance is dominated by glacier dynamics (Bown et al., 2019; Minowa et al., 2021). As mass balance is dominated by glacier dynamics in some instances, this leads to the decoupling of glaciers from climate and the initiation of a positive feedback loop with ice flow acceleration causing thinning and vertical straining (Benn and others, 2007; Felikson et al., 2017).

The current state of Alaskan glaciers can be used as an interesting proxy regarding the PIF, but especially the SPI. Like the current state of the SPI, Alaskan marine-terminating glaciers have retreated at a significant rate since the LIA playing a key role in the mass loss of the region (Larsen et al., 2015). However, many marine-terminating glaciers in the region have reached a stage in the unstable “tidewater glacier cycle” where they are now stable and, in some cases, even advancing (Mcnabb and Hock, 2014; Post et al., 2011). The stabilisation and advancement have reduced the control of frontal ablation on glacier dynamics, with thinning in the ablation zone maintaining negative mass balances (Larsen et al., 2015). Consequently, suggesting that surface melt is the current key driver behind the mass loss of Alaskan glaciers. Therefore, insinuating that the calving glaciers of Alaska have transitioned from climate decoupling to a more stable state dominated by climate forcing. A transition which could exist on the SPI in the future, modifying the role of frontal ablation on glacier dynamics. The relatively stable retreat of the NPI juxtaposes the heterogeneous retreat of the SPI, due to glacier characteristics supporting different glacier dynamics.

2.3 Marine and Lake-terminating Environments

Dynamic ice loss, which accounts for all losses other than the surface mass balance, is a key component in the mass balance of the PIF (Rignot et al., 2003). Between 2000 and 2019, 40 % of total ablation on the PIF was due to frontal ablation, as 90 % of the icefield margin terminates in calving glaciers (Minowa et al., 2021). The dominance of frontal ablation focusses on marine and lake-terminating environments and is evidenced by Jakob and

Gourmelen (2023) who finds a discharge anomaly of 13.3 ± 1.3 Gt yr^{-1} compared to a total mass loss of 29.9 ± 2.6 Gt yr^{-1} in the Southern Andes. Ice-ocean interactions are complex with continued thinning and the speed up of marine terminating glaciers on the PIF exacerbating changes in glacier geometry, longitudinal stresses and iceberg calving rates creating non-linear responses to climate forcing (Benn et al., 2017; Mouginot and Rignot, 2015; Podrasky et al., 2014).

The rapid retreat and thinning of marine-terminating glaciers can be explained by the "tidewater glacier cycle" (Post et al., 2011; Truffer and Motyka, 2016). The "tidewater glacier cycle" is initially linked to climate forcing after triggering fast unstable retreat over a few decades following a steady advancing phase spanning hundreds of years (Post et al., 2011). However, when in retreat the glacier becomes decoupled from climate and geometry becomes the key driver of behaviour (Enderlin and Howat, 2013; Pfeffer, 2007). The along flow shape dictates dynamic response, either a new steady state or multi-kilometre retreat, thinning and flow acceleration (Amundson, 2016; Enderlin and Howat, 2013). Regional studies of Alaska and Greenland reveal antithetical marine-terminating glacier fluctuations in terminus positions of adjacent glaciers exposed to similar climatic conditions (McNabb and Hock, 2014; Moon and Joughin, 2008). These observations are also evident on the SPI, where the northernmost marine-terminating glaciers on the icefield, Jorge Montt and Tempano show contrasting termini fluctuations. The contrasting nature of these glaciers is due to glacier bathymetry, with Tempano currently grounded and stabilised a few metres above sea level whilst Jorge Montt continues to retreat calving into waters up to 400 m deep (Rivera et al., 2012; Figure 3).

The physics of the ocean-ice interaction play a key role in determining dynamic glacier behaviour alongside glacier geometry. Ice-berg calving is stochastic in nature where complex physical relationships exist such as height above buoyancy calving laws linked to marine ice-cliff instability (Bassis and Walker, 2012), terminus strain rates (Benn and others, 2007; Nick et al., 2010) and water depth at the terminus (Warren, 1991). Furthermore, relationships involving subglacial discharge and fjord temperatures regulate subglacial melt, an important component of frontal ablation (Jenkins, 2011; Motyka et al., 2013). Although these complex physical relationships do play an important role in determining glacier dynamics, they are still poorly constrained. This indicates that dynamic mass loss patterns through marine-terminating boundaries are still not fully understood and must be investigated further on local and regional scales.

Whilst there has been significant focus on the instability of marine-terminating glaciers a lot less is known about the sensitivity of lake-terminating glaciers (Pfeffer et al., 2008; Trüssel et al., 2013). The PIF contains proglacial lake environments spanning small cirque glaciers,

valley glaciers and large icefield tributary glaciers. Proglacial lakes cause glaciers to respond through amplifications in ice flow, calving and terminus retreat (Warren and Kirkbride, 2003). As lake-terminating glaciers retreat into deeper water ice velocity amplifies, drawing down upstream ice, promoting widespread thinning and weakening the calving front (Trüssel et al., 2013). Low effective pressure driven by increasing subglacial water pressures from thinning linked to surface melt enhances basal motion at the terminus, thus amplifying ice velocity (Fowler, 1987; Vieli et al., 2000). The consequent amplification of surface velocity at the terminus increases the calving rate of lake-terminating glaciers, triggering glacier retreat (Tsutaki et al., 2011).

This process chain indicates that climatic forcing can be a catalyst for rapid retreat in lake-terminating glaciers through initial surface melt. An increase in glacier discharge may be coupled with extensional flow which causes longitudinal stress, resulting in dynamic thinning (Tsutaki et al., 2011). This leads to flotation at the terminus front, promoting ice instabilities, and ultimately glacier disintegration. Eight glacier tongues have disintegrated since 1985 on the NPI, including the 13-year breakdown of the San Quintin Glacier front (Aniya, 2017). The number of glacial lakes in mountainous regions in recent times has increased through the order of magnitudes in response to glacier retreat (Carrivick and Quincey, 2014). This pattern is replicated in Patagonia where the number of proglacial lakes increased by 43 % and increased in extent by 7 % between 1986 and 2016 (Wilson et al., 2018). Datasets from the glacierised regions of the world show that the presence of a proglacial lake alters the dynamics of the host glacier, indicating that for Patagonia terminus processes could become increasingly important, and thus, quantifying mass flux through these environments will provide useful insights into glacier system response through time.

Traditionally, a binary concept where non-calving glaciers are deemed to be climatically sensitive and calving glaciers insensitive exists (Warren and Kirkbride, 2003). However, studies indicate that marine-terminating glaciers calve at an order of magnitude larger than lake-terminating glaciers at similar water depths (Benn and others, 2007). Therefore, when considering the differential calving rates of marine-terminating and lake-terminating glaciers, the traditional binary framework can be split so that non-calving glaciers are the most sensitive to climate forcing, and lake-terminating glaciers then become more sensitive than marine-terminating glaciers (Warren and Kirkbride, 2003). Nef Glacier, a lake-terminating glacier on the NPI exhibits infrequent but significant calving events (Warren et al., 2001). This is facilitated by slow terminus retreat, rapid thinning, and the absence of ocean interaction (Warren et al., 2001). The combination of these factors enables the tongue to approach flotation, reducing shear stresses and creating buoyant uplift (Kirkbride and Warren, 1997).

This response enables melt to become the key ablation mechanism on the glacier, highlighting the glaciers climatic sensitivity (Warren et al., 2001).

Calving dynamics are driven by a combination of tidal forcing, density contrasts between freshwater and seawater, glacial lake stratification, the temperature and connectivity of the system, and sources of heat exchange (Van der Veen, 2002). Some of the factors outlined above were investigated by Sugiyama et al., (2016) in Patagonia, analysing the thermal structure and bathymetry of proglacial lakes linked to Perito Moreno, Upsala and Viedma glaciers (Figure 4). The study led to conclusions confirming significant differences in the thermal structure of lakes in contact with calving glaciers compared to marine-terminating glaciers and fjords (Sugiyama et al., 2016). Relatively warm (3 to 4°C) near-surface water transports heat to the lake-ice interface via wind-driven mixing; however, turbid subglacial meltwater is much colder and inhibits vertical mixing creating inefficient heat transfer to the surface (Sugiyama et al., 2016). In contrast, marine-terminating glaciers form an upwelling current due to the density contrast between freshwater and seawater (Jenkins, 2011). This buoyant plume effectively transfers heat vertically from water to ice, enhancing frontal ablation (Motyka et al., 2013; Xu et al., 2013). For example, a study by Bartholomaus et al., (2013) on Yahtse Glacier a marine-terminating glacier in Alaska found a large proportion of frontal ablation could be attributed to subaqueous melt. In contrast, Sugiyama et al., (2016) attributed < 10 % of subaqueous melt to frontal ablation on Upsala and Viedma Glaciers.

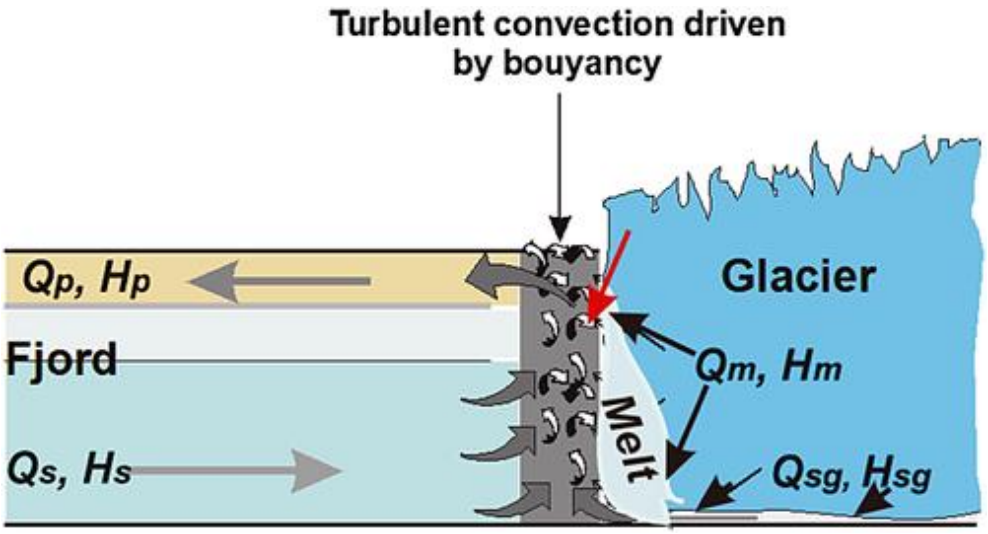

Figure 4 - Model symbolising proglacial convective flow. Subglacial discharge (Qsg) carrying heat (Hsg), drives convective flow, drawing saline water (Qs, Hs) towards the termini where the components mix and rise turbulently. As the water ascends ice melts along the face (Qm, Hm). Once the turbulent plume reaches the surface it flows away from the termini (Qp, Hp) (figure taken from Motyka et al., 2013).

Lake-terminating environments tend to be closed systems often isolated by their terminal moraines, with solar radiation being the only heat source whilst marine-terminating environments have steady heat supplies emanating from the open ocean (Funk and Röthlisberger, 1989; Gladish et al., 2015). The stark contrast in the efficiency of heat transfer at termini fronts in lake and marine environments controls frontal ablation mechanisms. These factors can partially explain the disparity in calving dynamics, but the magnitude of difference remains unsolved (Trüssel et al., 2013). Minowa et al., (2021) displays this calving dynamic loss disparity in F-fraction calculations (comparison of calculated frontal ablation with reported surface ablation) of major PIF outlet glaciers. Marine-terminating glaciers such as Penguin and Europa have F-fractions exceeding ~ 80 % compared to lake-terminating glaciers F-fractions which were often below ~ 20 % (e.g., Viedma and Tyndall) (Minowa et al., 2021).

Furbish and Andrews (1984) identified that glaciers with contrasting hypsometry exhibit differing termini behaviour under similar climatic forcing, highlighting hypsometry as a key factor influencing glacier behaviour (Jiskoot et al., 2009). Marine-terminating glaciers to the west of the ice divide on the PIF are generally found to have large accumulation areas and small steep ablation areas, reducing their sensitivity to climatic changes (Aniya et al., 1997; De Angelis, 2014). However, low mass balance sensitivities are offset by dynamic termini environments extremely sensitive to changes in equilibrium line altitude (ELA) due to their hypsometry (Furbish and Andrews, 1984; Mercer, 1961). In contrast, lake-terminating glaciers found to the east of the ice divide on the PIF predominantly exhibit large ablation areas leading to increased levels of mass loss via climatic forcing (Minowa et al., 2021). This implies that these glaciers are more sensitive to atmospheric warming, but the terminus environment is less sensitive to changes in ELA (De Angelis, 2014).

The presence or absence of supraglacial debris can also heavily impact glacier, thinning and recession. Supraglacial debris often deposited via rockfalls, mudflows and debris flow from mountain slopes alters surface ablation rates and spatial variations of mass loss (Kirkbride and Deline, 2013). The presence of debris acts as an insulator once a specific thickness is obtained however ice melt can also be enhanced when debris cover is below the threshold of insulation (1 to 2 cm) due to increased absorption of solar radiation (Nakawo and Rana, 1999; Østrem, 1959). Debris covered glaciers in Patagonia are different to debris covered glaciers in high-mountain regions such as the Himalayas, because of large ice fluxes, surface velocity and terminus recession compared to low surface velocities, surface lowering and terminus stagnation (Glasser et al., 2016). The juxtaposition of glacial behaviour is due to many complex factors but the rapid turnover of ice in Patagonia supresses the influence debris cover has on mass balance processes (Glasser et al., 2016).

In summary, glacier behaviour is determined by a complex interplay of physical factors, which is exemplified by the antithetical recessional trends present in adjacent glaciers. Therefore, due to the array of physical factors impacting glacier behaviour, this study will focus on attempting to quantify frontal ablation, providing useful insights into the nature of the Patagonian Icefields. This is an insight that is particularly useful when analysing the Patagonian Icefields due to the dominance of calving termini in the region.

3.0 Methodology

3.1 Datasets

Glacier, proglacial lake, marine boundaries, glacier surface velocity and ice thickness datasets were used in combination to delineate lake-ice and ocean-ice interfaces and to generate flux gates on the Northern and Southern Patagonian icefields (Table 3). Once the flux gates were generated, ice discharge (Gt yr^{-1}) was calculated for each of them for each period and then aggregated per glacier and per icefield sub-region.

Table 3 - Datasets used in his study and their utilisation.

Dataset	Utilisation	Source
2004 Ice Thickness	Discharge Calculation	Millan et al., (2022) and Hugonnet et al., (2021)
2004 Ice Velocity	Discharge Calculation	Mouginot and Rignot (2015)
2017 Ice Thickness	Discharge Calculation	Millan et al., (2022)
2017 Ice Velocity	Discharge Calculation	Millan et al., (2022)
Glacier Inventory	Glacier Identification	Aniya (1998)
Glacier Inventory	Glacier Identification	Aniya (1995)
Glacier Inventory	Glacier Identification	Barcaza et al., (2017)
Glacier Inventory	Glacier Identification	Casassa et al., (2014)
Glacier Inventory	Glacier Identification	Rivera et al., (2007)
GLIMS Outlines	Intersection Analysis	RGI V6.0
Landsat Imagery	Glacier Identification	NASA EarthExplorer
Marine Boundary	Intersection Analysis	Claus et al., (2014)
Proglacial Lake Outlines	Intersection Analysis	Shugar et al., (2020)

3.1.1 GLIMS Outlines

The Randolph Glacier Inventory version 6.0 (RGI_v6.0) provided glacier outlines via the GLIMS (Global Land Ice Measurements from Space) database, the most comprehensive dataset for both 2004 and 2017 (GLIMS, 2005). The outlines taken from the RGI_v6.0 were derived by multiple analysts and relate to a range of different time periods (Table 4). The methods used for deriving glacier outlines differed depending on which analyst performed the review. These methods ranged from semi-automated glacier classification, analysis of pre-processed Landsat images using band ratio methods at multiple thresholds and manual

delineation based on digital elevation models coupled with false colour composite images focusing on glacier features such as ice flow surface patterns, crevasses, and moraines. Previous glacier inventories such as Aniya (1988), Aniya (1995), Barcaza et al., (2017), Casassa et al., (2014) and Rivera et al., (2007) were compared and used to curate a comprehensive set of glaciers ready for analysis. In addition, manual identification of the small marginal glaciers not included in previous inventories required the use of Landsat imagery, the proglacial lake dataset (Section 3.1.2), and marine boundaries dataset (Section 3.1.3) to verify termini environments.

Table 4 - Summary of GLIMS outline source dates and analyst information.

Region and Time Period	Source Timestamp Dates	Analysts	Associated Publications
NPI (2004)	08/03/2000 – 04/08/2001	Gonzalo Barcaza (Universidad de Chile), Francisca Bown (Universidad de Chile) and Bethan Davies (University of Newcastle).	Barcaza et al., (2017) and Davies and Glasser (2012).
NPI (2017)	12/03/2016	Raymond Le Bris (University of Zurich)	n/a
SPI (2004)	15/06/2000 – 20/02/2005	Lidia Ferri Hidalgo (IANIGLA), Gonzalo Barcaza (Universidad de Chile), Bethan Davies (University of Newcastle), Frank Paul (University of Zurich) and Graham Cogley.	Zalazar et al., (2017), Barcaza et al., (2017) and Davies and Glasser (2012).
SPI (2017)	06/09/2007 – 12/03/2016 (apart from one unnamed glacier as the only	Raymond Le Bris (University of Zurich), Bethan Davies (University of	Davies and Glasser (2012).

	available outline was from 15/06/2000)	Newcastle) and Graham Cogley.	

3.1.2 Proglacial Lake Outlines

The approach used by Shugar et al., (2020) involves calculating and thresholding the Normalised Difference Water Index (NDWI) and the Normalised Difference Snow Index (NDSI) on optical satellite images, combining these indices with image processing and segmentation algorithms to derive individual lake outlines over a 30-year period stretching from 1990 to 2018. Shugar et al., (2020) leverages the processing power of Google Earth Engine to create a multi-sensor data cube from the Landsat archive including surface reflectance data from numerous missions. Data processing calculates NDWI and NDSI for each scene, generating an output where pixel values represent the proportion of scenes reaching the threshold (Shugar et al., 2020). Threshold values are determined empirically for each region, whilst various filtering steps involving proximity to glaciers, median slope and lake size were also applied (Shugar et al., 2020). The data are readily available to download in shapefile form and were used in this study to identify lake boundaries when the lake outlines intersected with the glacier outlines, ready for the generation of flux gates.

Aggregated lake outline shapefiles encompassing the years 1990 to 1999, 2000 to 2004, 2005 to 2009, 2010 to 2014 and 2015 to 2018 were used for providing context around the development of proglacial lakes in Patagonia. However, the subsets 2000 to 2004 and 2015 to 2018 were primarily used for the intersection analysis.

3.1.3 Marine Boundaries

Claus et al., (2014) provides a global dataset of marine boundaries that attempt to unify the depiction of boundaries in several other geospatial databases. The marine boundary used in this study was taken from the “maritime boundaries” geodatabase and was used to identify marine-terminating glaciers. The marine boundaries were derived from ESRI Countries 2014 and are therefore representative of this period also.

3.1.4 Ice Velocity and Ice Thickness 2017/18

Millan et al., (2022) provides a globally comprehensive dataset of ice thickness and velocity values provided in a raster format with 50 m spatial resolution, representing the period 1st January 2017 to 31st December 2018. Images acquired from numerous satellites, including Landsat 8, Sentinel-2, Venus and Sentinel-1 radar images, were used to calculate velocity (Millan et al., 2022). Velocity was calculated using a cross-correlation feature tracking approach using images with repeat cycles ranging from 16-100 days and 330-400 days (Millan et al., 2022). Repeat cycles are used in the context of velocity mapping for refining temporal resolution, reducing error and uncertainty, creating a holistic picture of ice velocity patterns and for validation purposes. Time-averaged surface velocity mosaics were computed via a cross-correlation algorithm called “ampcor” developed by NASA’s Jet Propulsion Laboratory (JPL) (Millan et al., 2022). This took patches of the satellite imagery pairs identified as the glacier surface and aimed to calculate their displacement (Millan et al., 2019). Outliers which sat outside one standard deviation from the median were automatically filtered. Once this had occurred time-averaged velocity maps were created using a post-treatment algorithm (Millan et al., 2019).

Millan et al., (2022) found that cloud cover and diminished correlation in optical data over icefields reduced the accuracy of the velocity product, so Sentinel-1 radar images were analysed using speckle tracking to amplify spatial coverage and reduce uncertainties. As well as using additional Sentinel-1 radar imagery to reduce uncertainties over icefields, final calibration aimed to fix minor errors (Millan et al., 2022). The rigorous process undertaken to assure velocity grids are consistent and robust indicate that Millan’s velocity mosaics are suitable to use for analysis of the Patagonian Icefields.

Ice thickness was estimated using the Shallow Ice Approximation (SIA), which works on the relationship between ice surface velocity and slope profile (Millan et al., 2022). The SIA is the most used ice dynamic simulation method because it provides a useful approximation of the full-stokes equations, reducing computational effort (Pattyn, 2017). The full-stokes equations consider the viscous flow and deformation of ice whilst accounting for the conservation of mass and momentum (Cuffey, 2010; Greve and Blatter, 2009). Through approximations based on the full-stokes equations a reasonable depiction of ice sheet flow is achieved, with the potential to capture dynamic ice sheets (Rückamp and others, 2022). However, there are still doubts over whether the SIA is suitable for representing mountain glaciers and glaciers constrained by valley topographies (Rückamp and others, 2022). This is because the SIA was developed for estimating the interior of ice sheets where the thickness to area ratio is heavily biased to the surface area and the ice surface slope is shallow (Egholm et al., 2011).

Therefore, these model conditions are unsuitable for representing valley and mountain glaciers due to their smaller surface area and steeper surface slopes (Hutter, 1983). Pelletier et al., (2010) also explains that the SIA fails to represent the complex sliding and erosion mechanisms evident in valley and mountain glaciers.

Millan et al., (2022) used in-situ ice thickness measurements to calibrate certain parameters in the model for regions where these measurements were available, in regions where field measurements were non-existent either average parameter values for adjacent regions were used, or a standard value was implemented. Therefore, as in-situ thickness measurements were used for model calibration, model validation was performed to differentiate results from measurements eliminating the possibility of over-fitting.

3.1.5 Ice Velocity and Ice Thickness 2004

Mouginot and Rignot (2015) derived surface velocity data covering both icefields equivalent to those found in 2004 at a 100 m resolution. They used data from five SAR satellites including NASA's SIR-C (autumn 1994), the European Space Agency's ERS-1 and ERS-2 (winter 1995 to 1996), the Canadian Space Agency's RADARSAT-1 (autumn 2004 to spring 2008) and the Japanese Space Agency's PALSAR (winter 2007 and autumn to winter 2010) (Mouginot and Rignot, 2015). Landsat data were also used across the whole observation period (1984 to 2014). Various methods to detect surface ice motion were used dependent on the satellite type with a speckle tracking algorithm developed by Michel and Rignot (1999) used for SIR-C, RADARSAT-1 and ALOS, an interferometry method developed by Joughin et al., (1998) used for ERS-1 and 2 and a feature tracking algorithm used for Landsat.

Interferometry works on the basis that surface displacement is the only factor that can't be simulated in total phase differences. A total phase difference occurs when synthetic aperture radar signals (SAR) from multiple sensors are returned to the satellite after reflecting from the surface below, this includes differences due to image geometry, topographic variability, earth curvature and surface displacement (Fatland, 1998). Image geometry and earth curvature can be calculated whilst topographic variability is nullified through high resolution elevation models such as SRTM. Thus, when observing icefields and valley glaciers an interferogram will display surface displacement and enable an estimation of surface velocity for a specific moment in time (Joughin et al., 1998).

In addition, an advanced filtering process eliminated false detection whilst calibration of the velocity composites was made using ice-free areas, providing "zero motion" targets (Mouginot et al., 2012; Mouginot and Rignot, 2015). In this study, the velocity mosaics were obtained in

X and Y vectors; to convert values from a vector to a scalar quantity, Pythagoras theorem was used.

To reconstruct the ice thickness in 2004, this study used a combination of Millan et al's., (2022) ice thickness estimates and Hugonnet et al's., (2021) elevation grids. Hugonnet et al., (2021) uses a geodetic based approach to delineate elevation differences in glaciers globally from 1st January 2000 to 31st December 2019. This method consisted of using ASTER, ArcticDEM and REMA digital elevation models (DEMs) to create co-registered DEM strips (30m resolution; 180 km x 60 km). A series of filtering methods removed DEM strips with anomalous elevation differences; two global-scale statistical modelling steps filtered and interpolated the DEMs into elevation time series (Hugonnet et al., 2021).

In this study, Millan's thickness estimates were used as a baseline (contemporary) thickness. Hugonnet et al's elevation change grids, which were downloaded in 5-year bins and quantified in meters per year (m/yr), were multiplied by five to give an absolute elevation change in metres. This process was repeated for multiple five-year bins, to derive cumulative elevation change from 2004 to 2017. These values were then added to Millan's contemporary ice thickness to yield the 2004 dataset.

3.2 Flux Gate Mapping and Ice Discharge Calculation

The use of flux gates to estimate ice discharge is a well-known and widely used methodology in the marine-terminating glacier literature, but also recently has been applied to lake-terminating glaciers (Carrivick et al., 2022; Kochtitzky et al., 2022; Minowa et al., 2021). In this study, flux gates were systematically generated. For lake-ice boundaries the GLIMS outlines were processed with Shugar et als., (2020) proglacial lake shapefiles to delineate boundaries. The same processing was applied to marine-ice boundaries with the marine boundary layer. For land-ice boundaries, Landsat imagery and past glacial lake outlines were used to assess suitable positions for flux gate generation by identifying where the termini used to be in contact with a lake environment (Figure 5).

A 500 m buffer was applied for all three types of termini because initial analysis indicated that ice thickness and ice surface velocity data right at ice margins was chaotic in magnitude and pattern and very likely erroneous so likely leading to unreliable estimations of ice discharge. These observations were also seen in Enderlin et al., (2014) who found that a ~ 16 % difference in discharge total for Greenland between their study and Rignot et al., (2011) was likely due to differences in data interpolation and availability at the margin. Furthermore, like

Mankoff et al., (2020), the buffer upstream was placed sufficiently close to the terminus such that the discharge did not need correcting for surface mass balances processes downstream.

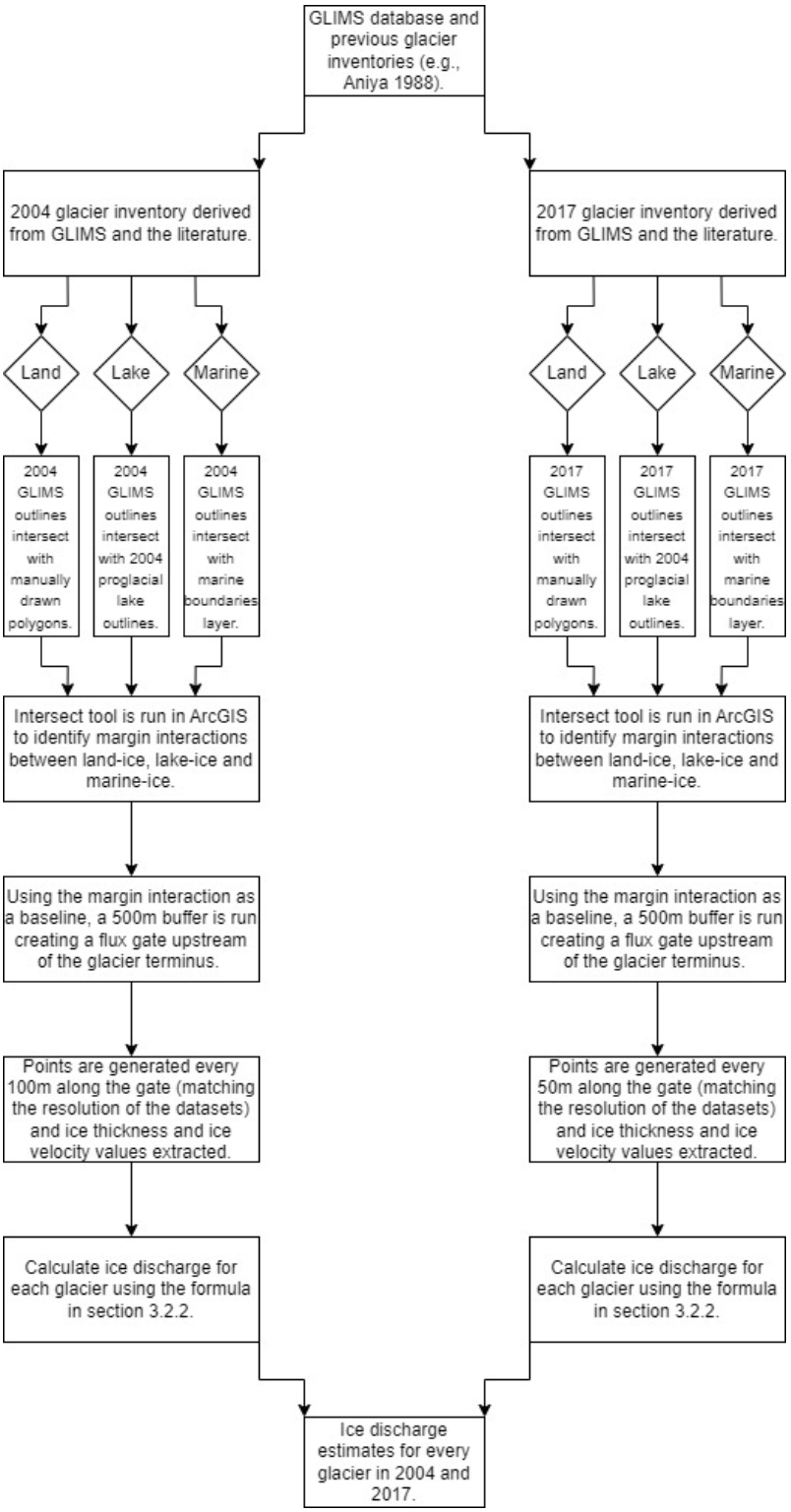

Figure 5 – A flow chart explaining the process of generating flux gates, the data extraction process and discharge calculation.

A systematic approach to flux gate generation across all termini environments removed uncertainty involved in the manual placement of flux gates (Enderlin et al., 2014; King et al., 2018). Mankoff et al., (2020) describes the manual placement of flux gates as “sub-optimal”. However, in this study there was a few exceptions to this rule, all occurring in the Southern Patagonian Icefield. A major exception to the rule being glacier Pio Xi, the only surge type glacier on the icefield, where the two major outlet termini have shown significant advancement (up to 1,400 m) and thickening trends since 2000, likely due to the compressive flow regime (Hata and Sugiyama, 2021). Therefore, due to the nature of this glacier the velocity and thickness datasets used did not cover the termini area. The other exceptions to the rule involve the fastest flowing marine-terminating glaciers on the icefield Calvo, Europa, HPS12, HPS13, HPS15, Jorge Montt and Penguin. For these glaciers rapid mass turnover at the calving front creates gaps in the velocity product close to the termini. Therefore, flux gates were placed manually as close to the termini as possible (Figure 6 and Figure 7).

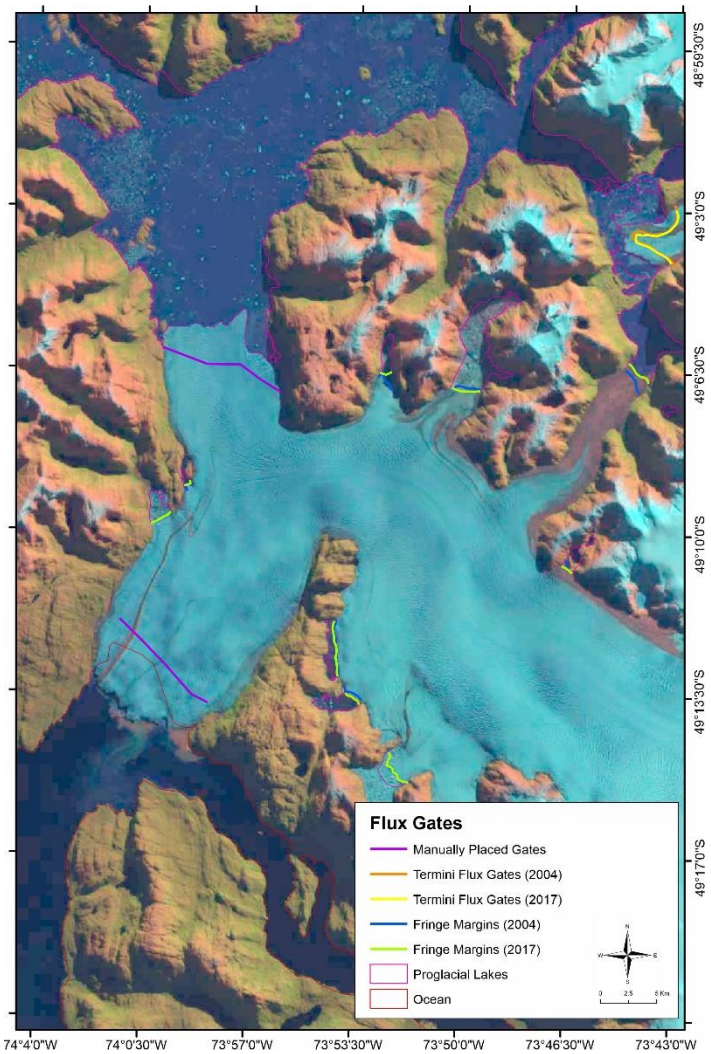

Figure 6 - Pio Xi and the surrounding environment with flux gates and interaction margins highlighted.

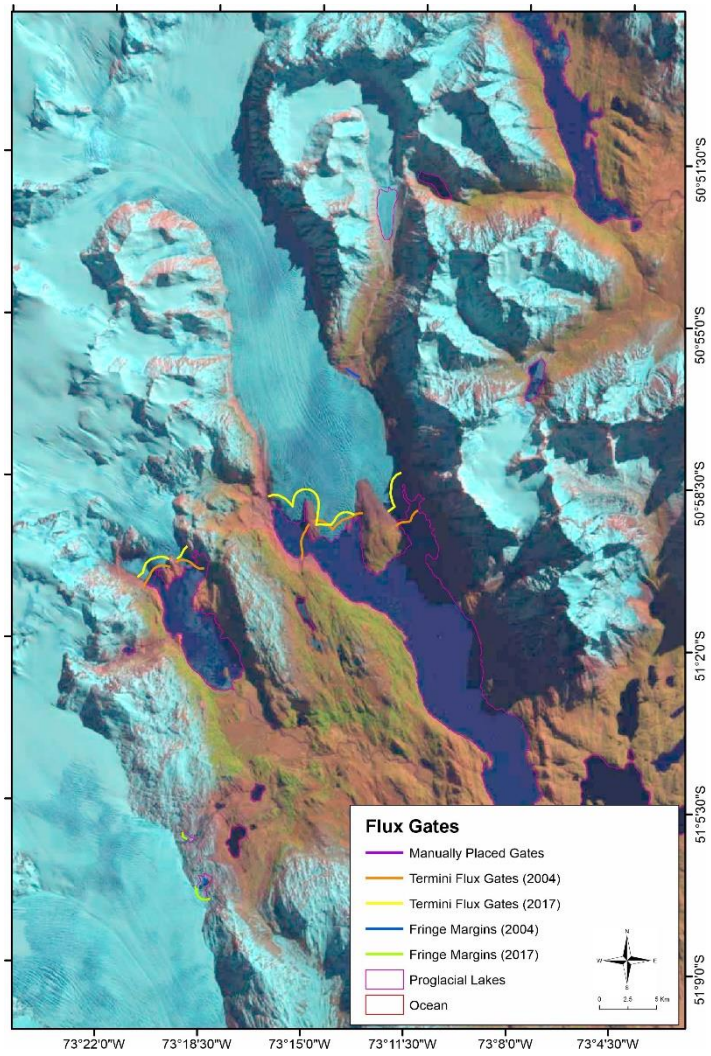

Figure 7 - Pingo and the surrounding environment with flux gates and interaction margins highlighted.

3.2.1 Transitional Environment Identification

In this study a transitional environment is where a glacier either retreats away from a proglacial lake causing the glacier to change from a lake-terminating to a land-terminating environment or vice versa where a proglacial lake forms at the snout of a land-terminating glacier resulting in the glacier changing from a land-terminating to a lake-terminating environment (Figure 8). Figure 8 gives examples of some transitional environments observed within this study. These environments were manually identified through checking ice-contact margins in both time periods for both icefields.

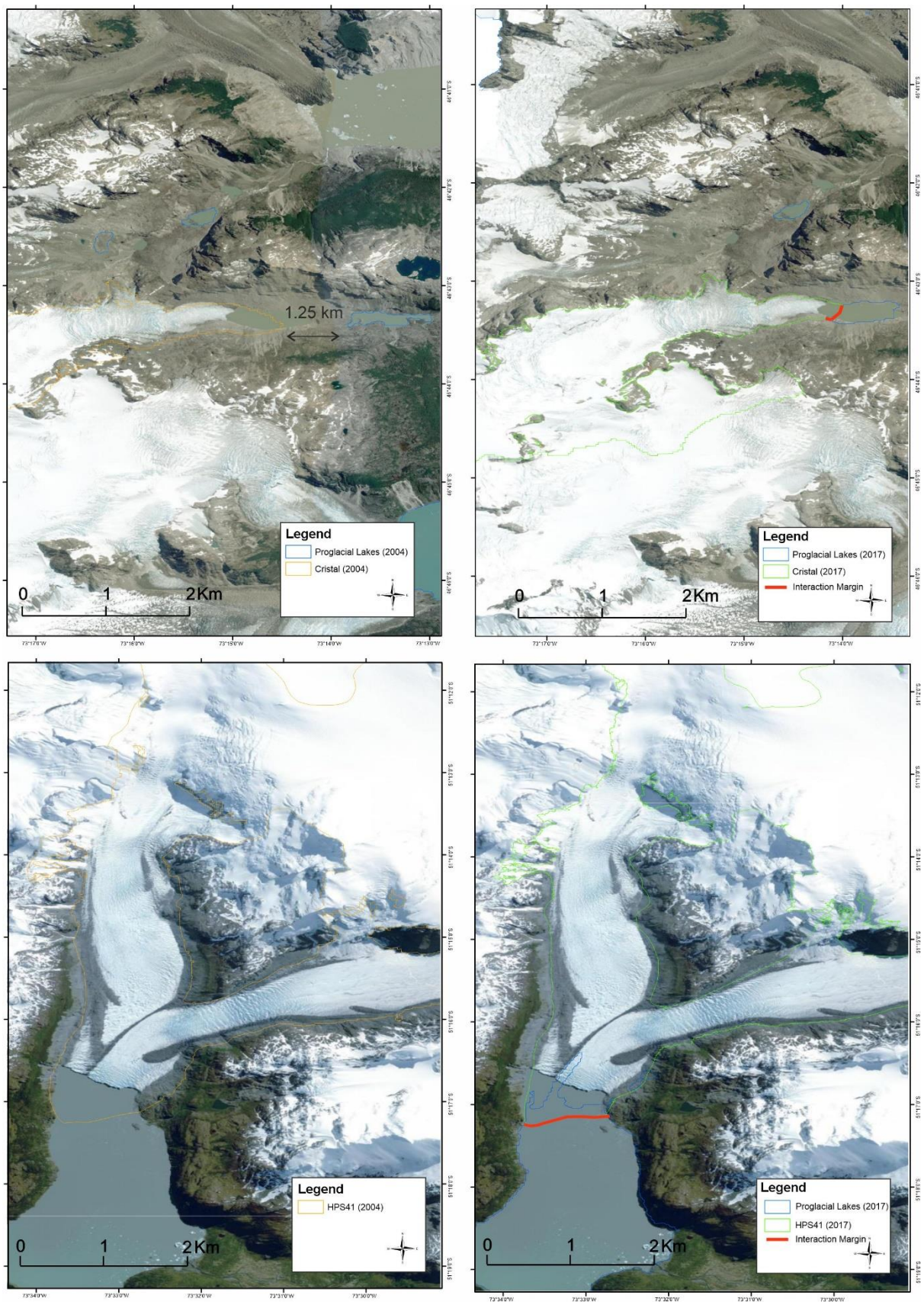

Figure 8 - Examples of transitional land to lake termini environments on the PIF. With annotations indicating distances and the delineated ice-contact margins (base map imagery dated 2022, source ESRI).

3.2.2 Ice Discharge Calculation

The flux of ice through each gate was calculated as a mass, by multiplying together the surface velocity perpendicular to the gate, with the ice thickness and the flux gate width. The use of depth averaged velocities in this discharge calculation is appropriate since both icefields are dominated by fast-flowing outlet glaciers where observed surface velocity is approximately equal to depth-averaged velocities (c.f. King et al., 2018; Mankoff et al., 2020). Ice discharge (Q_{ice}, Gt yr^{-1}) was calculated through each flux gate (Figure 9) and was given by:

$$Q_{ice} = \left(\rho \left(\sum_{n=1}^{n} (V_n \cdot T_n \cdot S_n \right) \right) \quad (1)$$

Where ρ equals the averaged density of the ice column (850 kg m^{-3}), *N* equals the number of points along the flux gate, V_n equals the velocity component at each point along the flux gate (m yr^{-1}), T_n equals ice thickness (m) and S_n equals flux gate segment width (50 m in 2017 and 100 m in 2004). An ice bulk density of 850 kg m^{-3} was used because of the relatively dry and high-elevation setting of the PIF and is a commonly applied value in glacier mass conversion studies (Zemp et al, 2019; Huss, 2013).

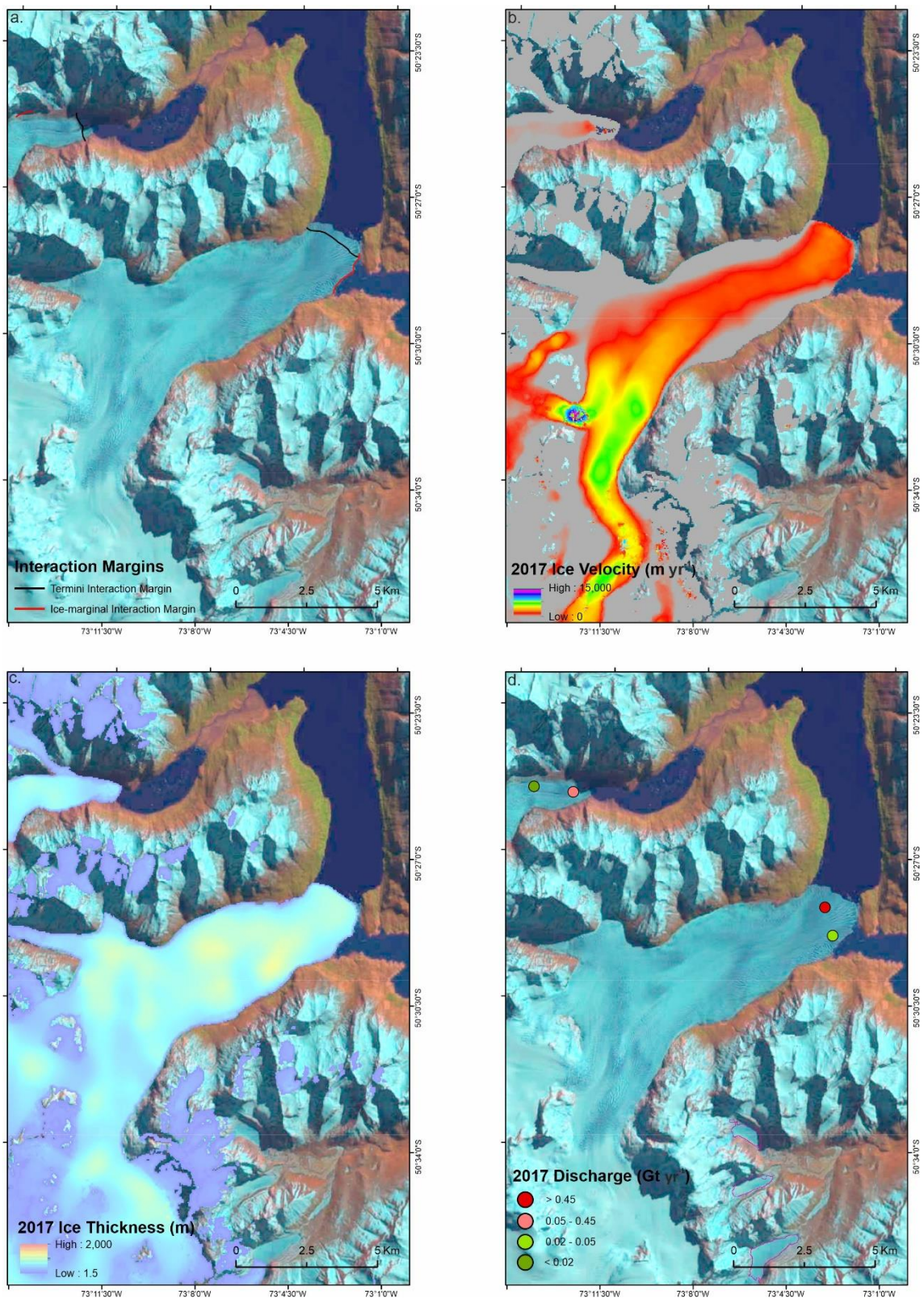

Figure 9 - Example of delineation of termini and glacier-lake interactions for Perito Moreno Glacier (a), association of enhanced velocity in the vicinity of lakes as well as termini boundaries (b), ice thickness grid displaying thickness distribution errors across the Perito Moreno Glacier (c), calculated discharges at each boundary (d).

3.3 Uncertainty Analysis

The uncertainty associated with the 2017 ice discharge data was calculated using the discharge maxima (Q_{max}) and minima (Q_{min}) provided in the spatially distributed error grids of Millan et al., (2022). At each pixel the minimum discharge (Q_{min}) was estimated using the following equation

$$\mathrm{Q_{min}} = \rho(\mathrm{V} - \sigma\mathrm{V})(\mathrm{T} - \sigma\mathrm{T})\mathrm{S} \quad (2)$$

and the maximum discharge (Q_{max}) from

$$\mathrm{Q_{max}} = \rho(\mathrm{V} + \sigma\mathrm{V})(\mathrm{T} + \sigma\mathrm{T})\mathrm{S} \quad (3)$$

where ρ equates to the averaged density of the ice column, V equates to the velocity component, T is ice thickness, σV equates to velocity error and σT equates to thickness error.

The uncertainty associated with the ice discharge calculations for 2004 required a different approach because spatially distributed error grids were not available for Mouginot's velocity mosaic or for the reconstructed ice thickness estimate. Although, Mouginot and Rignot (2015) did report error values of 3.5, 4.7, 17, 21, 52 and 28 m/yr for ALOS, RADARSAT, ERS, SIR-C and Landsat satellites respectively, there was no feasible method to identify where individual satellite contributions were on the mosaic, meaning no distributed error values could be assigned.

This study therefore first compared velocity on both icefields using random sampling of points to query both Mouginot's dataset and ITS_LIVE velocity dataset (Gardner et al., 2019). These data are provided as annual mean surface velocities derived from feature tracking Landsat 4, 5, 7 and 8 imageries (Gardner et al., 2019). While they provided a useful comparison for the random sampling used in the velocity validation, the ITS_LIVE data were evidently inferior to the Mouginot dataset due to the significantly lower spatial resolution and the missing velocity data at several of the major outlet glaciers on both icefields. Therefore, they were unable to provide the holistic coverage of the icefields and flux gates that is needed for robust validation.

Consequently, a combined random and systematic sampling approach was used on both icefields to validate velocity estimates for 2004 and delineate some error estimates. The R^2 values indicate that there is reasonably good agreement between the two velocity products. However, when looking in more detail, it quickly becomes clear that the samples with the highest velocity values have a large spread in their absolute values (Figure 10). This indicates

that the derived error values are not representative of these areas that are likely to yield the greatest flux values. The small R^2 values of the transformed data suggest that the two datasets have limited correlation. This is reinforced by the transformed R^2 values of 0.42 (Figure 10a), 0.47 (Figure 10b), 0.34 (Figure 10c) and 0.4 (Figure 10d). Consequently, the 2004 ice discharge estimates do not have any formal evaluation of uncertainty and figures will not be reported with any uncertainty. The impact of this will be considered with the discussion of study limitations.

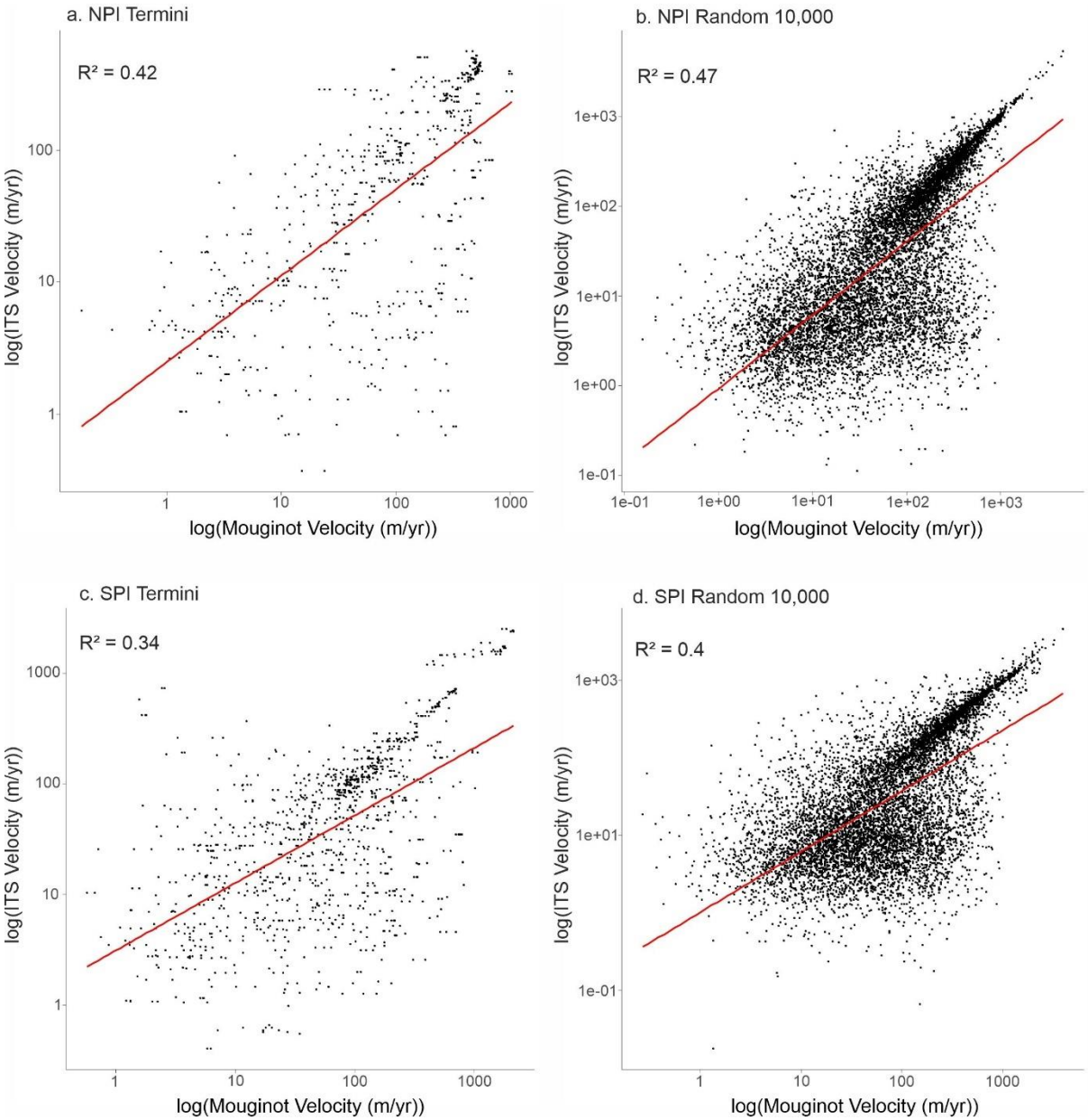

Figure 10 - Scatter plots displaying logarithmically transformed linear regression models for NPI termini points (a), 10,000 random points on the NPI (b), SPI termini points (c) and 10,000 random points on the SPI (d).

3.4 Sea Level Equivalent Estimates

The resulting discharge values were converted to sea level contributions using equation 4. To give a reasonable estimate of sea level equivalent, all ice below sea level must be removed. This is because any grounded ice below the surface and floating ice beneath the surface have already displaced water (Hock et al., 2009). Ergo, the glacial component above sea level is the only factor that needs accounting for (Pfeffer et al., 2008). Therefore, the assumption is made that all glacier termini are grounded, and consequently no floating ice exists on the PIF. Minowa et al., (2021) also makes this assumption as the combination of temperate ice and high surface velocities on the PIF reduce the likelihood of floating tongues.

$$\mathrm{SLE}\ (\mathrm{mm}) = \mathrm{Mass\ of\ ice}\ (\mathrm{Gt}) \times (1/\mathrm{area\ of\ the\ ocean}\ (\mathrm{km}^2)) \quad (4)$$

4.0 Results

4.1 Discharge Estimates for the Northern and Southern Patagonian Icefields

Combined, the NPI and SPI discharged 24.59 Gt yr^{-1} of ice in 2004 compared to 23.94 ± 7.18 Gt yr^{-1} in 2017, which is a 2.5 % decrease. This amount equates to 0.068 mm yr^{-1} sea level equivalent in 2004 and 0.066 mm yr^{-1} in 2017. Analysing both icefields, in 2004 marine-terminating glacier contributions dominated total discharge (13.89 Gt yr^{-1} or 56 %). However, in 2017, lake-terminating and marine-terminating glaciers contributed almost equally to total ice discharge (Figure 11).

This ice discharge total can be further separated into icefield contributions with the NPI contributing 7.07 Gt yr^{-1} of ice in 2004 (29 % of total) whilst 5.02 ± 1.57 Gt yr^{-1} of ice was discharged from the NPI in 2017 (21 % of total). This equates to 0.019 mm yr^{-1} sea level equivalent in 2004 and 0.014 mm yr^{-1} in 2017. On the other hand, the SPI contributed 17.52 Gt yr^{-1} (71 % of total) in 2004 compared to 18.92 ± 5.98 Gt yr^{-1} in 2017 (79 % of total), equating to 0.049 mm yr^{-1} sea level equivalent in 2004 and 0.052 mm yr^{-1} in 2017. Therefore, comparing 2004 and 2017 the NPI saw an 8 % decrease in contribution to total discharge whilst the SPI observed an 8 % increase (Figure 11).

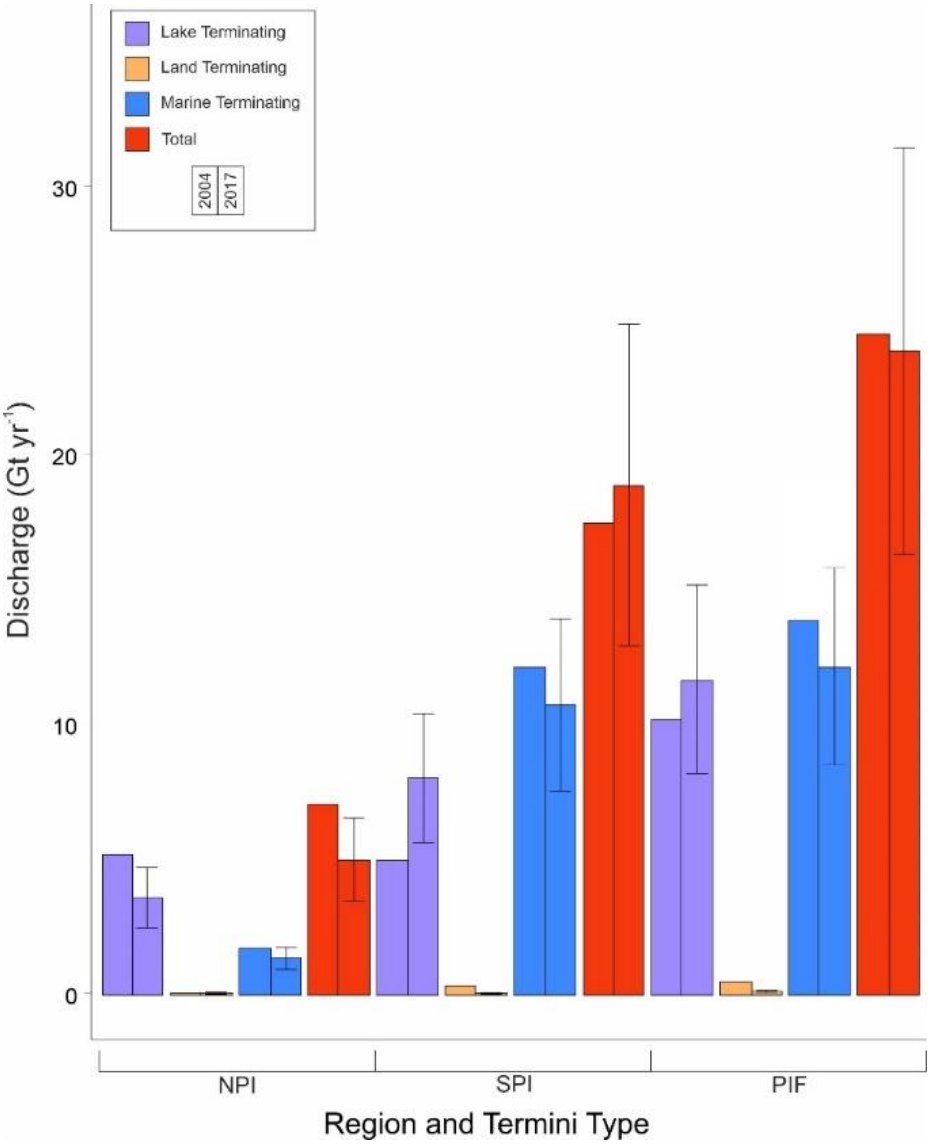

Figure 11 - Regional and termini totals of ice discharge estimates for the NPI, SPI and PIF for each of lake-terminating, land-terminating, and marine-terminating environments.

The NPI shows no significant change in ice discharge contributions between termini environments comparing both study periods (Figure 12a). While lake-terminating glaciers dominate the contribution to total discharge (2004 = 5.24 Gt yr^{-1} or 74 % and 2017 = 3.59 ± 1.07 Gt yr^{-1} or 71 %). There is a decrease in contribution of 3% when comparing 2004 to 2017 (Figure 10a). Proportionally, ice discharge contributions from each of the three terminus environments (Lake 2004 = 5.24 Gt yr^{-1} (74 % of total), Lake 2017 = 3.59 ± 1.07 Gt yr^{-1} (71 % of total), Marine 2004 = 1.73 Gt yr^{-1} (25 % of total), Marine 2017 = 1.37 ± 0.41 Gt yr^{-1} (28 % of total), Land 2004 = 0.087 Gt yr^{-1} (1 % of total), Land 2017 = 0.053 ± 0.0159 Gt yr^{-1} (1 % of total)) do not change significantly during the study period (Figure 12a). But in 2004 the outliers are consistently higher compared to the median value in 2017 (Figure 12b). For the NPI, the 2004 lake-terminating value (5.24 Gt yr^{-1}) exceeds the upper limit of 2017 lake-terminating

discharge (4.56 Gt yr^{-1}), showing greater disparity in lake-terminating contribution than marine-terminating. In comparison, the marine-terminating contribution for 2004 (1.74 Gt yr^{-1}) sits within the range of values calculated for 2017 (0.96 to 1.78 Gt yr^{-1}), which is driven by a singular glacier (San Rafael).

On the other hand, the SPI had significant changes in ice discharge when discriminated by terminus environment (changes) comparing 2004 and 2017. For example, Figure 12c indicates that marine-terminating glaciers dominate contributions to total discharge in both 2004 (12.16 Gt yr^{-1} or 69 % of total) and 2017 (10.77 ± 3.2 Gt yr^{-1} or 57 %). However, the lake-terminating contribution increased from 5 Gt yr^{-1} in 2004 to 8.06 ± 2.4 Gt yr^{-1}, i.e., by ~ 14 % (Figure 12c). An increase in lake-terminating boundary length and number is also observed (2004 = 73.5 km, 2017 = 92.5 km, 2004 = 48 margins, 2017 = 61 margins) (Figure 12g, h). This pattern is reinforced by lake-terminating contribution in 2004 (5 Gt yr^{-1}) sitting below the range of values calculated for 2017 (5.5 to 10.83 Gt yr^{-1}), whereas marine-terminating contribution remained steady between 2004 and 2017, with discharge values of 12.16 Gt yr^{-1} for 2004 and 10.77 ± 3.2 Gt yr^{-1} in 2017.

Figure 12f indicates that marine-terminating glaciers have a higher median ice discharge value than lake-terminating glaciers for the PIF in both time snapshots (Lake 2004 = 0.025 Gt yr^{-1}, Lake 2017 = 0.049 Gt yr^{-1}, Marine 2004 = 0.13 Gt yr^{-1}, Marine 2017 = 0.17 Gt yr^{-1}). However, analysing absolute values indicates that the highest discharge value calculated for a lake-terminating glacier (2004 San Quintin = 4.21 Gt yr^{-1}) is equivalent to the highest discharge value calculated for a marine-terminating glacier (2004 Jorge Montt = 4.14 Gt yr^{-1}) (Figure 12b, d). On both icefields median discharge values for lake-terminating glaciers have increased in 2017 compared to 2004 (NPI lake 2004 = 0.03 Gt yr^{-1}, NPI lake 2017 = 0.05 Gt yr^{-1}, SPI lake 2004 = 0.018 Gt yr^{-1}, SPI lake 2017 = 0.064 Gt yr^{-1}) (Figure 12b, d). However, median ice discharge values for marine-terminating glaciers decreased on the NPI but increased on the SPI (NPI marine 2004 = 1.73 Gt yr^{-1}, NPI marine 2017 = 1.37 Gt yr^{-1}, SPI marine 2004 = 0.13 Gt yr^{-1}, SPI marine 2017 = 0.16 Gt yr^{-1}) and land-terminating glaciers observed a negligible increase in median discharge values across both icefields (NPI land 2004 = 0.0005 Gt yr^{-1}, NPI land 2017 = 0.002 Gt yr^{-1}, SPI land 2004 = 0.0008 Gt yr^{-1}, SPI land 2017 = 0.003 Gt yr^{-1}).

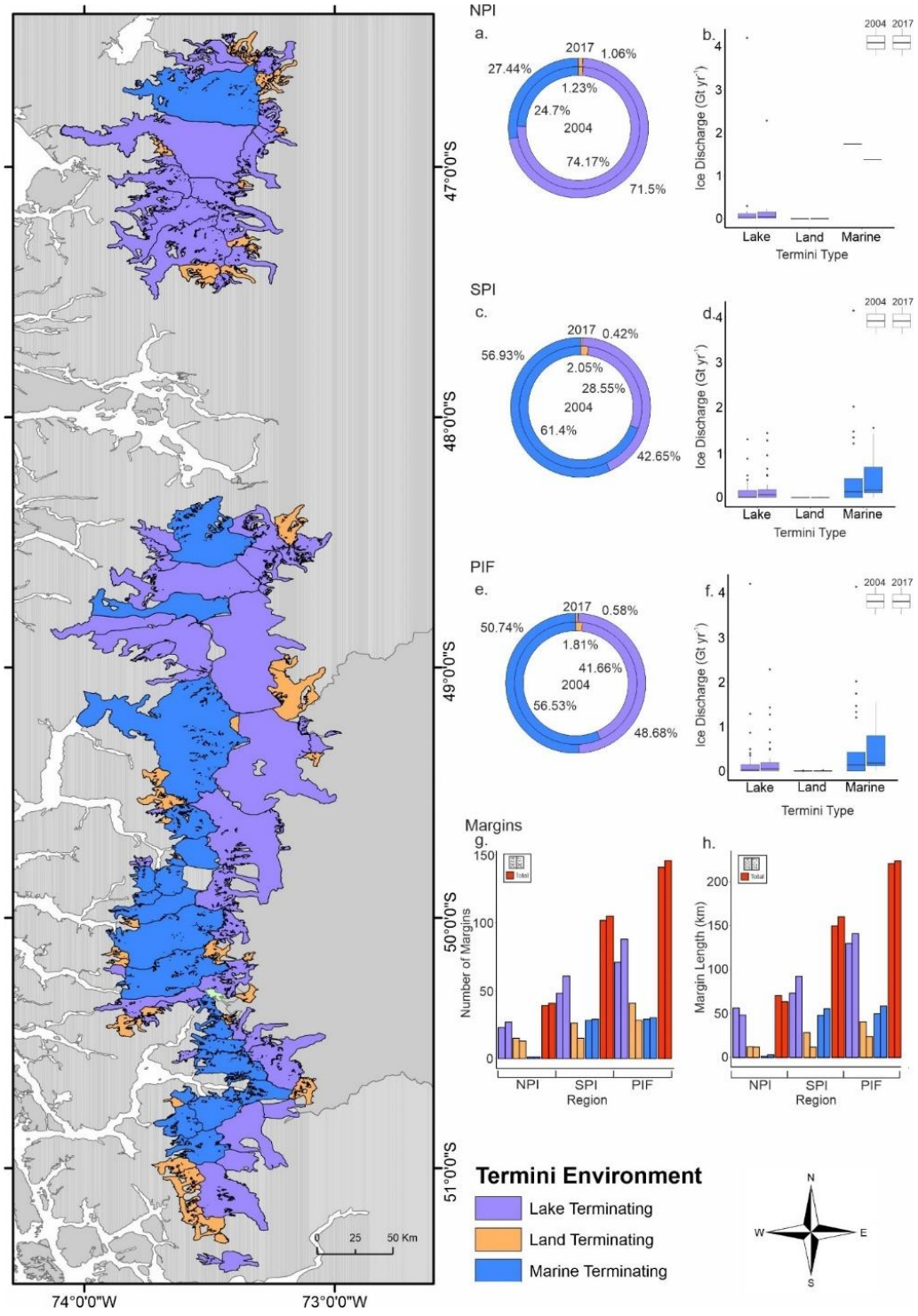

Figure 12 - The Patagonian Icefields (PIF) with termini environments associated with 2004. As well as corresponding doughnut charts showing breakdown in discharge contribution for termini environments (a, c, e) and box plots showing the spread of values for each termini type (b, d, f) for both time periods for the Northern Patagonian Icefield (NPI), Southern Patagonian Icefield (SPI) and both combined (PIF). Bar charts showing change in margin number (g) and margin length (h) for the NPI, SPI and PIF.

The western side of the NPI dominates glacier discharge in both time periods (2004 = 6.45 Gt yr^{-1} or 91 % of total, 2017 = 4.03 ± 1.2 Gt yr^{-1} or 80 % of total), exceeding all other regions combined (Figure 13a). The eastern side of the NPI had a glacier discharge total of 0.38 Gt yr^{-1} in 2004 (5 % of total) and 0.57 ± 0.17 Gt yr^{-1} (11 % of total). The general trend in the major contributing glaciers on the west of the NPI is of a reduction in magnitude of ice discharge whilst ice discharge on the eastern side of the icefield has increased when comparing 2004 to 2017. The contrasting trends in East and West are summarised by a 50 % increase in discharge in the East compared to a 40 % decrease in ice discharge in the West. The Northern and Southern regions of the NPI display no significant change in ice discharge comparing 2004 and 2017. Figure 13b shows that the greatest concentration of ice discharge on the icefield is through the north-west sector, where San Quintin Glacier reaches ice discharge rates between 2.29 and 4.41 Gt yr^{-1}. In comparison, the rest of the icefield shows a range of discharge totals between 0.000023 Gt yr^{-1} and 0.22 Gt yr^{-1}, considerably lower than San Quintin.

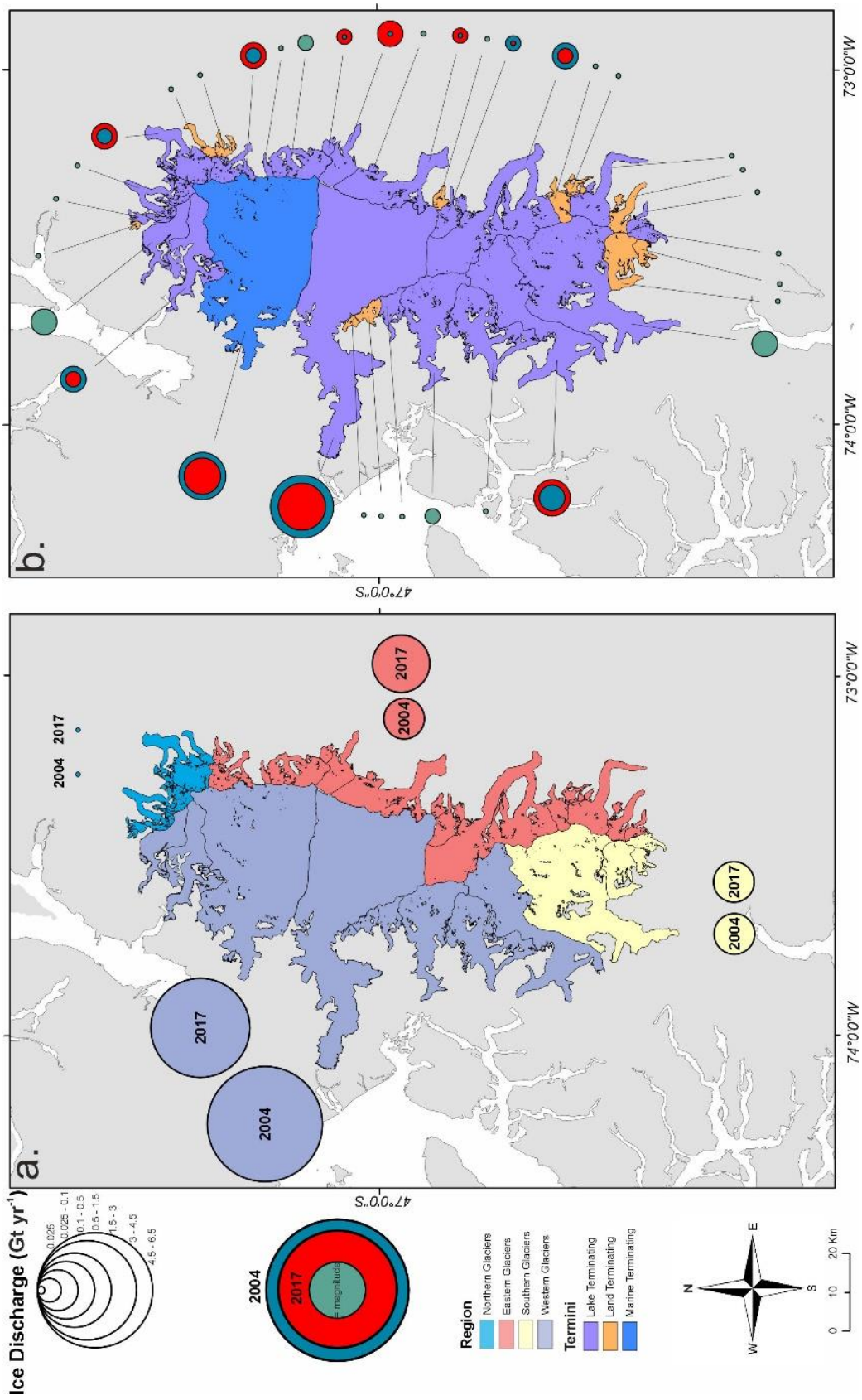

Figure 13 - Regional contributions to ice discharge split into North, East, South and West and for 2004 and 2017 for sub regions (a) and for individual glaciers (b).

Overall, Figure 14b indicates a strong trend of increasing ice discharge comparing 2004 and 2017. Indeed 93 % of the glaciers have had an increase in ice discharge comparing 2004 to 2017. Ice discharge from the SPI is predominantly from the Western sub-region of the icefield (2004 = 8.97 Gt yr^{-1} or 51 % of total, 2017 = 11.66 ± 3.5 Gt yr^{-1} or 62 % of total) compared to the Eastern sub-region (2004 = 4.03 Gt yr^{-1} or 23 % of total, 2017 = 6.29 ± 1.89 Gt yr^{-1} or 33 % of total) and Northern sub-region (2004 = 4.53 Gt yr^{-1} or 26 % of total, 2017 = 0.97 ± 0.3 Gt yr^{-1} or 5 % of total) (Figure 14a). The Western sub-region experienced a net 30 % increase in ice discharge comparing 2004 to 2017, and the Eastern sub-region of the icefield also follows this trend with a 60 % increase. However, the Northern region contrasts with the rest of the icefield as it has seen an ~ 80 % decrease in ice discharge comparing 2004 to 2017. This large decrease can be attributed to a single glacier (Jorge Montt), as the other glaciers in the Northern-sub region show no significant change.

In terms of termini environment on the SPI, land-terminating glaciers have not significantly changed in their ice discharge considering 2004 and 2017 values (2004 = 0.36 Gt yr^{-1} or 2 % of total, 2017 = 0.08 ± 0.024 Gt yr^{-1} or 0.5 % of total) many lake-terminating glaciers increased in ice discharge but ~ 60 % had no significant change. Marine-terminating glaciers varied in their ice discharge comparing 2004 to 2017 and whilst 25 % showed an increase in ice discharge two major outlet glaciers (Jorge Montt and Pio Xi) decreased in ice discharge. The south-west of the SPI has a particular concentration of glaciers where ice discharge increases significantly comparing 2004 to 2017 (Figure 14b). Furthermore, this region of the icefield should be noted as an area of interest due to its apparent discharge increase and concentration of glaciers. The highest frequency of glaciers which show no categorical change exists in the eastern region of the icefield, where 72 % of the glaciers fall into this category.

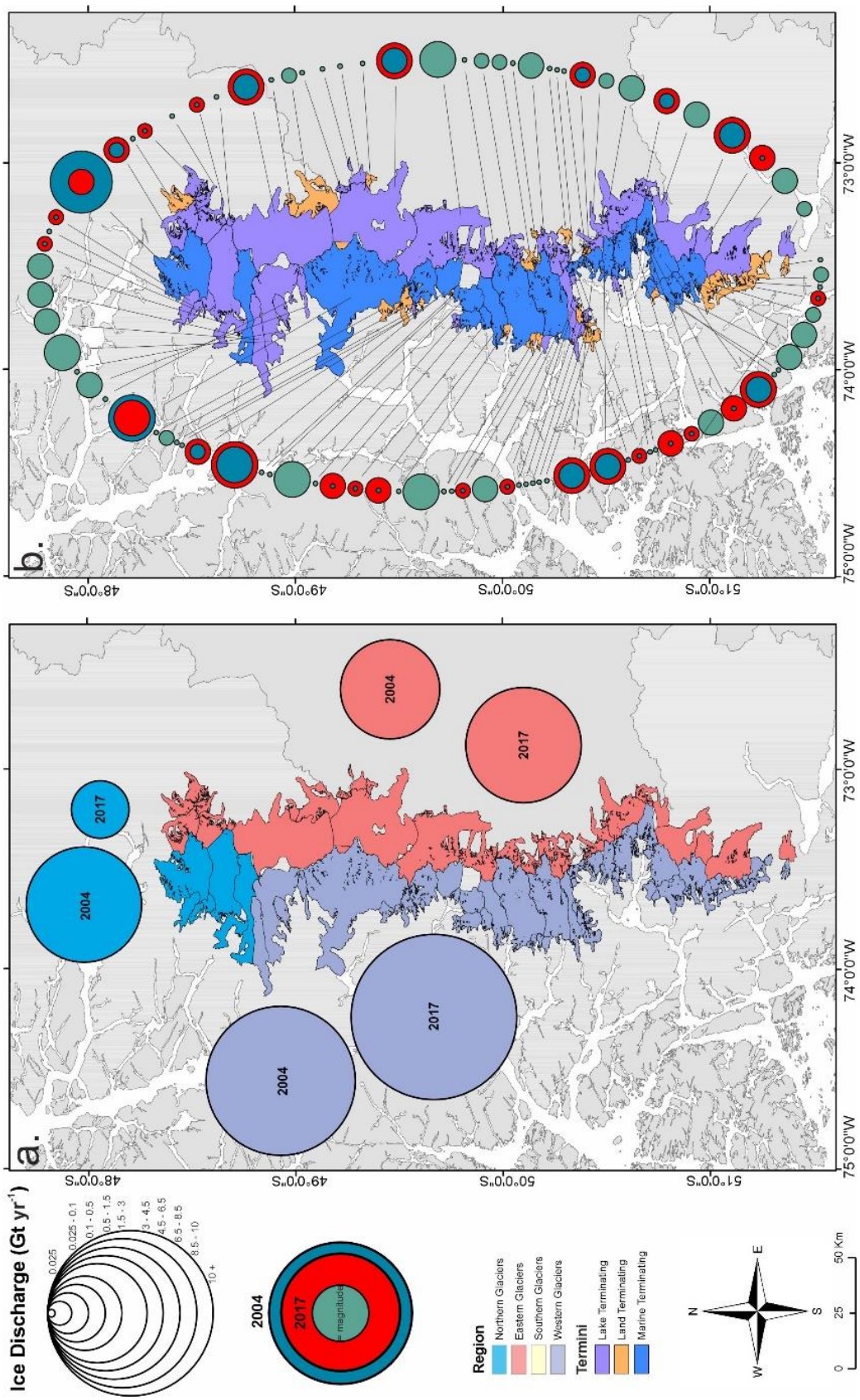

Figure 14 - Regional contributions to ice discharge of the SPI split into North, East, South and West and for 2004 and 2017 for sub regions (a) and for individual glaciers (b).

4.2 Transitional Glaciers

Figure 15a shows the glacier ice discharge totals discriminated by terminus environments for glaciers on both icefields. Whilst 80 % of glaciers display no categorical change in discharge comparing that in 2004 and 2017. This does not tell the whole story because 70 % of glaciers whose terminus transitioned from one environment to another show an increase in discharge over the time analysed (Figure 15b). Grande, Fiero and HPS41, all had termini that transitioned land to lake, and they show the greatest magnitude increase in absolute discharge (Figure 15b). For example, Fiero Glacier in the northern region of the NPI has a discharge total of 0.06 Gt a^{-1} but increases by 136 % to 0.15 Gt a^{-1} in 2017. Figure 15c indicates that lake to land transitional glaciers show the greatest percentage increase in discharge between 2004 and 2017 (median = 2396.97 %). Land-terminating glaciers are the next highest (median = 246.32 %) followed by marine-terminating glaciers (median = 195.87 %), land to lake transitional glaciers (Median = 142.32 %) and then lake-terminating glaciers (median = 90.3 %). It should be noted that the lake to land transitional glacier dataset is much smaller in terms of number of glaciers (4 glaciers) than the other datasets, hence the disparity in percentage change compared to the other termini environments.

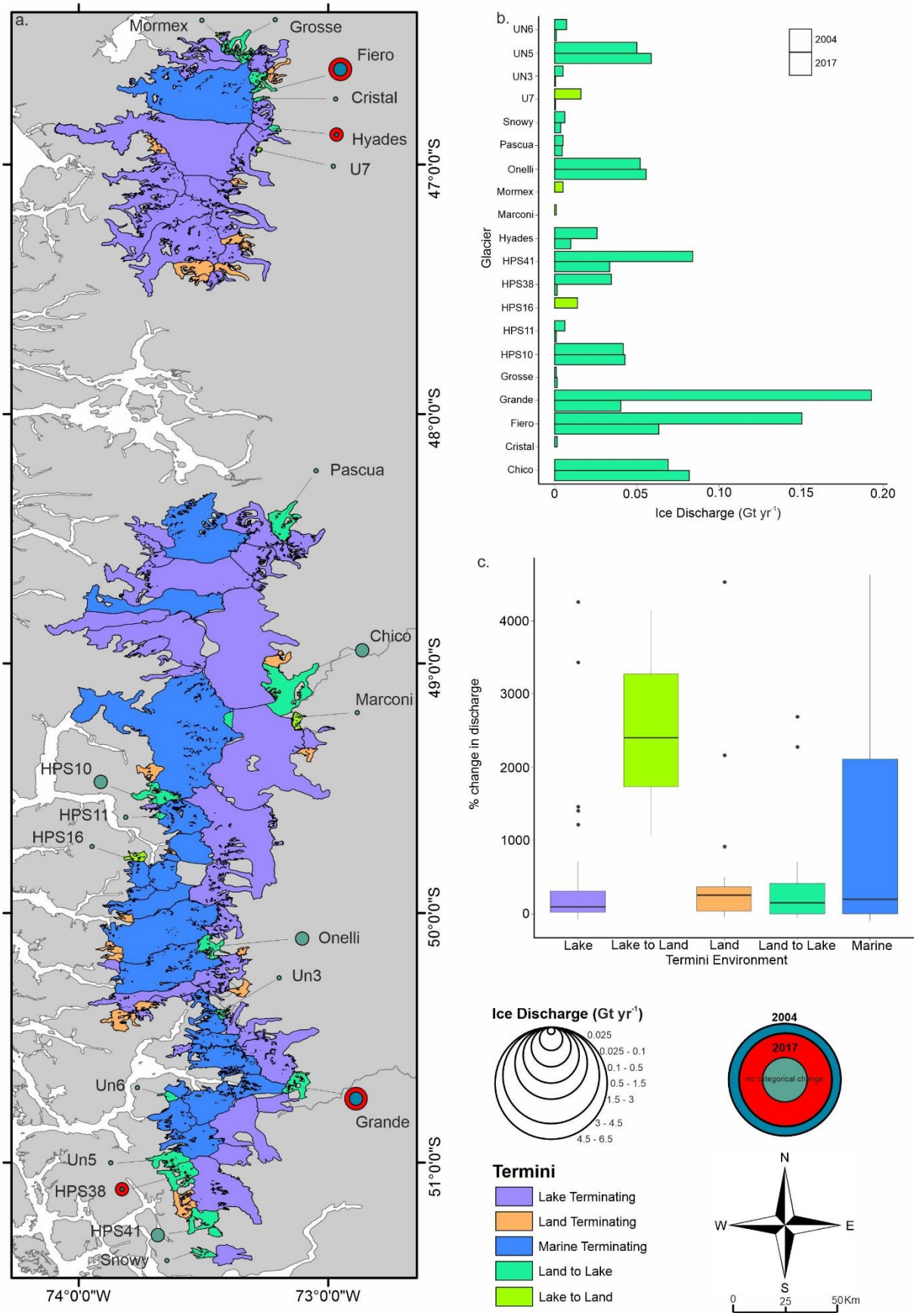

Figure 15 - Total discharge of glaciers whose terminus has transitioned from one environment to another (a), raw ice discharge values for 2004 and 2017 (b) and percentage change (c).

4.3 Results Summary

Overall, there was a 2.5% decrease in ice discharge comparing 2004 (24.59 Gt yr^{-1}) to 2017 (23.94 ± 7.18 Gt yr^{-1}) for the PIF. Most of the ice discharge from the PIF passed through marine-terminating boundaries (2004 = 56 % of total, 2017 = 50 % of total) which are concentrated on the western regions of both icefields. However, lake-terminating boundaries control (2004 = 5.24 Gt yr^{-1} or 74 % of total, 2017 = 3.59 ± 1.07 Gt yr^{-1} or 71 % of total) ice discharge on the NPI. The NPI shows a decrease in discharge totals from 2004 (7.06 Gt yr^{-1}) to 2017 (5.03 ± 1.5 Gt yr^{-1}) whereas the SPI shows an increase (2004 = 17.52 Gt yr^{-1}, 2017 = 18.92 ± 5.67 Gt yr^{-1}). A particular area of interest is identified in the south-western region of the SPI where there is a concentration of glaciers that display an increase in discharge comparing 2004 to 2017, collectively increasing from 0.67 Gt yr^{-1} to 3.58 ± 1.07 Gt yr^{-1}. In addition, this area predominantly consists of marine-terminating glaciers which are the most intense areas of ice discharge on both icefields. Marine-terminating environments contribute directly to sea level rise with equivalent estimates of total icefield discharge equating to 0.068 mm yr^{-1} in 2004 and 0.066 mm yr^{-1} in 2017. Finally, glaciers whose terminus environment has transitioned from lake to land provide the highest percentage change in discharge, but the results are likely to be skewed due to a very small dataset of 4 glaciers. Glaciers that transitioned from a land to a lake terminus environment saw a percentage increase in ice discharge of 142.32 %.

5.0 Discussion

5.1 Icefield-wide Comparisons

As described in section 2.2 there are numerous geodetic and surface mass balance model estimates of mass loss on the PIF. These estimates vary in time constraints, but the large majority are directly comparable in terms of period to this study. In this section, previous mass loss estimates from the NPI, SPI and the PIF will be directly compared to this study.

For the PIF, this study produced mass loss estimates of 24.59 Gt yr^{-1} for 2004 and 23.94 ± 7.18 Gt yr^{-1} for 2017, a negligible decrease (see section 4.1; Figure 11). The ice discharge estimates provided from this study show a remarkable agreement with geodetic mass loss estimates of the PIF. Each of Abdel Jaber et al., (2019), Chen et al., (2007), Foresta et al., (2018), Li et al., (2019), McDonnell et al., (2022), Richter et al., (2019), Willis et al., (2012a) and Willis et al., (2012b) cover a period between 2000 and 2017, matching this study. All the above studies apart from McDonnell et al., (2022) and Abdel Jaber et al., (2019) estimate mass loss from the PIF between 21.29 Gt yr^{-1} and 27.9 Gt yr^{-1}. With Li et al., (2019), Richter et al., (2019) and Willis et al., (2012b) providing mass loss estimates of 24.4 ± 1.4 Gt yr^{-1}, 23.5 ± 8.1 Gt yr^{-1} and 24.4 ± 4.7 Gt yr^{-1}. Compared to this study these mass loss estimates are all within ± 5 % of both the 2004 and 2017 ice discharge estimates. Indicating that on an icefield scale, the discharge estimates from this study provide an accurate representation of mass loss (Figure 16).

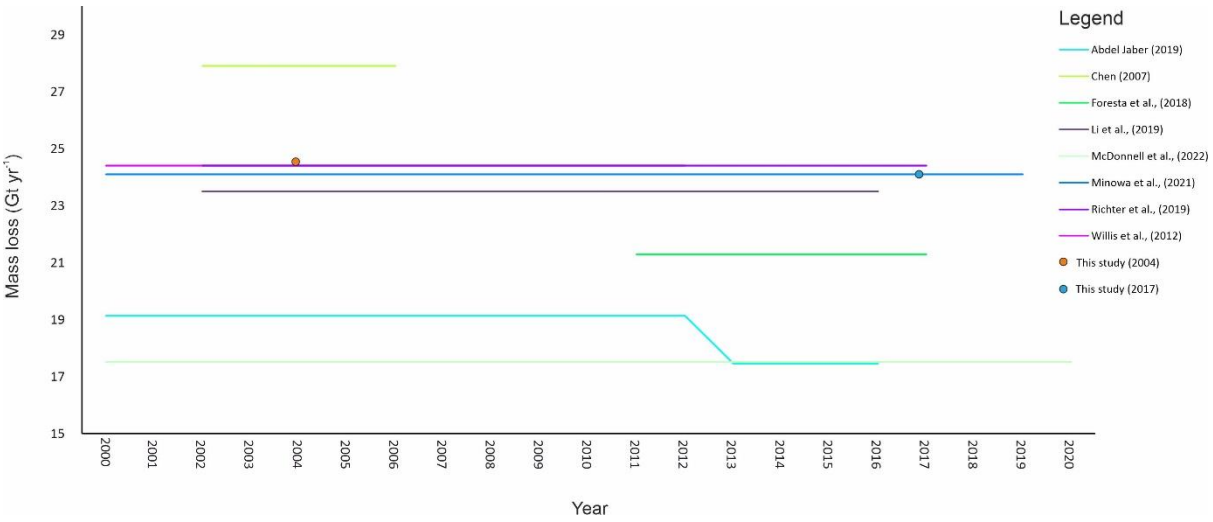

Figure 16 - Temporal comparison with mass loss estimates taken from the literature for the PIF alongside the ice discharge estimates calculated in this study.

Glasser et al., (2011) uses a geodetic method coupled with LIA reconstructions to determine PIF sea level equivalent contribution since LIA maximums, finding a 0.0018 ± 0.0004 mm yr^{-1} contribution for the NPI (1870 to 2010) and a 0.0034 ± 0.0007 mm yr^{-1} contribution for the SPI (1650 to 2010). Rignot et al., (2003) calculates a 0.042 ± 0.002 mm yr^{-1} contribution from the PIF between 1975/76 and 2000 but indicates a rapid acceleration of mass loss between 1995 and 2000 where sea level equivalent contribution amplified to 0.105 ± 0.011 mm yr^{-1}.

A review of the literature finds a few geodetic mass balance estimates; Gravity Recovery and Climate Experiment (GRACE) and frontal ablation estimates for the PIF or the individual icefields which cover various timeframes from 2000 to the present day and provide sea level equivalent estimates (Abdel Jaber et al., 2019; Chen et al., 2007; Foresta et al., 2018; Li et al., 2019; Malz et al., 2018; McDonnell et al., 2022; Minowa et al., 2021; Richter et al., 2019; Schaefer et al., 2015; Willis et al., 2012b). Within these estimates Minowa et al., (2021), Li et al., (2019), Richter et al., (2019) and Willis et al., (2012b) cover mass loss over the time periods, 2000 to 2012, 2002 to 2016, 2002 to 2017 and 2000 to 2019 respectively. Both the time periods and sea level rise estimate from these studies align with this study (2004: 0.068 mm yr^{-1}, 2017: 0.066 mm yr^{-1}, Willis et al., (2012b): 0.067 mm yr^{-1}, Li et al., (2019): 0.066 mm yr^{-1}, Richter et al., (2019): 0.067 mm yr^{-1}, Minowa et al., (2021): 0.066 mm yr^{-1}). The sea level rise estimates from Glasser et al., (2011) and Rignot et al., (2003) are a magnitude smaller than the estimates made in the 21st century – indicating a speed up in mass loss, which was also observed globally. Furthermore, due to the agreement between geodetic mass loss estimates and ice discharge estimates from this study and Minowa et al., (2021) the sea level rise estimates given appear to be robust.

For the NPI, this study produced mass loss estimates of 7.07 Gt yr^{-1} for 2004 and 5.02 ± 1.57 Gt yr^{-1} for 2017 (see section 4.1; Figure 11). There is general agreement in the literature for the NPI on mass loss rates between 2000 and 2014 ranging from 3.4 to 4.25 Gt yr^{-1} (Abdel Jaber, 2016; Abdel Jaber et al., 2019; Willis et al., 2012a), which is significantly lower than the estimate calculated in this study. Whilst for a later period (2011 to 2017) mass loss from geodetic estimates indicated an increase in mass loss, with absolute values from the NPI during this period ranging from 5.04 to 6.79 Gt yr^{-1} (Abdel Jaber et al., 2019; Foresta et al., 2018) (Figure 17).

The apparent overestimation in 2004 within this study is likely linked to the San Quintin Glacier where the radial piedmont lobe amplified calving flux margin length thus artificially increasing ice discharge. As the piedmont lobe collapsed and the San Quintin Glacier termini became more compact the flux gate methodology was able to better capture ice discharge thus aligning the results from this study in 2017 with the geodetic estimates from Abdel Jaber et al., (2019)

and Foresta et al., (2018). Furthermore, even if San Quintin Glacier is removed from the ice discharge estimates a reduction of ~ 30 % is still found across the time considered. This is interesting because it partially contradicts the amplification of inferred calving fluxes found in Schaefer et al., (2013) for the NPI from 1975/76 to 2000 and 2000 to 2009. However, the mean frontal ablation estimates from Minowa et al., (2021) for the NPI stretching between 2000 and 2019 are considerably lower than those found in Schaefer et al., (2013) indicating a shallower increase in discharge.

For the SPI, this study produced mass loss estimates of 17.52 Gt yr^{-1} for 2004 and 18.92 ± 5.98 Gt yr^{-1} (4.1 Discharge estimates; Figure 11). Rignot et al., (2003) estimates mass is lost from the SPI at a rate of 12.15 ± 0.72 Gt yr^{-1} from 1995 to 2000. Abdel Jaber (2019) (13.38 ± 0.47 Gt yr^{-1}) and Willis et al., (2012b) (20 ± 1.2 Gt yr^{-1}) mass loss estimates span 2000 to 2011/12, both of which imply an increase in mass loss from Rignot et al., (2003). Dussaillant et al., (2019) and Foresta et al., (2018) for the period 2010 to 2017 imply an increase in mass loss yet again if the average of Abdel Jaber et al., (2019) and Willis et al., (2012b) is taken (Figure 17). The geodetic mass loss estimates from the SPI seem to show a wider range in values compared to the NPI however the estimates of mass loss from this study do not contradict the general trend. Schaefer et al., (2015) inferred calving fluxes on the SPI and noticed a net increase from 1975 to 2000 and 2000 to 2011 whilst also dominating mass loss in the region. This trend transcends into this study and exemplifies the general increase in mass loss on the SPI.

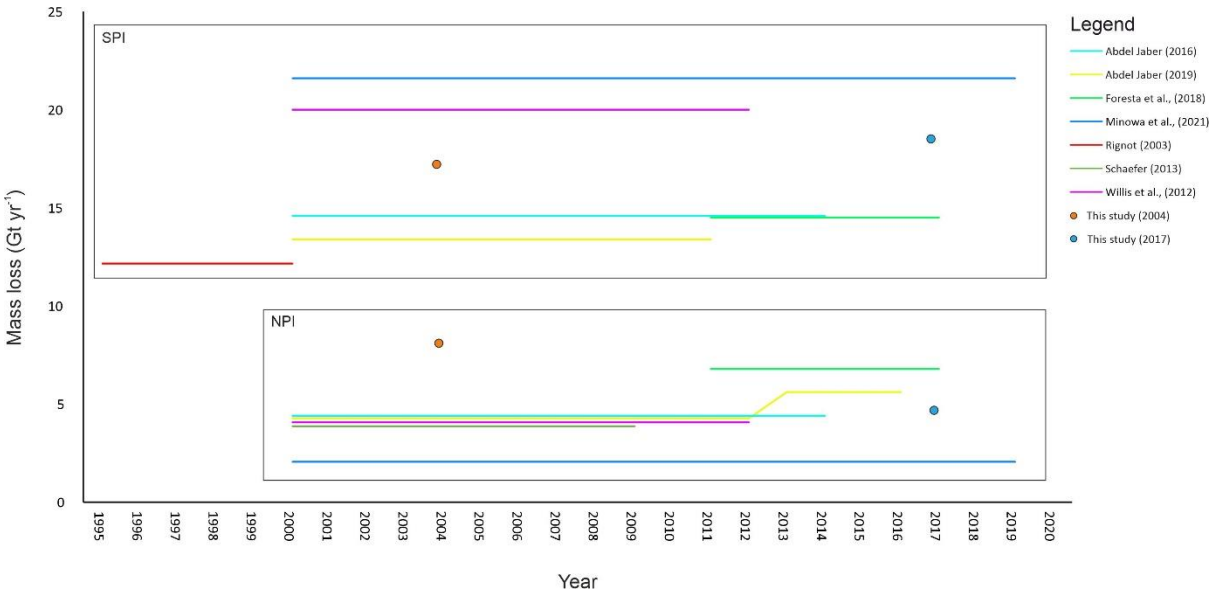

Figure 17 - Temporal comparisons of mass loss estimates taken from the literature for the NPI and SPI alongside the ice discharge estimates calculated in this study.

Comparing NPI, SPI and PIF ice discharge totals to published data surrounding mass loss estimates indicates that there is a disparity in suitability of using discharge estimates to accurately predicting mass loss trends through time for regions where calving is not the dominant ablation mechanism. This is exemplified by contradictory trends in geodetic and ice discharge estimates on the NPI (even with the exclusion of San Quintin, which is thought to have an overestimated ice discharge value in 2004) compared to the SPI where ice discharge estimates and geodetic mass loss trends were in general agreement. Geodetic mass loss estimates for the PIF being within ± 5% of the discharge totals in this study is likely driven by the domination of SPI in terms of areal extent and number of lake and marine terminating glaciers. A key driver behind the suitability of using ice discharge estimates is the % of total ablation attributed to frontal ablation, which for the NPI is ~ 20 % and the SPI ~ 50 % (McDonnell et al., 2022; Minowa et al., 2021). Calving is therefore a more dominant ablation mechanism on the SPI than the NPI.

Minowa et al., (2021) F-fraction calculations demonstrate that calving dominates most of the marine-terminating glaciers on the SPI (e.g., Penguin F-fraction = ~ 80 %) whilst lake-terminating glaciers in general show a significantly lower F-fraction. The NPI has a significantly higher ratio of lake-terminating to marine-terminating glaciers than the SPI (see section 4.1; Figure 12), forcing the disparity in the control of frontal ablation on total ablation (Minowa et al., 2021). Whilst ice discharge estimates through flux gates directly measure mass loss, geodetic methods capture elevation change, which can result from the drawdown of ice as glaciers calve (Post et al., 2011) as well as from surface melt. Therefore, as the NPI is likely more vulnerable to climate forcing than the SPI due to the feedbacks and climate decoupling involved with calving, ice discharge estimates struggle to accurately estimate actual volume loss (Schaefer et al., 2013; Bravo et al., 2021). However, as geodetic and ice discharge estimates align on the PIF this strengthens the overall understanding of mass loss on the PIF in general.

Both the NPI and SPI are found to be susceptible to climate forcing and therefore surface ablation as a mass loss mechanism (Minowa et al., 2021). This is driven by the relationship on some glaciers between F-fractions and accumulation area ratios (AAR), where on the PIF small F-fractions accompanied by large AAR's mean that frontal ablation is accounted for by accumulation (Minowa et al., 2021). However, on the SPI rapidly retreating glaciers such as Jorge Montt and Upsala negate this relationship becoming dominated by ice dynamics rather than surface ablation (Bown et al., 2019; Minowa et al., 2021; Skvarca et al., 2003). There are external factors which impact the retreat rate of glaciers on the PIF and both Jorge Montt and Upsala have shown considerable fluctuations in retreat rate, thus amplifying and nullifying ice dynamic control on mass balance (Bown et al., 2019; Naruse and Skvarca, 2000; Skvarca et

al., 2003). These variations in retreat rate which are decoupled from climate forcing, are mirrored in the heterogeneous discharge rates found in this study.

5.1.1 Comparisons of Estimates of Ice Discharge

Minowa et al., (2021) investigated the frontal ablation of 38 glaciers on the Patagonian icefields for the period 2000 to 2019. This period coincides with those analysed within this study. This study calculated discharge totals of 24.59 Gt yr^{-1} for 2004 and 23.94 ± 7.18 Gt yr^{-1} for 2017 (see section 4.1). In comparison, Minowa et al., (2021) calculated a mean frontal discharge value between 2000 and 2019 of 24.1 ± 1.7 Gt yr^{-1}. Therefore, indicating that the total discharge values calculated in this study are in conjunction with the total calculated by Minowa et al., (2021). This study delineates discharge through every (n = 124) glacier terminus on the PIF whereas Minowa et al., (2021) calculated ablation through the 38 largest glaciers. Considering this, on the NPI the glaciers excluded by Minowa et al., (2021) in 2004 contributed 0.13 Gt yr^{-1} or ~ 2 % of the calculated total; in 2017, the excluded glaciers contributed 0.48 ± 0.19 Gt yr^{-1} or ~ 10 %. For the SPI, the excluded glaciers contributed 1.51 Gt yr^{-1} or ~ 8 % of the calculated total; in 2017, the excluded glaciers contributed 4.52 ± 1.8 Gt yr^{-1} or ~ 25 % of the calculated total.

Consequently, the excluded glaciers by Minowa et al., (2021) contribute a significant amount to total frontal discharge amounts, especially on the SPI in 2017. This indicates that the discharge estimates in this study underestimate frontal discharge as the Minowa et al., (2021) mean estimate matches the totals in this study but with 86 fewer glaciers. This overestimation can be seen in Figure 15a where the vertical spread of the data in most glaciers indicates that the estimate made by Minowa et al., (2021) is often greater than the estimate made in this study. This is also reflected in the R^2 values (2004 R^2 = 0.3, 2017 R^2 = 0.48) (Figure 18).

Jakob and Gourmelen (2023) calculated discharge anomaly (D_a), hereafter referred to as ice discharge (Gt yr^{-1}), on a global scale between 2010 and 2020. Jakob and Gourmelen (2023) generated ice discharge values for 16 glaciers on the PIF for comparison with Minowa et al., (2021), providing another dataset for comparison with this study. However, this study is less comparable to Jakob and Gourmelen (2023) because of the geodetic partitioning method they used to delineate ice discharge (Gt yr^{-1}). This creates a significant disparity in all estimates when comparing the results of Jakob and Gourlemen (2023) to this study, as demonstrated via the small R^2 value of 0.07 and statistically insignificant p value (0.32). When comparing the estimates derived in Jakob and Gourlemen (2023) and Minowa et al., (2021) a similar pattern is observed, where there is disparity in values (R^2 = 0.28).

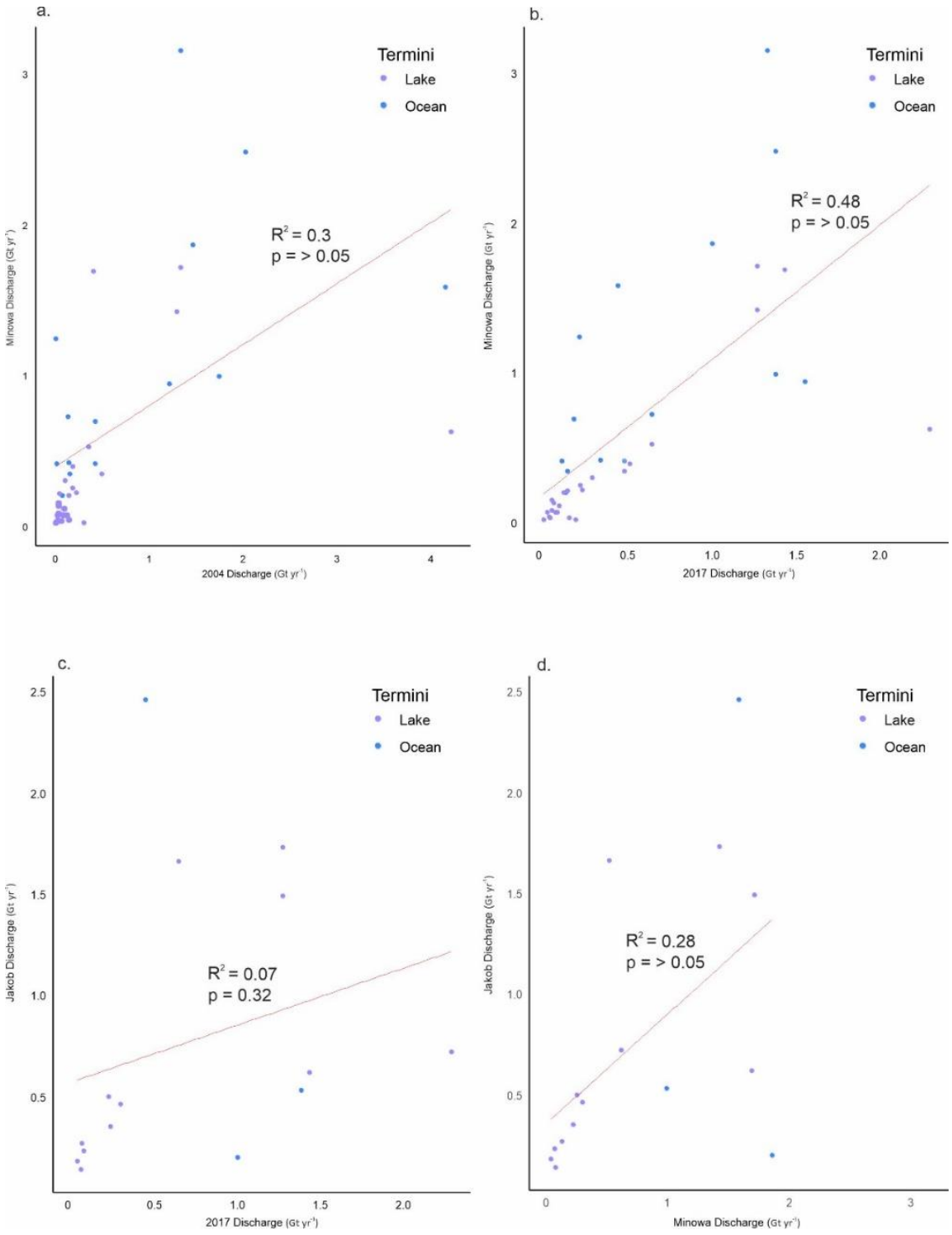

Figure 18 - (a) glacier-specific comparison between estimates of ice discharge for this study (2004) and the frontal ablation estimates of Minowa et al., (2021). (b) glacier-specific comparison between estimates of ice discharge for this study (2017) and the frontal ablation estimates of Minowa et al., (2021). (c) glacier-specific comparison between estimates of ice discharge for this study (2017) and the discharge anomaly estimates of Jakob and Gourmelen (2023). (d) glacier specific comparison between the frontal ablation estimates of Minowa et al., (2021) and the discharge anomaly estimates of Jakob and Gourmelen (2023).

5.1.2 Individual Glacier Mass Loss Comparisons

Glacier San Rafael is the only glacier on the NPI which has multiple historical estimates of ice discharge, outside of Minowa et al., (2021) and Jakob and Gourmelen (2023) (Figure 19). This is because San Rafael is the largest glacier on the NPI and the only marine-terminating glacier whilst being one of the fastest glaciers in the world with ice velocities exceeding 7,000 m/yr (Mouginot and Rignot, 2015; Willis et al., 2012a). For context, since the end of the LIA (1870) San Rafael has retreated 10 km and deteriorated to the point where a ~ 7 km piedmont lobe has disintegrated into a ~ 2 km calving front (Colloa-Barrios et al., 2018; Davies and Glasser, 2012). A modelling study by Koppes et al., (2011) indicated that since the 1950's the ice discharge at San Rafael has decreased steadily from 8.05 Gt yr^{-1} to 1.4 Gt yr^{-1} in 2001.

In addition, Koppes et al., (2011) indicated that consistent "rapid calving rates" in the future may diminish the current termini and initiate rapid retreat as seen in other marine-terminating glaciers around the world (Howat et al., 2008). The ice discharge estimates from this study for San Rafael are consistent with the results from Schaefer et al., (2013) and Willis et al., (2012a) – considerably larger than the estimates provided by Collao-Barrios et al., (2018), Koppes (2007), Koppes et al., (2011) and Warren et al., (1995) (Figure 17). Therefore, the estimates from this study, alongside those from Schaefer et al., (2013) and Willis et al., (2012a), indicate that the San Rafael Glacier has sustained a significant level of ice discharge from the early 2000's up until 2017, aligning with Koppes et al's., (2011) prediction. Further work should focus on San Rafael in the future as a significant retreat could alter the landscape of the NPI.

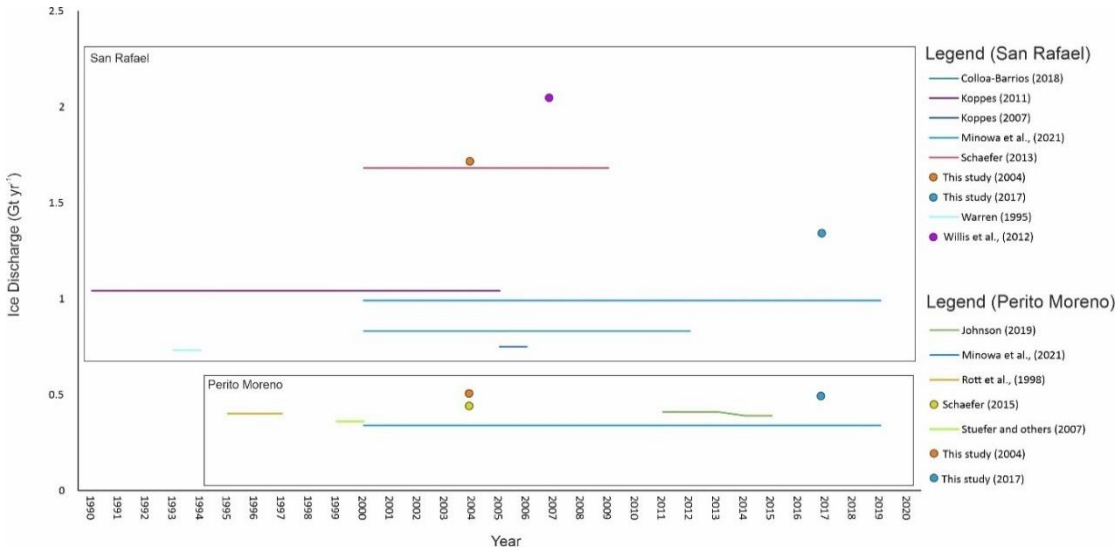

Figure 19 - Published ice discharge estimates for San Rafael and Perito Moreno glaciers alongside ice discharge estimates calculated in this study.

The SPI has a collection of high-profile glaciers that have been the subject of detailed research in recent decades. Therefore, ice discharge estimates are much more readily available for individual glaciers on the SPI than they are on the NPI.

Perito Moreno Glacier is a relatively stable glacier (± 500m since 1920) located in the south of the SPI which has some of the highest net accumulation rates in the world (Lodolo et al., 2020; Skvarca and Naruse, 1997). Minowa et al., (2017) reports that Perito Moreno has a high ratio of calving flux to total ablation (56 %). In addition, pinning points at the terminus on the Magellanes peninsula have caused several instances of damming at the Brazo River over the last century, whilst also halting advancement (Minowa et al., 2017). Ice discharge estimates from the literature for Perito Moreno span from 1995 to 2015. Figure 19 shows that all estimates are close in magnitude, even though numerous methods of ice discharge calculation were used. Lodolo et al., (2020) indicates that the balance between frontal ablation and accumulation keeps Perito Moreno Glacier stable, juxtaposing the retreat rates of glaciers nearby. This is a reasonable assumption to make due to the number of discharge estimates over the last 20 years indicating that the calving flux has remained constant.

Glacier Upsala in this study showed a negligible change in ice discharge (see section 4.1; Figure 14b) (2004 = 1.29 Gt yr^{-1}, 2017 = 1.26 ± 0.5 Gt yr^{-1}). When comparing these results to estimates found in the literature, there has been a general increase in discharge from 1985 to 2020. Skvarca et al., (1995) reported discharge values ranging from 0.8 to 1.4 Gt yr^{-1} between 1985 and 1993. In comparison, Minowa et al., (2021) reported mean frontal ablation estimates for Upsala between 2000 and 2019 as 1.42 Gt yr^{-1} (a 78 % increase on the lowest estimate made by Skvarca et al., (1995)) whilst Jakob and Gourmelen (2023) estimated ice discharge from Upsala between 2010 and 2020 as 1.73 ± 0.1 Gt yr^{-1} (a 116 % increase on the lowest estimate made by Skvarca et al., (1995)). Both Minowa et al., (2021) (2004 = + 10 %, 2017 = + 12 %) and Jakob and Gourmelen (2023) (2004 = + 34 %, 2017 = + 37 %) provide discharge estimates that are greater than the estimate made in this study.

Extensive research has commenced on Upsala due to its rapid retreat in recent decades and the subsequent velocity acceleration at the terminus (Minowa et al., 2023). Sakakibara and Sugiyama (2014) discovered a ~ 20 % increase in velocity at the termini in association with a rapid retreat, thinning and longitudinal stretching in 2008 at Upsala (Muto and Furuya, 2013). The bed geometry of Upsala is the likely cause of rapid retreat, thinning and an increase in ice flux at Upsala and climatic control can be ruled out as a contributing factor due to negligible changes in air temperature being detected at a nearby climate station (Sakakibara et al., 2013; Skvarca et al., 2002). This dynamic control on glacier behaviour is a consistent theme which

runs throughout Patagonia whereby rapid retreats, velocity acceleration and widespread thinning are common.

Glacier Viedma has displayed an increase in ice discharge within this study increasing from 0.35 Gt yr^{-1} in 2004 to 0.64 ± 0.26 Gt yr^{-1} in 2017 (4.1 Discharge estimates; Figure 14b). Ice discharge estimates found in the literature also follow this trend. Schaefer et al., (2015) indicated that Viedma had an ice discharge rate of 0.36 ± 0.3 Gt yr^{-1} in 2004 whilst Minowa et al., (2021) estimate Viedma to have a mean ice discharge of 0.52 Gt yr^{-1} between 2000 and 2019 and Jakob and Gourmelen (2023) calculate Viedma to have a mean discharge rate of 1.66 Gt yr^{-1} from 2010 to 2020. An increase of 82 % was observed in this study and this can be reinforced by using Schaefer et al., (2015) as an independent baseline. For example, the ice discharge estimate for Viedma taken from Minowa et al., (2021) found an 44 % increase in ice discharge over a similar period. This apparent increase in ice discharge is directly linked to an amplification of frontal retreat on Viedma. Joughin et al., (2004) explains that surface velocity acceleration causes calving flux to increase which causes thinning and glacier retreat. This relationship is observed at Viedma. Sakakibara and Sugiyama (2014) found a deceleration at Viedma between 2000 and 2011 of -5.3 ± 1.4 % which coincided with a relatively slow front retreat rate of 35.5 m/yr in context with some of the glaciers on the SPI. The average velocity along the flux gate used in this study at Viedma in 2004 was 499 m/yr but increased drastically in 2017 where the average velocity was 689 m/yr, which consequently corresponded with a drastic increase in frontal retreat of 281 m yr^{-1} between 2010 and 2016 (Vecchio et al., 2018). Therefore, on Glacier Viedma we can observe a clear example of how calving flux can control the state of glacier retreat.

5.2 Influence of Terminus Environments

5.2.1 Marine-terminating Glaciers

The total frontal discharge of marine-terminating glaciers had a negative trend comparing 2004 and 2017 (see section 4.1; Figure 11). However, this trend masks the changing nature of frontal discharge at individual marine-terminating glaciers. Out of the 25 marine-terminating glaciers, 18 saw an increase in frontal discharge, which can partially be explained by an amplification of ice velocity. Indeed, 16 of these glaciers had a statistically significant increase in surface velocity comparing 2004 to 2017 (see appendix C.2). For example, HPS29 observed an increase in average surface velocity of 1042 m/yr. Sakakibara and Sugiyama (2014) identified 1.1% of the SPI where an increase of > 1,000 m/yr was observed between

1984 and 2000, indicating that the amplified values extracted from the flux gates in this study are entirely feasible within the context of the SPI.

The associated accelerated surface velocities of these marine-terminating glaciers could be due to numerous factors. One factor could be geothermal heating at the base, lubricating the glacier bed, increasing frictional heating, and enabling faster flows (Näslund et al., 2005; Larour et al., 2012). On the PIF there are 5 volcanoes, all of which have shown activity within the Holocene (Gonzalez-Ferran, 1995; Motoki et al., 2003; Orihashi et al., 2004). Killan (1990) found evidence that the latest eruption from Viedma volcano occurred in 1988, indicating that there remain active volcanoes on the icefields.

Looking at the SPI specifically marine-terminating glaciers and lake-terminating glaciers display different characteristics. The marine-terminating glaciers are characterised by large F-fractions and small elevation changes (Minowa et al., 2021). This consequently promotes a stable set of glaciers, where surface mass balance is moderated by small steep ablation areas (Aniya et al., 1997; De Angelis, 2014). A key finding in this study is the increase in discharge through time of ~ 70 % of marine-terminating glaciers, with a particular concentration in the south-west of the SPI (see section 4.1; Figure 14b). Minowa et al., (2021) reports that several glaciers in this region are in fact thickening, contributing to the fact that these marine-terminating glaciers are increasing in discharge. However, Glacier Pio Xi and Jorge Montt show reductions in ice discharge through time due to a complex interplay of processes. This once again highlights the heterogeneous nature of marine-terminating environments on the PIF.

Another key influence on marine-terminating glaciers is the critical role the ocean plays on the dynamics of the glacier termini. The calving flux of marine-terminating glaciers can be directly influenced by submarine melting at the termini, fjord bathymetry and fjord stratification (Jenkins, 2011; Schild and Hamilton, 2013). Submarine melting at the termini influences calving fluxes through buoyant plumes which emanate from subglacial channels, the plumes then dwell at the glacier front enhancing melt (Motyka et al., 2003; Rignot et al., 2015). Enhanced melt at the termini amplifies calving, causing the ice surface to steepen, increasing driving stress which subsequently increases ice discharge (Sutherland et al., 2020; Walker and Gardner, 2017). Fjord bathymetry and stratification controls glacier behaviour at the same time.

The network of fjords that connects the SPI to the Pacific Ocean is intricate in nature, with marine-terminating glaciers in the region experiencing varied exposure to ocean-ice interaction (Dowdeswell et al., 2016). For example, a narrow sill and channel constriction in the Messier channel restricts flow, hindering fjord circulation patterns and reducing the

influence of subsurface waters from the Pacific ocean south of 49° (Dowdeswell and Vásquez, 2013; Moffat et al., 2018). On the other hand, in the northern section of the icefield the subsurface waters in the fjord systems are usually warmer in the spring (Moffat et al., 2018). This restriction of the Messier channel reduces the exposure of Pio Xi Glacier to ocean forcing potentially contributing to the apparent advance of the termini (Moffat et al., 2018). Observations of fjords and the oceanic conditions surrounding the marine-terminating glaciers in Patagonia is minimal, the few case studies that do exist can only provide a brief insight into specific glaciers. Moffat et al., (2018) investigated the ocean-ice interactions in the fjord connected to Jorge Montt and found that the melting of the glacier is caused by “some of the warmest” oceanic water reaching a marine-terminating glacier anywhere in the world. This indicates that oceanic forcing does have a significant impact on glacier dynamics in Patagonia but most likely does not solely explain the heterogeneous behaviour of marine-terminating glaciers.

The prominent losses in ice discharge from marine-terminating glaciers within the PIF are found on San Rafael, Europa, Jorge Montt and Pio Xi (see section 4.1; Figure 14b). Glacier Jorge Montt in the northern region of the SPI has undergone rapid retreat in recent years with retreat rates of up to 640 m yr^{-1} being reported between 2011 and 2018, and a 1 km retreat being reported in 2011 alone (Bown et al., 2019; Rivera et al., 2012). Within the time constraints of this study, frontal discharge estimates from Jorge Montt vary considerably with estimates in 2003 equating to 1.63 ± 0.61 Gt yr^{-1} compared to 4.38 ± 1.23 Gt yr^{-1} in 2011 and 2.14 ± 0.6 Gt yr^{-1} in 2017 (Bown et al., 2019). These values agree with the value extracted for 2004 but not for the value extracted in 2017 (Jorge Montt 2004 = 4.15 Gt yr^{-1}, Jorge Montt 2017 = 0.44 Gt yr^{-1}). The significant variability in frontal discharge estimates can be attributed to significant phases of acceleration and deceleration in the last 25 years driven by changes in fjord bathymetry at the termini (Rivera et al., 2012).

Acceleration occurred between 1985 and 2001 and 2009 to the present day on Jorge Montt, ice stream velocities increased by 130 % between 2003 and 2011 (Muto et al., 2013). The significant variation in velocities and frontal discharge at Jorge Montt exemplifies the dynamic nature of termini environments on the SPI. Analysing Jorge Montt further, there was no significant difference ($P = 0.09973$) in velocity values taken from the flux gates in 2004 and 2017 within this study. Therefore, the variable velocities alone cannot explain the reduction in frontal discharge at Jorge Montt. Alongside rapid retreat, surface lowering within the ablation zone between 2000 and 2018 ranged from - 2 m yr^{-1} to - 21 m yr^{-1} (Bown et al., 2019). Dynamic thinning is thought to control glacier dynamics on Jorge Montt as a negative mass balance trend between 1980 and 2015 continued even though snow accumulation increased at the same time (Bravo, 2019; Mouginot and Rignot, 2015).

A significant difference comparing 2004 and 2017 velocity values extracted at the flux gate on Europa was found (P = > 0.05) with average values for 2004 (7208.92 m/yr) being much higher than the average value for 2017 (296.23 m/yr) (see appendix B.2). Therefore, indicating that the terminus velocities have decelerated. Previous research has suggested that Europa glacier has remained relatively balanced in terms of surface elevation between 2012 and 2016 but followed a negative trend from 2000 and 2012 (Dussaillant et al., 2019; Malz et al., 2018). This is reinforced by the ice thickness data extracted from the flux gate on Europa, where a significant difference was found in a negative trend (P = > 0.05). Consequently, a reduction in frontal discharge between the two snapshots in time is therefore understandable. Glacier San Rafael follows a similar trend, with a modelling study initiated by Koppes et al., (2010) simulating a steadily decreasing estimate of frontal discharge from 1959 to 2001, a trend which is mirrored within this study (see appendix B.1).

Glacier Pio Xi is the exception to the rule for marine-terminating glaciers which have shown a reduction in frontal discharge on the SPI. Pio Xi has advanced significantly in the 20th and 21st centuries, the only glacier to follow this trend on the SPI (Hata et al., 2021; Rivera et al., 1997; Warren and Rivera, 1997). As well as advancing, the bifurcated tongues of Pio Xi have thickened at a rate equivalent to 2 m/yr between 2000 and 2012 (Willis et al., 2012b). The mechanisms controlling the advancing Pio Xi are relatively unknown. Rivera et al., (1997) connects a large accumulation area (AAR = 0.81) with positive precipitation anomalies as a possible explanation of Pio Xi advance during the late 20th century. Differing theories point towards a surge type glacier, but a triggering mechanism is still yet to be found (Wilson et al., 2016).

A possible explanation for the reduction of discharge at Pio Xi glacier is the formation of a sediment barrier in front of the southern terminus. Therefore, isolating the terminus from external stimuli from the fjord, stabilising the calving front and reducing calving flux (Hata et al., 2021). This barrier developed in 2011 and expanded to cover the entire front in 2019, through a combination of disturbed fjord sediment and subglacial meltwater deposits (Hata et al., 2021) (Figure 20). Furthermore, ITS_LIVE data confirmed that the southern terminus has followed a decelerating trend from 2000 to 2018 due to the buffer provided by the sediment barrier (Hata et al., 2021). Therefore, the sediment barrier is a likely explanation for the trend found within this study of a reduction in frontal discharge at Pio Xi glacier.

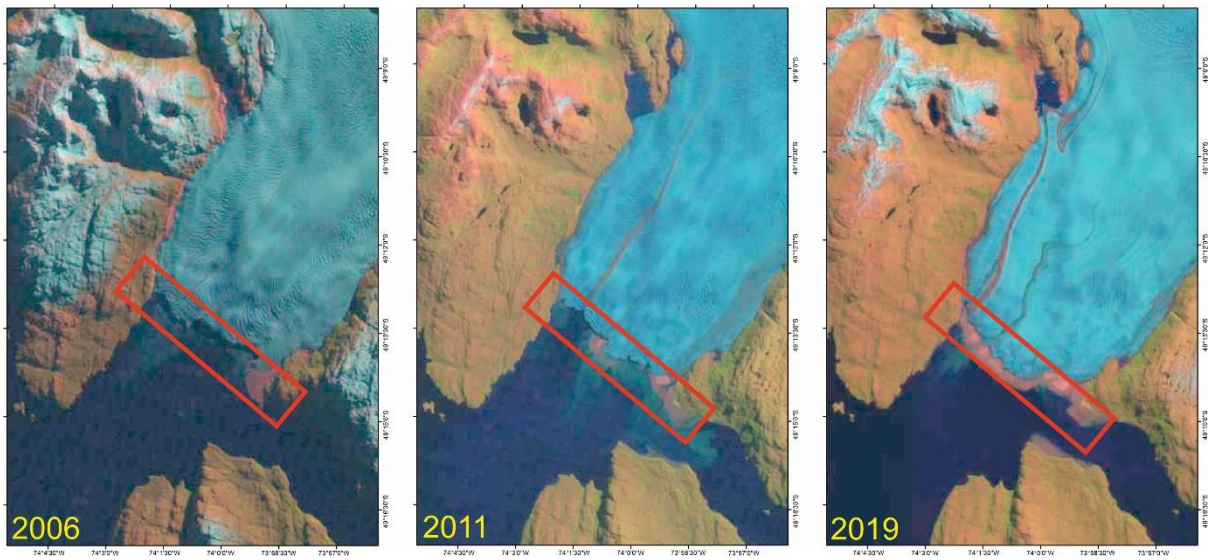

Figure 20 - Landsat 5 and Landsat 8 imagery of the southern tongue of Pio Xi glacier terminating in Eyre fjord. A clear accumulation of the sediment at the glacier terminus is visible.

5.2.2 Lake-terminating Glaciers

Overall, lake-terminating glaciers across the PIF had an increase in ice discharge comparing 2004 to 2017 (see section 4.1; Figure 11). However, the NPI and SPI icefields displayed opposite trends; the NPI saw a net decrease in ice discharge from lake-terminating glaciers (dominated by losses from San Quintin), compared to a net increase in ice discharge from lake-terminating glaciers on the SPI (NPI 2004 lake = 5.24 Gt yr^{-1}, NPI 2017 lake = 3.59 ± 1.07 Gt yr^{-1}, SPI 2004 lake = 5.02 Gt yr^{-1}, SPI 2017 lake = 8.06 ± 2.42 Gt yr^{-1}). A net increase in ice discharge from lake-terminating glaciers is likely due to an increase in new proglacial lake margins coupled with an acceleration of ice surface velocity.

A key influence on an increase in ice discharge through lake-terminating environments is the expansion of lake-ice contact margins. For example, in 2004 the total margin length equalled 220.77 km on the PIF but in 2017 this had expanded to 223.93 km (see section 4.1; Figure 12h). This trend was exemplified by Loriaux and Casassa (2013) who identified a ~ 65 % increase in proglacial lake area on the NPI between 1945 and 2011; the findings of this study support the continued growth of proglacial lakes on the PIF. An overarching trend on the PIF in lake-terminating environments is that of retreat and thinning (Minowa et al., 2021), as these glaciers retreat proglacial lakes expand and form enhancing freshwater calving (Carrivick and Tweed, 2013; Malz et al., 2018).

A well-documented example of this is Glacier Exploradores on the NPI. Exploradores has remained in a stable state since the LIA, having only retreated 100 m to 200 m from its LIA moraine (Aniya et al., 2007). However, termini disintegration coupled with the expansion of proglacial lakes on the east and west margins of the glacier indicate this could soon change (Irarrazaval et al., 2022; Wilson et al., 2018). Termini disintegration has been driven by the coalescence of supraglacial ponds at the terminus, glacier down wasting and crevasse formation consequently advancing the development of a larger proglacial lake at the terminus (Irarrazaval et al., 2022). The proglacial lake on the western margin doubled in size from 0.5 km^2 to 1.1 km^2 between 2010 and 2019 – with the development of a calving front enhancing mass loss from the glacier (Irarrazaval et al., 2022). The development of a proglacial lake amplifies mass loss by introducing mechanisms such as calving and subaerial melting, increasing ice flow, and altering ice dynamics (Benn and others, 2007; Robertson et al., 2012; Sakai et al., 2009). Ergo, explaining the increase in discharge for Exploradores found within this study. It should be noted that the introduction of proglacial lakes to a glacier system often represent a “tipping point” or a decoupling from the climate which can alter a glacial landscape significantly, forcing the glacier from a slow retreat into a rapid retreat (Kirkbride, 1993; Sutherland et al., 2020). It is likely that these relationships also exist on other glaciers of the PIF where a proglacial lake has amplified surface velocity and consequently ice discharge.

In addition, not only has there been an expansion of the lake-contact margins which interact with the glaciers of the PIF, there also has been an apparent speed up of glacier surface velocity. This is evidenced by 36 out of the 43 lake-terminating glaciers which displayed an increase in discharge showing a statistically significant increase in surface velocity from 2004 to 2017 (see appendix C.1). Sakakibara and Sugiyama (2014) examined ice velocity trends for two epochs (1984 to 2000 and 2000 to 2011) finding a net accelerating trend in the first and a net decelerating trend in the second. However, this was caveated with the fact that velocity trends on the PIF were not homogenous. The findings of Sakakibara and Sugiyama (2014) at first seem to contradict the findings in this study likely due to the prominence of marine-terminating glaciers dominating the velocity signal. However, the lake-terminating glaciers which were examined in Sakakibara and Sugiyama (2014) and this study show a correlation in general, that they are accelerating.

The apparent amplification of surface velocity is likely due to a positive feedback mechanism involving lake-ice contact margins. Thermomechanical processes drive interactions at the glacier-lake contact margin (Carrivick and Tweed, 2013; Carrivick et al., 2020; Tsutaki et al., 2011). Calving draws down ice from upstream which steepens the surface slope whilst lubrication at the bed reduces basal friction (Carrivick et al., 2020). The combination of these two feedback mechanisms initiates dynamic thinning which further decreases longitudinal

stresses and amplifies flow velocity (Nishimura et al., 2013; Trüssel et al., 2013). This occurs in conjunction with surface ablation due to climatic forcing, exacerbating dynamic changes to glacier dynamics even further.

The thermomechanical processes driving these interactions have been investigated in Patagonia with research focussing on proglacial lake temperature providing important insights into frontal ablation. As mentioned previously at marine-terminating glaciers fjord circulation, ocean-fjord connectivity and fjord stratigraphy can play a key role in determining calving flux from a marine-terminating glacier (Jackson et al., 2014; Sciascia et al., 2013; Xu et al., 2013). These subsequent investigations highlighted that subaqueous melting plays a key role in frontal ablation suggesting that calving is not the main catalyst. The processes surrounding subaqueous melting at a marine-terminating glacier are relatively well understood however at lake-terminating glaciers this is not the case.

In Patagonia, Sugiyama et al., (2016) examined the calving fronts of Perito Moreno, Upsala and Viedma for insights into the behaviour of ice-contact proglacial lakes. Observations show that wind-driven circulation dominated heat convection down to a depth of ~ 180 m whilst below this depth cold glacier water is abundant (Sugiyama et al., 2016). The turbid glacial discharge has a higher density than the warmer water at the surface, creating well stratified layers and nullifying the impact of buoyant plumes on heat transfer (Sugiyama et al., 2016). Thus, implying a different subaqueous melting mechanism is in force at lake-terminating glaciers in Patagonia compared to marine-terminating glaciers. In addition, it appears that proglacial lake stratification in Patagonia is heavily influenced by an external force (i.e., wind) and therefore any future change in wind patterns could impact glacier-lake interaction through the amplification of wind driven heat convection.

Patagonian climate is dominated by the Southern Annular Mode (SAM) and El-Niño Southern Oscillation (ENSO) (Swart and Fyfe, 2012). The precipitation and temperature trends of Patagonia are controlled by westerlies which in turn are mediated by the SAM and ENSO (Garreaud et al., 2009; Gillet et al., 2006). Marshall (2003) has indicated that changes in the positive phase of the SAM shifting southward has created a windier environment in southern South America. As changes are predicted for both the SAM and ENSO due to human-induced climate forcing this “windier” environment may be exacerbated (Jones et al., 2016). Therefore, conceptually a “windier” environment driven by changes in the SAM and ENSO could have further implications on proglacial lakes in Patagonia and ultimately calving rates of lake-terminating glaciers.

Minowa et al., (2021) categorises lake-terminating glaciers on the SPI as having lower F-fractions than marine-terminating glaciers and smaller AARs, leading to surface mass balance

losses at a greater rate across larger ablation areas. This study found a general increase in ice discharge at lake-terminating boundaries through time likely due to the expansion of lake-ice contact margins and an apparent increase in ice velocity at the termini (Wilson et al., 2018). However, yet to be considered in this discussion is the impact of surface melt on surface velocity. Temperatures across the PIF have risen across the 20th century but temperature trends in recent decades have been weak (Garreaud et al., 2009; Rasmussen et al., 2007; Rosenblüth et al., 1997). Correlations have been found between air surface temperature and surface velocities on Perito Moreno glacier on the SPI (Minowa et al., 2017; Sugiyama et al., 2011). Thus, suggesting that meltwater percolating into the subglacial hydrology, manipulates basal water pressure at this glacier, increasing basal sliding and overall surface velocity (Bravo et al., 2021). This is an important relationship as we know lake-terminating glaciers have experienced extreme thinning on the SPI often outweighing the losses via frontal ablation (Weidemann et al., 2018). This thinning can be attributed to a combination of dynamically controlled processes but also their susceptibility to climate forcing and therefore production of meltwater and speed up in surface velocity.

Even though marine-terminating glaciers have larger F-fractions than lake-terminating glaciers, their rates of ice discharge in terms of the largest glaciers are equivalent (2004 San Quintin (lake) = 4.21 Gt yr^{-1}, 2004 Jorge Montt (marine) = 4.14 Gt yr^{-1}). In essence, marine-terminating glaciers are generally dominated by frontal ablation, but lake-terminating glaciers are controlled by surface ablation and frontal ablation. The equivalency in ice discharge found in the larger glaciers comes from the large lake-terminating glaciers such as Upsala where there is evidence of dynamic control overbearing climatic control and decoupling the glacier from climate via cycles of recession and advancement (Skvarca et al., 2003). Furthermore, this contradicts the traditional view that marine-terminating glaciers calve at an order of magnitude higher than lake-terminating glaciers (Warren and Kirkbride, 2003). However, the median ice discharge values of marine-terminating glaciers in 2004 (0.13 Gt yr^{-1}) and 2017 (0.17 Gt yr^{-1}) are greater than the median ice discharge values of lake-terminating values in 2004 (0.025 Gt yr^{-1}) and 2017 (0.049 Gt yr^{-1}). Therefore, indicating that in general the relationship does exist on the PIF where marine-terminating glaciers calve at an order of magnitude higher than lake-terminating glaciers (Warren and Kirkbride, 2003). Further highlighting the complex array of factors which need to be considered when analysing trends in frontal discharge in both marine and lake-terminating environments.

San Quintin Glacier juxtaposes the general increasing trend found in lake-terminating glaciers with a reduction of 1.93 Gt yr^{-1} from 2004 to 2017. Between 1986 and 2019 San Quintin Glacier retreated 5 km, its piedmont lobe collapsed, and the calving front became much more “compact” (Pętlicki et al., 2023). A detachment from the terminal moraine and consequent

development of a proglacial lake since 1986 has led to the disintegration of the piedmont lobe, promoting thinning and surface acceleration (Pętlicki et al., 2023). Trends observed within the data used in this study. However, even though surface velocity has generally increased from 2004 to 2017 the collapse and compaction of the piedmont lobe has greatly reduced the calving front of San Quintin Glacier. This reduces the glacier-lake contact margin and ice discharge fluxes through the termini. In addition, for context San Quintin Glacier has the highest ice discharge value for 2017 for the entire PIF even though its flux has halved. This indicates that the rapid disintegration of San Quintin Glacier is still occurring, and further research should be undertaken to assess what this may mean for the future of the NPI.

5.2.3 Glaciers Whose Termini Transition from one Environment to Another

Within this discussion the development of proglacial lakes has been used as a tangible reason for the amplification of ice discharge at termini boundaries in lake-terminating glaciers (e.g., Exploradores Glacier on the NPI). An ongoing trend in high-mountain glaciated areas is the development of proglacial lakes in recent decades, exemplified by a ~ 50 % increase in lake volume and ~ 50 % increase in frequency from 1990 to 2018 (Shugar et al., 2020), thus increasing the opportunities for glaciers to become lake-terminating. For example, Watson et al., (2020) discover an increase in glacier surface velocity at the terminus of the Lower Barun glacier coinciding with the formation of a proglacial lake. The associated speed up in velocity is driven by the introduction of a calving front, which consequently lubricates the bed, drawing ice down from up-glacier whilst accelerating thinning (Tsutaki et al., 2011). The associated increase in the multitude and magnitude of proglacial lakes according to Shugar et al., (2020) should increase mass loss from lake-terminating glaciers globally.

However, the relationship between lake-terminating glaciers and proglacial lakes is not one dimensional and several factors need to be considered. The interaction between glaciers and proglacial lakes can be manipulated by water depth and temperature, debris cover, air temperature, solar insolation, lake fluctuation and circulation patterns and the surface velocity and ice thickness at the calving front (Benn and others, 2007; Sakai et al., 2009; Watson et al., 2020). This study only considers velocity and thickness changes, indicating that for a true representation of the calving regime in transitional environments all the above must be considered. In Patagonia, research has been done on lake circulation, temperature, and depth properties (Haresign and Warren, 2005; Sugiyama et al., 2016), lake fluctuation trends (Pasquini et al., 2008), ice surface velocity (Sakakibara et al., 2014; Mouginot and Rignot, 2015) and debris cover (Glasser et al., 2016). However, these studies either focus on case

studies or the larger lake-terminating glaciers of the PIF. Thus, making assumptions for the smaller peripheral glaciers where most of these transitional environments exist difficult.

On the other hand, in environments where glaciers are detaching themselves from proglacial lakes the dynamics are poorly understood as this is the antithesis of the general worldwide trend. Therefore, there is almost no scientific literature which explains the behaviour of glaciers as they detach from proglacial lakes. We assume that the opposite occurs compared to what happens when a glacier connects with a proglacial lake. For example, the retraction of a calving front results in limited drawdown of ice from up glacier consequently resulting in the slowdown of surface velocity. Examples of glacier-lake detachment have been observed in the Bolivian Andes, Karakoram, and Austrian Alps (Cook et al., 2016; Emmer et al., 2015; Gardelle et al., 2011). Reasons forcing these detachments vary from surging glaciers, mass loss deceleration, sedimentation, changing subglacial hydrology and recession past any previous erosional maximum (Cook et al., 2016; Emmer et al., 2015; Gardelle et al., 2011).

These transitional environments appear to exist on the PIF according to this study. In total, glaciers whose termini transition from one environment to another account for ~ 15 % of glaciers on the PIF (see section 4.2; Figure 14a). Land to lake shifts equate to ~ 12 % of the total glaciers on the PIF compared to lake to land shifts which equate to ~ 3 %. It should also be noted that the delineations of these ‘transitions’ are reliant on the proglacial lake database used from Shugar et al., (2020) – where some glacial lakes could be missed due to low resolution satellite imagery. Therefore, the delineations made in this study are taken as a best estimate of which glaciers are detaching or harbouring proglacial lakes.

Patagonia much like the global trend has observed an increase in the multitude and magnitude of proglacial lakes between 1986 and 2016 (Wilson et al., 2018). The transitions delineated however are all found on the periphery of the PIF with a negligible impact on total discharge (~ 2 % of 2004 total and ~ 3 % of 2017 total). The small nature of these glaciers in terms of ice discharge and area hinders a robust mass loss acceleration or deceleration signal dependent on which way the glacier environment has transitioned. Furthermore, the added factors which must be considered when analysing lake-terminating glacier discharge will also impact any signals found within the data. Thus, likely explaining the sporadic nature of % change in discharge found in this study for transitional environments (Land-lake % change median = 142.3 %, Lake-land % change median = 2396.9 %) (see section 4.2; Figure 14b).

Therefore, this study finds commonalities with Wilson et al., (2018) that lakes have expanded in Patagonia in recent history. This expansion in part explains the transition of numerous glaciers on the PIF from land-terminating to lake-terminating, where proglacial lakes have developed in glacial overdeepenings moulded by LIA maximums (Wilson et al., 2018; Davies

and Glasser, 2012). This is a relationship outlined by Truffer and Motyka (2016) where the presence of glacial overdeepenings in formation and expansion is expected to continue; however, glacier decoupling and insufficient space in glacial overdeepenings could cause expansion and formation to stagnate or even decrease (Shugar et al., 2020). We know these environments exist on the PIF and further research should focus on determining the small-scale mechanisms that accommodate these changes.

5.3 Patagonian Icefield: Sea Level Rise Contribution

5.3.1 Global Marine-terminating Environment Mass Trend

Overall, between 2010 and 2020, Jakob and Gourmelen (2023) calculated a mean global glacier mass loss of 272 ± 11 Gt yr^{-1}. Frontal ablation was attributed to account for 28 ± 2 % of this total when corrected through the removal of land-terminating glaciers whilst atmospheric forcing dominates global mean mass loss (72 ± 5 %) (Jakob and Gourmelen, 2023). Jakob and Gourmelen (2023) provided a frontal ablation estimate of 13.3 ± 1.3 Gt yr^{-1} for the Southern Andes equating to ~ 46 % of the global frontal ablation between 2010 and 2020. Using the estimate made in this study for 2017 ~ 86 % of the global frontal ablation between 2010 and 2020 can be attributed to the PIF. The differences are likely driven by uncertainties within the datasets used in this study and the different methods used to obtain frontal discharge estimates (see section 5.1.1). However, the mass lost through frontal ablation in the PIF is the highest in the world outside of the ice sheets (Jakob and Gourmelen, 2023).

Outside of the Greenland Ice Sheet, Southern Andes, Svalbard, Antarctic Periphery, and the Russian Arctic mass loss in glaciated areas is dominated by atmospheric forcing (Huss and Hock, 2015; Kochtitzky et al., 2022). These regions which negate the domination of atmospheric forcing have high concentrations of marine-terminating glaciers which are dynamically active. This dynamicity is reinforced by proportional glacial volume losses of 66 % (Greenland Ice Sheet), 61 ± 8 % (Southern Andes), 38 ± 5 % (Svalbard), 51 % (Antarctic Periphery) and 77 ± 9 % (Russian Arctic) to frontal ablation (Gardner et al., 2018; Jakob and Gourmelen, 2023; Mouginot et al., 2019). Focussing on regions with a high concentration of marine-terminating glaciers various patterns emerge within ice discharge trends over the last 20 years. Calculating ice discharge through marine-terminating environments is important because of the direct influence on sea level estimates, the disturbance of marine ecosystems and the implications of resolving the components of mass loss underpinning glacial change (Huss and Hock, 2015; Kochtitzky et al., 2022). Figure 21 indicates that 54 % of the regions

displayed below show a negative trend in rates of ice discharge. When removing the Antarctic regions this increases to 70 %, indicating that most regions dominated by marine-terminating glaciers are undergoing a reduction in rates of ice discharge. The only outliers in the Northern Hemisphere are Novaya Zemyla, Severnaya Zemyla and Svalbard and Jan Mayen.

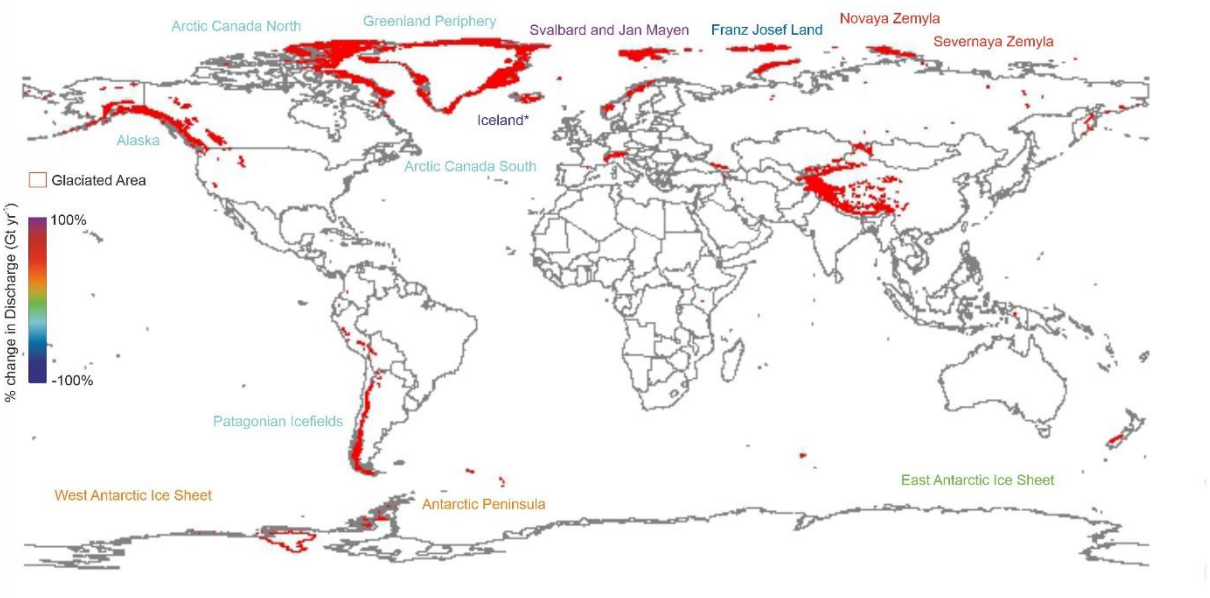

Figure 21 - Global map with glaciated areas outlined. The colours of the region titles correlate with marine-terminating glacier discharge % change between 2000 and 2020 taken from Kochtitzky et al., (2022) and Gardner et al., (2018), with the Patagonian icefields data taken from this study. *Iceland has only one marine-terminating glacier.

There is a significant variability in trends associated with marine-terminating glaciers on a global scale (Figure 21). For example, in regions where there is an increase in marine-terminating ice discharge a strong ocean connectivity is observed as the ‘Atlantification’ of the Barants and Kara Sea has been linked to increases frontal ablation in the Russian Arctic (Barton et al., 2018; Polyakov et al., 2017), whilst changing ocean circulations and warming of the Antarctic deep water current has accelerated mass loss on the Antarctic peninsula (Dutrieux et al., 2014; Jacobs et al., 2013). On the other hand, McNabb and Hock (2014) indicates a reduction in regional marine-terminating discharge in Alaska between 1985 and 2013, driven by a depletion in mass resource due to retreating and therefore failing to sustain levels of frontal ablation. This pattern was also observed in Greenland where 200 glaciers examined by Moon et al., (2012) slowed between 2000 and 2010 due to a loss of resistive stress and lowering of the surface slope. The highlighted variability shows the complexity of marine-terminating environments and indicates that alongside regional heterogeneity in ice discharge trends from marine-terminating environments there is also global heterogeneity.

5.3.2 Global Estimates of Eustatic Sea Level Rise

Marine-terminating environments globally therefore indicate contrasting trends in recent decades. Understanding the ongoing trends in these marine-terminating environments is important because projections indicate that widespread glacier retreat is inevitable due to ongoing anthropogenic forcing resulting in direct contributions to eustatic sea level rise (Huss and Hock, 2015; Marzeion et al., 2012). Several applied global glacier models exist aiming to quantify future global glacier mass loss and consequent contribution to sea level rise (Bliss et al., 2014; Hirabayashi et al., 2013; Marzeion et al., 2012; Radić and Hock, 2011; Radić et al., 2014).

Huss and Hock (2015) explain that these “highly simplified” models depend heavily on volume-area or volume-length scaling relations inadequately representing geometric adjustments, thinning and glacier dynamics (Huss and Hock, 2015). In addition, none of the previously mentioned models include frontal ablation in their projections which is problematic since approximately 30 % of the global glaciated area flows directly into the ocean (Gardner et al., 2013). Recent studies such as Huss and Hock (2015), Rounce et al., (2023) and Zemp et al., (2019) have managed to introduce frontal ablation estimates into mass loss projections and sea level rise estimations. This advancement has improved the accuracy of projections and estimates of mass loss. This is important because analysis has indicated that previous evaluations cannot match ice-mass loss, thermal expansion, and the storage of water on land to observed sea level rise, indicating that some of these factors are poorly quantified (Frederikse et al., 2020).

Church et al., (2013) suggests that mass losses from land-ice command uncertainty surrounding sea level rise estimates. The IPCC AR6 report however reports that although there remains uncertainty in the sea level budget, there is currently a closer agreement between observed mean sea level rise and the quantified processes (i.e., glacier mass loss) than in previous IPCC assessments (Church et al., 2013; Fox-Kemper et al., 2021; Oppenheimer et al., 2019). Regional frontal ablation estimates provide important insights into trends and patterns which are occurring in marine-terminating environments thus enabling for more accurate estimates on mass loss patterns and consequent sea level rise (Frederikse et al., 2020; Rounce et al., 2023). For example, the insights derived from Minowa et al., (2021) and this study on ice discharge patterns on the PIF will provide a platform for future projections of Patagonian contribution to sea level rise. Rounce et al., (2023) used near global frontal ablation estimates from Kochtitzky et al., (2022), Minowa et al., (2021), Osmanoğlu et al., (2013) and Osmanoglu et al., (2014), to force their projections. Hence, frontal ablation

estimates are clearly an important factor for considering projections of global sea level rise from glacier mass loss.

The variety of methods used to calculate glacier mass loss on a global scale make estimates difficult to compare directly. However, estimates generally agree that since the turn of the millennium anywhere between 150 and 400 Gt yr^{-1} of ice has been lost equating to ~ 0.4 mm yr^{-1} and ~ 1 mm yr^{-1} of sea level rise (Gardner et al., 2013; Hugonnet et al., 2021; Jacob et al., 2012; Marzeion et al., 2017; Wouters et al., 2019; Zemp et al., 2019). In the period spanning 2003 to 2009 Gardner et al., (2013) and Zemp et al., (2019) found that ~ 30 % of observed sea level rise originated from glaciers outside of the major ice sheets. Using the frontal discharge estimates calculated in this study we demonstrate that the PIF contributed 16 %, 11 %, 12 %, 7 % and 9 % to global sea level rise from glaciers outside of the major ice sheets in the time spanning 2000 to 2019 depending on which estimate of global glacier mass loss is used (Gardner et al., 2013; Hugonnet et al., 2021; Jacob et al., 2012; Wouters et al., 2019; Zemp et al., 2019). Furthermore, each of the global estimates provide a regional breakdown of where mass is lost; we find a strong agreement with the regional mass loss estimates for the Southern Andes from the global estimates compared to this study (Gardner et al., 2013 = 13 % of contribution, Hugonnet et al., 2021 = 8 % of contribution, Jacob et al., 2012 = 16 % of contribution, Wouters et al., 2019 = 15 % of contribution, Zemp et al., 2019 = 10 % of contribution). The PIF dominates mass loss in the Southern Andes, so it is a reasonable comparison to make (Wouters et al., 2019). However, it should be noted that the frontal discharge estimate does not account for subaerial melting at the calving front and is therefore likely an underestimation of the true volume of water reaching the ocean (Hock et al., 2019).

Gregory and Oerlemans (1998), Leclercq et al., (2011) and Zuo and Oerlemans (1997) estimated that glacier contributions to global sea level rise equated to somewhere between 0.15 and 0.4 mm yr^{-1} from 1800 to 2000. These estimates come with a significant level of uncertainty but when compared to the estimates post 2000, they are certainly lower. This suggests that glacier contribution to sea level rise has amplified past 2000.

Furthermore, there also exists several studies that estimate global glacier mass loss into the future in conjunction with the various warming targets set within the Paris Agreement (Rounce et al., 2023). Rounce et al., (2023) predicts that glaciers are set to lose ~ 25 % to ~ 40 % of their mass by 2100 equating to 90 and 154 mm of sea level rise (0.7 to 2.23 mm yr^{-1}). For high emission scenarios (+ 4°C) there are continuous losses through until 2100 however the + 1.5°C scenario indicates a slowdown of mass loss past 2035 (Rounce et al., 2023). These patterns are also found within Edwards et al., (2021) and Marzeion et al., (2020) who find equivalent losses to Rounce et al., (2023) throughout the next century. For example, in

simulations ran by Edwards et al., (2021) for the + 1.5°C warming scenario glacier mass loss almost halved compared to the higher warming scenarios. By holistically analysing global glacier mass loss estimates from 1800 to 2100 a clear increase in contribution to global sea level rise is observed.

5.4 Wider implications

This study has quantified and analysed trends in ice discharge emanating from the PIF across two different time periods. Thus, giving an indication of the mass loss from the icefield, the transition of termini environments and sea level equivalent contributions. These factors consequently influence the surrounding environment of the PIF and must be considered when discussing the results of this research. A highly dynamic icefield where the continuation of significant mass loss is observed will have wider implications on its surrounding environment. Some of these implications include Glacial Lake Outburst Floods (GLOFs), the influence of meltwater on downstream ecology and hydrology, hydropower, and human impacts such as water resource dependency and tourism.

Ongoing mass loss in Patagonia has forced the frequency and formation of proglacial lakes to increase (Shugar et al., 2020; Wilson et al., 2018). This is inextricably linked to the possibility of amplifications in the number of GLOFs in the 21st century, which is likely to be a prominent feature in Patagonia as it is experiencing lake formation at some of the highest rates globally (Harrison et al., 2018; Shugar et al., 2020; Wilson et al., 2018). The instantaneous release of large volumes of water has potential serious impacts on infrastructure and communities downstream, exemplified by over 12,000 deaths globally being attributed to GLOFs in the last century (Carrivick and Tweed, 2016). Iribarren et al., (2014) analysed trends in historic GLOFs in the Baker region of Patagonia and summarised that proglacial lakes in contact with glaciers and that have a steep dam outlet slope (> 8°) are more likely to fail. This was exemplified in summer 2020 when Lago Greve (proglacial lake in contact with Greve Glacier) underwent “one of the largest GLOFs in the satellite era” resulting in an estimated discharge of 3.7 ± 0.2 km^3 (Hata et al., 2021). Thus, indicating that GLOFs directly associated to the PIF are a serious possibility and have the potential to be some of the largest observed globally. In addition, not only do GLOFs have the potential to cause significant damage and harm they also alter the physical and biological characteristics of downstream hydrology in Patagonia (Meerhoff et al., 2019).

Turbid glacier fed lake systems where nutrient rich meltwater dominates often have simplified food webs and lower biodiversity by proxy whereas clear and warmer disconnected glacier

lakes tend to have more complex food webs and higher biodiversity (Sommaruga, 2015; Tiberti et al., 2020). This indicates that some of the transitional environments on the PIF where glaciers have detached from their lakes may be undergoing similar changes in biodiversity. However, it is important to notice that it is difficult to quantify direct changes in biodiversity in these remote locations (Tiberti et al., 2020). Furthermore, as explained above glacial discharge and retreat can have a strong influence on biodiversity in the lakes, they are associated with but there are also teleconnections with fjord ecoystems, fjord circulation and river hydrological characteristics. These teleconnections are observed in the Baker River where an influx of freshwater from a GLOF increased discharge by 3-5 times the norm and altered the sediment load carrying capacity and sediment concentration significantly (Bastianon et al., 2012). This is the same catchment in which Meerhoff et al., (2019) also observed a change in hydrographic and biological characteristics of the fjord system connected to the Baker River. Thereby, introducing a cascading effect due to an influx of glacier meltwater on downstream hydrological and biological characteristics. Modelled reconstructions of glacial lake drainage stemming from PIF deglaciation (between 13 and 8 kyr ago) by Glasser et al., (2016) imply that an influx of freshwater from glacial lake drainage altered salinity characteristics in near coastal east Pacific zones. Thus, resulting in changes to thermohaline circulation in the near coastal zones and modifying regional climate (Glasser et al., 2016). Glacial meltwater drainage and influx from GLOFs has significant capabilities to modify the environment in which it drains into. Thus, promoting the importance of characterising trends in mass loss emanating from the icefields.

As well as impacts on the natural environment the PIF has strong links and impacts to the human environment as well. Immerzeel et al., (2020) indicates that ~ 1.9 billion people are reliant on “water towers” originating from mountainous areas. In the context of the PIF, Immerzeel et al., (2020) denotes that the Patagonian Andes are a key “water tower” for the surrounding area but dependence is difficult to predict in the future. The dependence of the local communities to the water provided by the PIF is exemplified by the cancellation of the HIDROAYSEN hydropower project in the river Baker catchment (Ponce et al., 2011). A 5-dam project was proposed which would flood 36 km^2 of the river Baker catchment, flooding important tourism locations but also altering the hydrology of the catchment significantly (Ponce et al., 2011). Even though this project was blocked by the Chilean government it demonstrated how largescale hydropower projects connected to glacially fed rivers could impact local communities (Hernando-Arrese and Tironi, 2019). With the projection of ‘peak water’ to be reached in 2035 in many glacial catchments such as high-mountain Asia the exploration of possible hydropower projects in these regions is likely to continue (Rowan et al., 2017; Soncini et al., 2016).

5.5 Limitations

5.5.1 Ice Surface Velocity and Thickness Estimation Inaccuracies

The velocity dataset used for ice discharge calculations in 2017 was developed by Millan et al., (2019) who found good agreement between in-situ GPS velocity measurements and surface velocities obtained from the time-averaged velocity mosaic the study had produced, comparing results in the French Alps, Cordillera Blanca and Southern Alps in New Zealand. However, it should be noted that during this comparison several limitations with the velocity mosaic were found. Glaciers with widths less than 250 m are not well captured in the processing chain; although, this has a minimal impact on this study since approximately 2 % of the glaciers on the PIF have a width less than 250 m (Millan et al., 2019).

In addition, the sensors used (Landsat, Venμs and Sentinel) struggled to capture velocity changes for glaciers with annual velocities below 200 m/yr due to their resolution (Millan et al., 2019). Therefore, this inability to capture velocity changes on the slower moving glaciers could have a reasonable impact on this study because outside of the major outlet glaciers, a lot of the periphery glaciers on the PIF fall below this threshold. Consequently, exemplified by ~ 40 % of the glaciers on the SPI and ~ 75 % on the NPI failing to reach this threshold. On the other hand, even though the resolution of the sensors may not capture the slower flowing glaciers, Millan et al., (2019) indicated that the sensors used are “perfectly suited” to capturing glaciers with velocities greater than 500 m/yr. This is entirely compatible with the PIF as ~ 30 % of the glaciers reach speeds of greater than 500 m/yr at their termini and is a notion that is also supported by Mouginot and Rignot (2015) who use a similar set of sensors for their velocity analysis of the icefields, the 2004 velocity dataset which is used in this study.

Approximations are made for ice surface velocity estimates when multiple look angles for individual glaciers are not available. The alignment of ice flow being parallel at the equilibrium line altitude when the glacier is in a steady state is consequently used (Joughin et al., 1998; Mouginot and Rignot, 2015; Nye, 1952). These assumptions are made when we use the velocity mosaics provided by Millan et al., (2022) and Mouginot and Rignot (2015). Furthermore, the nature of analysing a singular snapshot of velocity should be considered in the sense that it may not capture the entire story of velocity changes on the icefields, with marine-terminating boundaries being a key example due to their significant annual mass turnover (Warren and Kirkbride, 1993; Glasser et al., 2011).

The challenges surrounding modelling marine-terminating glaciers continues when we examine ice thickness estimates which becomes important because ~ 20 % of the glaciers on the PIF are marine-terminating. The SIA which Millan et al., (2022) uses to estimate ice thickness is heavily dependent on surface slope and surface flow velocity (Pattyn, 2012). Minowa et al., (2021) and Mouginot and Rignot (2015) both analyse velocity trends on the icefields and indicate that a much larger portion than previously realised is dominated by sliding over the bed as a flow mechanism. The SIA focusses on the relationship of vertical shear stress and ice thickness. Therefore, in environments where basal sliding is prominent, the SIA struggles to accurately capture ice thickness (Millan et al., 2022). In addition, for glaciers such as marine-terminating glaciers where the ratio between surface slope and surface velocity is heavily biased towards velocity, overestimations exist (Blatter et al., 2011; Millan et al., 2022). Furthermore, SIA models are approximations that rely on simplifications of the Full-stokes equations which can accurately capture ice dynamics. However, due to the simplifications of the SIA, they struggle to model dynamic ice behaviour including fast ice streams and ice margins (Hutter, 1983; Gudmundsson, 2003).

Therefore, it is important to realise that the use of SIA ice thickness estimates for analysis on the PIF should be used with caution. However, suitable alternatives such as models which use the Full-stokes equations are computationally expensive and not readily available or like Millan's thickness estimations encounter similar problems in terms of approximations and struggling to accurately depict highly dynamic icefields. For example, Farinotti et al., (2019) published a global ice thickness estimate dataset which used an ensemble of different models. These include models developed by Frey et al., (2014), Fürst et al., (2017), Huss and Farinotti (2012), Maussion et al., (2018) and Ramsankaran et al., (2018). Each of these models either uses inversions of the basal shear stress equation, the shallow ice approximation model or volume-area scaling methods to delineate ice thickness, having the same fundamental limitations as the SIA.

5.5.2 Flux Gate Placement and Discharge Calculation Assumptions

The flux gate approach and subsequent calculation of discharge requires several assumptions due to the lack of sufficient in-situ observations, the basic physics involved within the calculation and the extensive spatial detail required. Some of these assumptions are summarised by McNabb and Hock (2014) and constitute of assumptions surrounding ice thickness, terminus fluctuations, surface mass balance and seasonal velocity oscillations. For example, a study that assumes a constant mean ice thickness across the flux gate, neglects the shape of the bed profile. McNabb and Hock (2014) found that on average the discharge flux was underestimated by 27 % when neglecting the bed profile. However, this assumption is negated in this study as the thickness is taken from each flux gate segment and not averaged across the flux gate (Figure 22).

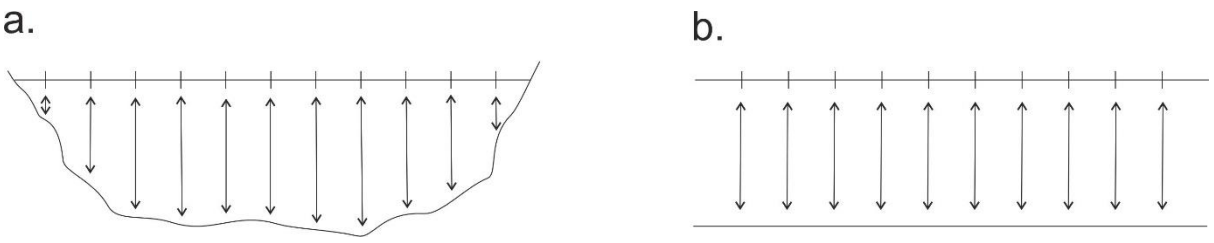

Figure 22 - Diagrams showing the difference between mean thickness assumption and sampling multiple thicknesses. (a) depicts the method used in this study where ice thickness is taken at each flux gate segment. (b) depicts a method which uses a mean ice thickness measurement across the flux gate, ignoring the shape of the bed.

Variations in glacier advance and retreat can impact discharge calculations, where ignoring rapidly retreating glaciers can lead to overestimations of frontal ablation (McNabb and Hock, 2014; Rignot et al., 2008). Glaciers, especially marine-terminating ones, that have no significant length change are well represented by flux calculations that neglect glacier advance or retreat. This is because rates of ice discharge are well represented by ice supply to the terminus (Post et al., 2011). In Patagonia, both icefields are retreating at a steady rate proportional to their area (Malz et al., 2018). However, especially on the SPI, some marine-terminating glaciers such as Jorge Montt and HPS-12 have retreated over 6 km since 1984 (Sakakibara and Sugiyama, 2014). In essence, both icefields have a mix of rapidly retreating and steady-state glaciers, so the impact of neglecting glacier length change on ice discharge calculations is difficult to delineate.

By excluding surface mass balance estimates from ice discharge calculations, ice flux could be overestimated (McNabb and Hock, 2014; O'Neel et al., 2003). This factor impacting ice discharge calculations is dependent on the distance between the flux gate and the terminus,

where the greater the distance increases the likelihood of surface mass balance impacting discharge calculations (McNabb and Hock, 2014). A 6 km^2 average distance between flux gate and termini was observed in McNabb and Hock (2014), which led to a 10 % regional overestimation of frontal ablation. The systematic approach used in this study sets flux gates at 500 m from the termini (unless manually derived), a significantly smaller distance than in the McNabb and Hock (2014) study. Therefore, the impact of surface mass balance fluxes is likely to be negligible on discharge calculations within this study, although, having flux gates close to the termini can influence discharge estimations due to bed thickness errors at the margin (Mankoff et al., 2020; Wood et al., 2018). Mankoff et al., (2020) tested this hypothesis, finding that discharge estimates along a transect stretching from the glacier termini to 10 km upstream tended to decrease as you moved towards the termini.

Seasonal velocity variations are the final parameter that needs to be discussed when calculating ice discharge estimates using flux gates. This is highlighted by Mouginot and Rignot (2015) who warn that “care should be exercised” when using the 2004 composite velocity mosaic because of temporal seasonal changes in velocity (Mouginot and Rignot, 2015, p. 2). Further developing this point, glaciers such as Jorge Montt and Pio Xi exhibit seasonal velocity fluctuations ranging between 200 m/yr and 400 m/yr peaking in October/November (Mouginot and Rignot, 2015). On the other hand, O’Higgins glacier exhibits seasonal velocity fluctuations of ~ 3 % mean annual speed (Mouginot and Rignot, 2015). All the previously mentioned glaciers are major outlet glaciers of the SPI, yet the variation in seasonal velocity fluctuations indicate that there are significant differences in peak seasonal velocities. McNabb and Hock (2014) found that using seasonal velocities in Alaska to calculate ice discharge led to overestimations of 1 %, 6 %, 8 % and 14 %. Due to the complex pattern of seasonal velocity variations on the PIF, the best approach would be to partition and treat each glacier on a case-by-case basis to calculate peak discharge. However, the feasibility of obtaining accurate velocity estimates for each season for the delineation of peak velocity is non-existent. Therefore, the use of a holistic velocity mosaic is the only viable approach.

A complex array of factors can be included when calculating ice discharge through a flux gate. Most of these factors require a granularity of data which is simply not available for the entirety of the NPI and SPI. For example, surface mass balance grids in a 10 km and 5 km resolution for the NPI and SPI exist and have been statistically downscaled to a smaller resolution, but the compounded uncertainty involved would impact discharge estimates negatively (Bravo et al., 2021; Schaefer et al., 2013; Schaefer et al., 2015). Studies such as McNabb and Hock (2014) and O’Neel et al., (2003) include the extra variables because of the limited spatial and temporal coverage evident in their study region. The methods used in this study are robust

and have consistently been used within the scientific literature in studies such as Carrivick et al., (2022), Enderlin et al., (2014), Gardner et al., (2018), King et al., (2018) and Osmanoğlu et al., (2013). Therefore, although some contributing factors are missing from the discharge calculations, the most appropriate and accurate methodology was used for this scenario.

5.5.3 Limitations Synthesis

The key limitations of this study involve the use of global datasets estimating ice velocity and thickness (Millan et al., 2022) to calculate ice discharge. Prominent factors influencing these global datasets include sensor limitations, compatibility with the PIF, assumptions in ice flow, overestimation of ice thickness in certain scenarios and Sheer Ice Approximation (SIA) thickness estimate downfalls. Furthermore, limitations involving the flux gate methodology to calculate ice discharge involves several assumptions which are made due to a lack of in-situ data on a regional scale. A few glacier characteristics are ignored in this study such as surface mass balance processes, glacier advance/retreat and seasonal velocity variations. Although, these limitations do exist the methodology used in this study has been used previously in the scientific literature and provides a robust estimate of mass loss on the PIF. This is confirmed by the apparent agreement between the total mass loss from the PIF found in this study for both time periods compared to geodetic estimates found in the scientific literature.

6.0 Conclusion

This study aimed to address the following research question “How has the volume of ice being discharged through Patagonian glacier outlets changed in two separate periods 2004 and 2017?”. The research question was answered by creating flux gates for 124 glaciers on the Patagonian Icefields for two time periods (2004 and 2017) and calculating ice discharge at each glacier. This enabled a spatial analysis comparing the Northern Patagonian Icefield and the Southern Patagonian Icefield as well as icefield wide comparisons (e.g., East vs West). Furthermore, temporal analysis was also performed, comparing a period equivalent to 2004 and a period equivalent to 2017. In addition, glaciers whose termini transitioned from one environment to another (i.e., from land-terminating to lake-terminating or vice versa) were identified and any associated change in ice discharge was quantified. By adhering to the research objectives set, the following key findings based on ice discharge estimates were identified for the 124 outlet glaciers used in this study.

A negligible decrease in ice discharge was observed on the PIF comparing 2004 to 2017 (2.5 % decrease). The NPI underwent an overall decreasing trend from 7.06 Gt yr^{-1} in 2004 compared to 5.03 ± 1.5 Gt yr^{-1} in 2017 whereas the SPI observed a net increase in discharge when comparing 2004 to 2017 (2004 = 17.52 Gt yr^{-1}, 2017 = 18.92 ± 5.67 Gt yr^{-1}). Marine-terminating environments dominate ice discharge contributions on the PIF in 2004 (13.84 Gt yr^{-1} or 56 %) but in 2017 there is an apparent shift towards equilibrium where lake-terminating glaciers match the contribution of marine-terminating glaciers to total ice discharge (2017 Lake = 10.97 ± 3.29 Gt yr^{-1}, 2017 Marine = 8.19 ± 2.46 Gt yr^{-1}). Spatially, on both icefields most of the estimated ice discharge passes through the western margins (2004 = 62.7 %, 2017 = 65.5 %) in both time periods which coincides with a clear contrast in termini environments with the west being dominated by marine-terminating environments and the east being dominated by lake-terminating environments. This is reinforced by the fact that the median ice discharge values for marine-terminating glaciers (2004 = 0.13 Gt yr^{-1}, 2017 = 0.17 Gt yr^{-1}) are higher than the median ice discharge values for lake-terminating glaciers (2004 = 0.025 Gt yr^{-1}, 2017 = 0.049 Gt yr^{-1}) in 2004 and 2017. Although these general spatial trends in ice discharge do exist on the PIF it should be noted that on a glacier-by-glacier basis heterogeneous changes spatially and temporally are common. In general, glaciers whose termini environment has transitioned display a net increase in discharge, either from a lake to land terminating or vice versa. However, these results should be interpreted with caution due to these types of glaciers only comprising of 13 % of the glaciers analysed and the fact that they are small in nature and on the periphery of the icefields. The PIF contributed 0.068 mm yr^{-1} to sea level rise in 2004 compared to 0.066 mm yr^{-1} in 2017.

The findings of this study are important because highly dynamic environments like the PIF contribute significantly to global glacier mass loss outside of the major ice sheets, yet the behaviour and trends linked to frontal ablation have limited regional understanding. Therefore, this study provides a quantitative estimate of sea level equivalent contribution from the PIF based on independent estimates from the literature and widens the understanding of mass loss on the PIF in a global context. This is important because the quantification indicates that the PIF have the highest contribution from glacier mass loss to global sea level rise outside of the major ice sheets between 2000 and 2019. On a regional scale this study finds contrasting agreements in geodetic estimates from the literature and the ice discharge estimates made in this study. The NPI geodetic estimates compared to the ice discharge estimates show limited agreement whereas the SPI geodetic estimates are aligned with the ice discharge estimates. This reinforces previous findings in the literature that the NPI is more susceptible to climate forcing compared to the SPI, which is dominated by frontal ablation, as even though geodetic estimates do capture ice dynamics, they are better suited to capturing surface mass balance processes. Overall, the geodetic estimates provided for the entire PIF in the literature show remarkable agreement with this study of ± 5 %, strengthening the general understanding of mass loss on the PIF. One trend found within this study was the overall increase in discharge from lake-terminating environments on the PIF which is consequently linked to an increase in magnitude and multitude of lake-terminating environments and an apparent speed up of ice velocity. This relationship underlines the importance of monitoring proglacial lakes and their expected expansion globally and in Patagonia.

This study provided a holistic overview of ice discharge estimates for the outlet glaciers on the PIF, which has not been achieved before. Minowa et al., (2021) examined the 38 largest calving glaciers on the PIF but did not consider smaller periphery glaciers which in 2017 contributed ~ 25 % of the total ice discharge on the SPI. Thus, exemplifying the need to investigate ice discharge trends in the smaller periphery glaciers as well as the major calving glaciers. Furthermore, this study delineated the emergence of transitional environments on the PIF and quantified any associated changes in discharge. This is an important factor to consider when analysing trends in frontal ablation because the introduction or reduction of a calving front can play a key role in the dynamics of a glacial system. Therefore, as well as reinforcing the overall trends found in Minowa et al., (2021) this study provides further insight into frontal ablation trends on the PIF.

Further research however needs to be directed towards the improvement of velocity and thickness datasets in terms of their accuracy at the icefield margins. This would directly contribute to the improved accuracy of ice discharge calculation in highly dynamic environments but also enable accurate relationships to be developed between ice discharge

changes and transitional environments. In addition, as the flux gate methodology used in this study provided an agreeable mass loss estimate compared to the geodetic estimates already published this methodology can be used as a robust estimate of mass loss in highly dynamic environments such as Alaska and Greenland. Furthermore, a hybrid study using both surface mass balance modelling and ice discharge flux calculation for the PIF would be beneficial. For example, this could be based on a criterion where if a glacier is dominated by surface ablation the mass loss is estimated via geodetic estimates but if the glacier is dominated by frontal ablation, then ice flux calculations should be used to calculate mass loss. This stems from the notion that the NPI is more susceptible to climate forcing than the SPI. Finally, further research should focus on using robust frontal ablation estimates in global glacier mass loss modelling projections to reduce uncertainties surrounding the role of glaciers outside the major ice sheets in future global sea level rise.

The overall domination of frontal ablation on the PIF and it's estimated ice discharge volume cement the PIF as a crucial region in determining glacier mass loss through ice discharge estimates. The heterogeneous changes in ice discharge accompanied by a complex interplay of processes at marine-terminating and lake-terminating boundaries show that determining mass loss through these environments is essential to understand the evolution of the icefield in the future. This has implications for global sea level rise, Glacial Lake Outburst Floods, water scarcity and the livelihoods of the surrounding communities making it of upmost importance to continue to study this region.

7.0 References

Abdel Jaber, W., 2016. *Derivation of mass balance and surface velocity of glaciers by means of high resolution synthetic aperture radar: application to the Patagonian Icefields and Antarctica* (Doctoral dissertation, Technische Universität München).

Abdel Jaber, W., Rott, H., Floricioiu, D., Wuite, J. and Miranda, N., 2019. Heterogeneous spatial and temporal pattern of surface elevation change and mass balance of the Patagonian ice fields between 2000 and 2016. *The Cryosphere*, *13*(9), pp.2511-2535.

Amundson, J.M., 2016. A mass-flux perspective of the tidewater glacier cycle. *Journal of Glaciology*, *62*(231), pp.82-93.

Aniya, M., 1988. Glacier inventory for the Northern Patagonia Icefield, Chile, and variations 1944/45 to 1985/86. *Arctic and Alpine Research*, *20*(2), pp.179-187.

Aniya, M., 1995. The use of satellite and airborne imagery to inventory outlet glaciers of the Southern Patagonia Icefield, South America.

Aniya, M., 2013. Holocene glaciations of hielo patagónico (Patagonia icefield), South America: a brief review. *Geochemical Journal*, 47(2), pp.97-105.

Aniya, M., 2017. Glacier variations of Hielo Patagónico Norte, Chile, over 70 years from 1945 to 2015. *Bulletin of Glaciological Research*, *35*, pp.19-38.

Aniya, M., Enomoto, H., AOKI, T., Matsumoto, T., Skvarca, P., Barcaza, G., Suzuki, R., Sawagaki, T., Sato, N., Isenko, E. and IWASAKI, S., 2007. Glaciological and geomorphological studies at Glaciar Exploradores, Hielo Patagonico Norte, and Glaciar Perito Moreno, Hielo Patagonico Sur, South America, during, 2003-2005 (GRPP03-05). *Bulletin of Glaciological Research*, *24*, pp.95-107.

Aniya, M., Enomoto, H., AOKI, T., Matsumoto, T., Skvarca, P., Barcaza, G., Suzuki, R., Sawagaki, T., Sato, N., Isenko, E. and IWASAKI, S., 2007. Glaciological and geomorphological studies at Glaciar Exploradores, Hielo Patagonico Norte, and Glaciar Perito Moreno, Hielo Patagonico Sur, South America, during, 2003-2005 (GRPP03-05). *Bulletin of Glaciological Research*, *24*, pp.95-107.

Aniya, M., Sato, H., Naruse, R., Skvarca, P. and Casassa, G., 1997. Recent glacier variations in the Southern Patagonia icefield, South America. *Arctic and Alpine Research*, *29*(1), pp.1-12.

Bamber, J.L., Westaway, R.M., Marzeion, B. and Wouters, B., 2018. The land ice contribution to sea level during the satellite era. *Environmental Research Letters*, *13*(6), p.063008.

Barcaza, G., Nussbaumer, S.U., Tapia, G., Valdés, J., García, J.L., Videla, Y., Albornoz, A. and Arias, V., 2017. Glacier inventory and recent glacier variations in the Andes of Chile, South America. *Annals of Glaciology*, *58*(75pt2), pp.166-180.

Bartholomaus, T.C., Larsen, C.F. and O'Neel, S., 2013. Does calving matter? Evidence for significant submarine melt. *Earth and Planetary Science Letters*, *380*, pp.21-30.

Barton, B.I., Lenn, Y.D. and Lique, C., 2018. Observed Atlantification of the Barents Sea causes the Polar Front to limit the expansion of winter sea ice. *Journal of Physical Oceanography*, *48*(8), pp.1849-1866.

Bassis, J.N. and Walker, C.C., 2012. Upper and lower limits on the stability of calving glaciers from the yield strength envelope of ice. *Proceedings of the Royal Society A: Mathematical, Physical and Engineering Sciences*, *468*(2140), pp.913-931.

Bastianon, E., Bertoldi, W. and Dussaillant, A., 2012. Glacial-lake outburst flood effects on Colonia River morphology, Chilean Patagonia. In *River Flow 2012-Proceedings of the International Conference on Fluvial Hydraulics* (pp. 573-579). Taylor & Francis Group.

Benn, D.I., Åström, J.A.N., Zwinger, T., Todd, J.O.E., Nick, F.M., Cook, S., Hulton, N.R. and Luckman, A., 2017. Melt-under-cutting and buoyancy-driven calving from tidewater glaciers: new insights from discrete element and continuum model simulations. *Journal of Glaciology*, *63*(240), pp.691-702.

Benn, D.I., Warren, C.R. and Mottram, R.H., 2007. Calving processes and the dynamics of calving glaciers. *Earth-Science Reviews*, *82*(3-4), pp.143-179.

Blatter, H., Greve, R. and Abe-Ouchi, A., 2011. Present state and prospects of ice sheet and glacier modelling. *Surveys in geophysics*, *32*, pp.555-583.

Bliss, A., Hock, R. and Radić, V., 2014. Global response of glacier runoff to twenty-first century climate change. *Journal of Geophysical Research: Earth Surface*, *119*(4), pp.717-730.

Bown, F., Rivera, A., Pętlicki, M., Bravo, C., Oberreuter, J. and Moffat, C., 2019. Recent ice dynamics and mass balance of Jorge Montt Glacier, Southern Patagonia Icefield. *Journal of Glaciology*, *65*(253), pp.732-744.

Braun, M.H., Malz, P., Sommer, C., Farías-Barahona, D., Sauter, T., Casassa, G., Soruco, A., Skvarca, P. and Seehaus, T.C., 2019. Constraining glacier elevation and mass changes in South America. *Nature Climate Change*, *9*(2), pp.130-136.

Bravo, C., Bozkurt, D., Ross, A.N. and Quincey, D.J., 2021. Projected increases in surface melt and ice loss for the Northern and Southern Patagonian Icefields. *Scientific Reports*, *11*(1), p.16847.

Bravo, C., Quincey, D.J., Ross, A.N., Rivera, A., Brock, B., Miles, E. and Silva, A., 2019. Air temperature characteristics, distribution, and impact on modeled ablation for the South Patagonia Icefield. *Journal of Geophysical Research: Atmospheres*, *124*(2), pp.907-925.

Bury, J., Mark, B.G., Carey, M., Young, K.R., McKenzie, J.M., Baraer, M., French, A. and Polk, M.H., 2013. New geographies of water and climate change in Peru: Coupled natural and social transformations in the Santa River watershed. *Annals of the Association of American Geographers*, *103*(2), pp.363-374.

Carrasco, J.F., Casassa, G. and Rivera, A., 2002. Meteorological and climatological aspects of the Southern Patagonia Icefield. In *The Patagonian Icefields: A unique natural laboratory for environmental and climate change studies* (pp. 29-41). Boston, MA: Springer US.

Carrivick, J.L. and Quincey, D.J., 2014. Progressive increase in number and volume of ice-marginal lakes on the western margin of the Greenland Ice Sheet. *Global and Planetary Change*, *116*, pp.156-163.

Carrivick, J.L. and Tweed, F.S., 2013. Proglacial lakes: character, behaviour and geological importance. *Quaternary Science Reviews*, *78*, pp.34-52.

Carrivick, J.L. and Tweed, F.S., 2016. A global assessment of the societal impacts of glacier outburst floods. *Global and Planetary Change*, *144*, pp.1-16.

Carrivick, J.L., How, P., Lea, J.M., Sutherland, J.L., Grimes, M., Tweed, F.S., Cornford, S., Quincey, D.J. and Mallalieu, J., 2022. Ice-marginal proglacial lakes across Greenland: Present status and a possible future. *Geophysical Research Letters*, *49*(12), p.e2022GL099276.

Casassa, G., Rodríguez, J.L. and Loriaux, T., 2014. A new glacier inventory for the Southern Patagonia Icefield and areal changes 1986–2000. In *Global land ice measurements from space* (pp. 639-660). Berlin, Heidelberg: Springer Berlin Heidelberg.

Chauche, N., Hubbard, A., Gascard, J.C., Box, J.E., Bates, R., Koppes, M., Sole, A., Christoffersen, P. and Patton, H., 2014. Ice–ocean interaction and calving front morphology at two west Greenland tidewater outlet glaciers. *The Cryosphere*, *8*(4), pp.1457-1468.

Chen, J.L., Wilson, C.R., Tapley, B.D., Blankenship, D.D. and Ivins, E.R., 2007. Patagonia icefield melting observed by gravity recovery and climate experiment (GRACE). *Geophysical Research Letters*, *34*(22).

Church, J.A., P.U. Clark, A. Cazenave, J.M. Gregory, S. Jevrejeva, A. Levermann, M.A. Merrifield, G.A. Milne, R.S. Nerem, P.D. Nunn, A.J. Payne, W.T. Pfeffer, D. Stammer and A.S. Unnikrishnan, 2013: Sea Level Change. In *Climate Change 2013: The Physical Science Basis*. Contribution of Working Group I to the Fifth Assessment Report of the Intergovernmental Panel on Climate Change [Stocker, T.F., D. Qin, G.-K. Plattner, M. Tignor, S.K. Allen, J. Boschung, A. Nauels, Y. Xia, V. Bex and P.M. Midgley (eds.)]. Cambridge University Press, Cambridge, United Kingdom and New York, NY, USA.

Ciracì, E., Velicogna, I. and Swenson, S., 2020. Continuity of the mass loss of the world's glaciers and ice caps from the GRACE and GRACE Follow-On missions. *Geophysical Research Letters*, *47*(9), p.e2019GL086926.

Claus, S., De Hauwere, N., Vanhoorne, B., Deckers, P., Souza Dias, F., Hernandez, F. and Mees, J., 2014. Marine regions: towards a global standard for georeferenced marine names and boundaries. *Marine Geodesy*, *37*(2), pp.99-125.

Cogley, J.G., 2009. Geodetic and direct mass-balance measurements: comparison and joint analysis. *Annals of Glaciology*, *50*(50), pp.96-100.

Collao-Barrios, G., Gillet-Chaulet, F., Favier, V., Casassa, G., Berthier, E., Dussaillant, I., Mouginot, J. and Rignot, E., 2018. Ice flow modelling to constrain the surface mass balance and ice discharge of San Rafael Glacier, Northern Patagonia Icefield. *Journal of Glaciology*, *64*(246), pp.568-582.

Cook, S.J., Kougkoulos, I., Edwards, L.A., Dortch, J. and Hoffmann, D., 2016. Glacier change and glacial lake outburst flood risk in the Bolivian Andes. *The Cryosphere*, *10*(5), pp.2399-2413.

Cuffey, K.M. and Paterson, W.S.B., 2010. *The physics of glaciers*. Academic Press.

Davies, B.J. and Glasser, N.F., 2012. Accelerating shrinkage of Patagonian glaciers from the Little Ice Age (~ AD 1870) to 2011. *Journal of Glaciology*, *58*(212), pp.1063-1084.

De Angelis, H., 2014. Hypsometry and sensitivity of the mass balance to changes in equilibrium-line altitude: the case of the Southern Patagonia Icefield. *Journal of Glaciology*, *60*(219), pp.14-28.

Dowdeswell, J.A. and Vásquez, M., 2013. Submarine landforms in the fjords of southern Chile: implications for glacimarine processes and sedimentation in a mild glacier-influenced environment. *Quaternary Science Reviews*, *64*, pp.1-19.

Dowdeswell, J.A., Dowdeswell, E.K., Rodrigo, C. and Diaz, J., 2016. Assemblage of glacial and related landforms in the fjords of southern Chile. *Geological Society, London, Memoirs*, *46*(1), pp.131-134.

Dussaillant, I., Berthier, E. and Brun, F., 2018. Geodetic mass balance of the Northern Patagonian Icefield from 2000 to 2012 using two independent methods. *Frontiers in Earth Science*, *6*, p.8.

Dussaillant, I., Berthier, E., Brun, F., Masiokas, M., Hugonnet, R., Favier, V., Rabatel, A., Pitte, P. and Ruiz, L., 2019. Two decades of glacier mass loss along the Andes. *Nature Geoscience*, *12*(10), pp.802-808.

Dutrieux, P., De Rydt, J., Jenkins, A., Holland, P.R., Ha, H.K., Lee, S.H., Steig, E.J., Ding, Q., Abrahamsen, E.P. and Schröder, M., 2014. Strong sensitivity of Pine Island ice-shelf melting to climatic variability. *Science*, *343*(6167), pp.174-178.

Dyurgerov, M., Bring, A. and Destouni, G., 2010. Integrated assessment of changes in freshwater inflow to the Arctic Ocean. *Journal of Geophysical Research: Atmospheres*, *115*(D12).

Edwards, T.L., Nowicki, S., Marzeion, B., Hock, R., Goelzer, H., Seroussi, H., Jourdain, N.C., Slater, D.A., Turner, F.E., Smith, C.J. and McKenna, C.M., 2021. Projected land ice contributions to twenty-first-century sea level rise. *Nature*, *593*(7857), pp.74-82.

Egholm, D.L., Knudsen, M.F., Clark, C.D. and Lesemann, J.E., 2011. Modeling the flow of glaciers in steep terrains: The integrated second-order shallow ice approximation (iSOSIA). *Journal of Geophysical Research: Earth Surface*, *116*(F2).

Emmer, A., Merkl, S. and Mergili, M., 2015. Spatiotemporal patterns of high-mountain lakes and related hazards in western Austria. *Geomorphology*, *246*, pp.602-616.

Enderlin, E.M. and Howat, I.M., 2013. Submarine melt rate estimates for floating termini of Greenland outlet glaciers (2000–2010). *Journal of Glaciology*, *59*(213), pp.67-75.

Enderlin, E.M., Howat, I.M., Jeong, S., Noh, M.J., Van Angelen, J.H. and Van Den Broeke, M.R., 2014. An improved mass budget for the Greenland ice sheet. *Geophysical Research Letters*, *41*(3), pp.866-872.

Farinotti, D., Huss, M., Fürst, J.J., Landmann, J., Machguth, H., Maussion, F. and Pandit, A., 2019. A consensus estimate for the ice thickness distribution of all glaciers on Earth. *Nature Geoscience*, *12*(3), pp.168-173.

Fatland, D.R. and Lingle, C.S., 1998. Analysis of the 1993-95 Bering Glacier (Alaska) surge using differential SAR interferometry. *Journal of Glaciology*, *44*(148), pp.532-546.

Felikson, D., Bartholomaus, T.C., Catania, G.A., Korsgaard, N.J., Kjær, K.H., Morlighem, M., Noël, B., Van Den Broeke, M., Stearns, L.A., Shroyer, E.L. and Sutherland, D.A., 2017. Inland thinning on the Greenland ice sheet controlled by outlet glacier geometry. *Nature Geoscience*, *10*(5), pp.366-369.

Fernández, R. and Rivera Ibañez, A., 2003. Variaciones recientes de los glaciares entre 41o y 49o de latitud sur y su relación con cambios climáticos.

Ferrán, O.G., 1995. *Volcanes de Chile*. Instituto Geográfico Militar.

Foresta, L., Gourmelen, N., Weissgerber, F., Nienow, P., Williams, J.J., Shepherd, A., Drinkwater, M.R. and Plummer, S., 2018. Heterogeneous and rapid ice loss over the Patagonian Ice Fields revealed by CryoSat-2 swath radar altimetry. *Remote Sensing of Environment*, *211*, pp.441-455.

Fowler, A.C., 1987. A theory of glacier surges. *Journal of Geophysical Research: Solid Earth*, *92*(B9), pp.9111-9120.

Fox-Kemper, B., H.T. Hewitt, C. Xiao, G. Aðalgeirsdóttir, S.S. Drijfhout, T.L. Edwards, N.R. Golledge, M. Hemer, R.E. Kopp, G. Krinner, A. Mix, D. Notz, S. Nowicki, I.S. Nurhati, L. Ruiz, J.-B. Sallée, A.B.A. Slangen, and Y. Yu, 2021: Ocean, Cryosphere and Sea Level Change. In *Climate Change 2021: The Physical Science Basis*. Contribution of Working Group I to the Sixth Assessment Report of the Intergovernmental Panel on Climate Change [Masson-Delmotte, V., P. Zhai, A. Pirani, S.L. Connors, C. Péan, S. Berger, N. Caud, Y. Chen, L. Goldfarb, M.I. Gomis, M. Huang, K. Leitzell, E. Lonnoy, J.B.R. Matthews, T.K. Maycock, T. Waterfield, O. Yelekçi, R. Yu, and B. Zhou (eds.)]. Cambridge University Press, Cambridge, United Kingdom and New York, NY, USA, pp. 1211–1362, doi:10.1017/9781009157896.011.

Frederikse, T., Landerer, F., Caron, L., Adhikari, S., Parkes, D., Humphrey, V.W., Dangendorf, S., Hogarth, P., Zanna, L., Cheng, L. and Wu, Y.H., 2020. The causes of sea-level rise since 1900. *Nature*, *584*(7821), pp.393-397.

Frey, H., Machguth, H., Huss, M., Huggel, C., Bajracharya, S., Bolch, T., Kulkarni, A., Linsbauer, A., Salzmann, N. and Stoffel, M., 2014. Estimating the volume of glaciers in the Himalayan–Karakoram region using different methods. *The Cryosphere*, *8*(6), pp.2313-2333.

Funk, M. and Röthlisberger, H., 1989. Forecasting the effects of a planned reservoir which will partially flood the tongue of Unteraargletscher in Switzerland. *Annals of Glaciology*, *13*, pp.76-81.

Furbish, D.J. and Andrews, J.T., 1984. The use of hypsometry to indicate long-term stability and response of valley glaciers to changes in mass transfer. *Journal of glaciology*, *30*(105), pp.199-211.

Fürst, J.J., Gillet-Chaulet, F., Benham, T.J., Dowdeswell, J.A., Grabiec, M., Navarro, F., Pettersson, R., Moholdt, G., Nuth, C., Sass, B. and Aas, K., 2017. Application of a two-step approach for mapping ice thickness to various glacier types on Svalbard. *The Cryosphere*, *11*(5), pp.2003-2032.

Gardelle, J., Arnaud, Y. and Berthier, E., 2011. Contrasted evolution of glacial lakes along the Hindu Kush Himalaya mountain range between 1990 and 2009. *Global and Planetary Change*, *75*(1-2), pp.47-55.

Gardner, A. S., M. A. Fahnestock, and T.A. Scambos, 2019 (October 2022): MEaSUREs ITS_LIVE Landsat Image-Pair Glacier and Ice Sheet Surface Velocities: Version 1. Data archived at National Snow and Ice Data Center. https://doi.org/10.5067/IMR9D3PEI28U.

Gardner, A.S., Moholdt, G., Cogley, J.G., Wouters, B., Arendt, A.A., Wahr, J., Berthier, E., Hock, R., Pfeffer, W.T., Kaser, G. and Ligtenberg, S.R., 2013. A reconciled estimate of glacier contributions to sea level rise: 2003 to 2009. *Science*, *340*(6134), pp.852-857.

Gardner, A.S., Moholdt, G., Scambos, T., Fahnstock, M., Ligtenberg, S., Van Den Broeke, M. and Nilsson, J., 2018. Increased West Antarctic and unchanged East Antarctic ice discharge over the last 7 years. *The Cryosphere*, *12*(2), pp.521-547.

Garreaud, R., Lopez, P., Minvielle, M. and Rojas, M., 2013. Large-scale control on the Patagonian climate. *Journal of Climate*, *26*(1), pp.215-230.

Garreaud, R.D., Vuille, M., Compagnucci, R. and Marengo, J., 2009. Present-day south american climate. *Palaeogeography, Palaeoclimatology, Palaeoecology*, *281*(3-4), pp.180-195.

Gillett, N.P., Kell, T.D. and Jones, P.D., 2006. Regional climate impacts of the Southern Annular Mode. *Geophysical Research Letters*, *33*(23).

Gladish, C.V., Holland, D.M., Rosing-Asvid, A., Behrens, J.W. and Boje, J., 2015. Oceanic boundary conditions for Jakobshavn Glacier. Part I: Variability and renewal of Ilulissat Icefjord waters, 2001–14. *Journal of Physical Oceanography*, *45*(1), pp.3-32.

Glasser, N.F., Harrison, S., Jansson, K.N., Anderson, K. and Cowley, A.J.N.G., 2011. Global sea-level contribution from the Patagonian Icefields since the Little Ice Age maximum. *Nature Geoscience*, *4*(5), pp.303-307.

Glasser, N.F., Holt, T.O., Evans, Z.D., Davies, B.J., Pelto, M. and Harrison, S., 2016. Recent spatial and temporal variations in debris cover on Patagonian glaciers. *Geomorphology*, *273*, pp.202-216.

GLIMS Consortium. 2005. GLIMS Glacier Database, Version 1. Boulder, Colorado USA. NASA National Snow and Ice Data Center Distributed Active Archive Center. doi: https://doi.org/10.7265/N5V98602. [October 2022].

Gregory, J.M. and Oerlemans, J., 1998. Simulated future sea-level rise due to glacier melt based on regionally and seasonally resolved temperature changes. *Nature*, *391*(6666), pp.474-476.

Greve, R. and Blatter, H., 2009. *Dynamics of ice sheets and glaciers*. Springer Science & Business Media.

Gudmundsson, G.H., 2003. Transmission of basal variability to a glacier surface. *Journal of Geophysical Research: Solid Earth*, *108*(B5).

Haresign, E. and Warren, C.R., 2005. Melt rates at calving termini: a study at Glaciar León, Chilean Patagonia. *Geological Society, London, Special Publications*, *242*(1), pp.99-109.

Harrison, S., Kargel, J.S., Huggel, C., Reynolds, J., Shugar, D.H., Betts, R.A., Emmer, A., Glasser, N., Haritashya, U.K., Klimeš, J. and Reinhardt, L., 2018. Climate change and the global pattern of moraine-dammed glacial lake outburst floods. *The Cryosphere*, *12*(4), pp.1195-1209.

Hata, S. and Sugiyama, S., 2021. Changes in the ice-front position and surface elevation of Glaciar Pío XI, an advancing calving Glacier in the Southern Patagonia Icefield, From 2000–2018. *Frontiers in Earth Science*, *8*, p.576044.

Hernando-Arrese, M. and Tironi, M., 2019. Worlding hydropower: river realities in the Chilean Patagonia. *Tapuya: Latin American Science, Technology and Society*, *2*(1), pp.295-309.

Hirabayashi, Y., Zang, Y., Watanabe, S., Koirala, S. and Kanae, S., 2013. Projection of glacier mass changes under a high-emission climate scenario using the global glacier model HYOGA2. *Hydrological Research Letters*, *7*(1), pp.6-11.

Hock, R., Bliss, A., Marzeion, B.E.N., Giesen, R.H., Hirabayashi, Y., Huss, M., Radić, V. and Slangen, A.B., 2019. GlacierMIP–A model intercomparison of global-scale glacier mass-balance models and projections. *Journal of Glaciology*, *65*(251), pp.453-467.

Hock, R., De Woul, M., Radić, V. and Dyurgerov, M., 2009. Mountain glaciers and ice caps around Antarctica make a large sea-level rise contribution. *Geophysical Research Letters*, *36*(7).

Howat, I.M., Joughin, I., Fahnestock, M., Smith, B.E. and Scambos, T.A., 2008. Synchronous retreat and acceleration of southeast Greenland outlet glaciers 2000–06: ice dynamics and coupling to climate. *Journal of Glaciology*, *54*(187), pp.646-660.

Hugonnet, R., McNabb, R., Berthier, E., Menounos, B., Nuth, C., Girod, L., Farinotti, D., Huss, M., Dussaillant, I., Brun, F. and Kääb, A., 2021. Accelerated global glacier mass loss in the early twenty-first century. *Nature*, *592*(7856), pp.726-731.

Huss M, Hock R. Global-scale hydrological response to future glacier mass loss. *Nature Climate Change*. 2018 Feb;8(2):135-40.

Huss, M. and Farinotti, D., 2012. Distributed ice thickness and volume of all glaciers around the globe. *Journal of Geophysical Research: Earth Surface*, *117*(F4).

Huss, M. and Hock, R., 2015. A new model for global glacier change and sea-level rise. *Frontiers in Earth Science*, *3*, p.54.

Huss, M., 2013. Density assumptions for converting geodetic glacier volume change to mass change. *The Cryosphere*, *7*(3), pp.877-887.

Hutter, K. and Hutter, K., 1983. The Application of the Shallow-Ice Approximation. *Theoretical Glaciology: Material Science of Ice and the Mechanics of Glaciers and Ice Sheets*, pp.256-332.

Immerzeel, W.W., Lutz, A.F., Andrade, M., Bahl, A., Biemans, H., Bolch, T., Hyde, S., Brumby, S., Davies, B.J., Elmore, A.C. and Emmer, A., 2020. Importance and vulnerability of the world's water towers. *Nature*, *577*(7790), pp.364-369.

Irarrazaval, I., Dussaillant, A., Vivero, S., Iribarren-Anacona, P. and Mariethoz, G., 2022. Ice Dynamics and Morphological Changes During Proglacial Lake Development at Exploradores Glacier, Patagonia. *Frontiers in Earth Science*, *10*, p.791487.

Iribarren Anacona, P., Norton, K.P. and Mackintosh, A., 2014. Moraine-dammed lake failures in Patagonia and assessment of outburst susceptibility in the Baker Basin. *Natural Hazards and Earth System Sciences*, *14*(12), pp.3243-3259.

Ivins, E.R., Watkins, M.M., Yuan, D.N., Dietrich, R., Casassa, G. and Rülke, A., 2011. On-land ice loss and glacial isostatic adjustment at the Drake Passage: 2003–2009. *Journal of Geophysical Research: Solid Earth*, *116*(B2).

Jaber, W.A., Floricioiu, D., Rott, H. and Eineder, M., 2013, July. Surface elevation changes of glaciers derived from SRTM and TanDEM-X DEM differences. In *2013 IEEE International Geoscience and Remote Sensing Symposium-IGARSS* (pp. 1893-1896). IEEE.

Jackson, R.H., Straneo, F. and Sutherland, D.A., 2014. Externally forced fluctuations in ocean temperature at Greenland glaciers in non-summer months. *Nature Geoscience*, *7*(7), pp.503-508.

Jacob, T., Wahr, J., Pfeffer, W.T. and Swenson, S., 2012. Recent contributions of glaciers and ice caps to sea level rise. *Nature*, *482*(7386), pp.514-518.

Jacobs, S., Giulivi, C., Dutrieux, P., Rignot, E., Nitsche, F. and Mouginot, J., 2013. Getz Ice Shelf melting response to changes in ocean forcing. *Journal of Geophysical Research: Oceans*, *118*(9), pp.4152-4168.

Jakob, L. and Gourmelen, N., 2023. Glacier mass loss between 2010 and 2020 dominated by atmospheric forcing. *Geophysical Research Letters*, *50*(8), p.e2023GL102954.

Jenkins, A., 2011. Convection-driven melting near the grounding lines of ice shelves and tidewater glaciers. *Journal of Physical Oceanography*, *41*(12), pp.2279-2294.

Jiskoot, H., Curran, C.J., Tessler, D.L. and Shenton, L.R., 2009. Changes in Clemenceau Icefield and Chaba Group glaciers, Canada, related to hypsometry, tributary detachment, length–slope and area–aspect relations. *Annals of Glaciology*, *50*(53), pp.133-143.

Jones, J.M., Gille, S.T., Goosse, H., Abram, N.J., Canziani, P.O., Charman, D.J., Clem, K.R., Crosta, X., De Lavergne, C., Eisenman, I. and England, M.H., 2016. Assessing recent trends in high-latitude Southern Hemisphere surface climate. *Nature Climate Change*, *6*(10), pp.917-926.

Joughin, I., Tulaczyk, S., MacAYEAL, D.R. and Engelhardt, H., 2004. Melting and freezing beneath the Ross ice streams, Antarctica. *Journal of Glaciology*, *50*(168), pp.96-108.

Joughin, I.R., Kwok, R. and Fahnestock, M.A., 1998. Interferometric estimation of three-dimensional ice-flow using ascending and descending passes. *IEEE Transactions on Geoscience and Remote Sensing*, *36*(1), pp.25-37.

Kaser, G., Cogley, J.G., Dyurgerov, M.B., Meier, M.F. and Ohmura, A., 2006. Mass balance of glaciers and ice caps: consensus estimates for 1961–2004. *Geophysical Research Letters*, *33*(19).

Kilian, R., 1990. The Austral Andean Volcanic Zone (South Patagonia). In *Intemational Symposium on Andean Geology (ISAG)* (Vol. 1, pp. 301-304).

King, M.D., Howat, I.M., Jeong, S., Noh, M.J., Wouters, B., Noël, B. and van den Broeke, M.R., 2018. Seasonal to decadal variability in ice discharge from the Greenland Ice Sheet. *The Cryosphere*, *12*(12), pp.3813-3825.

Kirkbride, M.P. and Deline, P., 2013. The formation of supraglacial debris covers by primary dispersal from transverse englacial debris bands. *Earth Surface Processes and Landforms*, *38*(15), pp.1779-1792.

Kirkbride, M.P. and Warren, C.R., 1997. Calving processes at a grounded ice cliff. *Annals of glaciology*, *24*, pp.116-121.

Kirkbride, M.P., 1993. The temporal significance of transitions from melting to calving termini at glaciers in the central Southern Alps of New Zealand. *The Holocene*, *3*(3), pp.232-240.

Kochtitzky, W., Copland, L., Van Wychen, W., Hugonnet, R., Hock, R., Dowdeswell, J.A., Benham, T., Strozzi, T., Glazovsky, A., Lavrentiev, I. and Rounce, D.R., 2022. The unquantified mass loss of Northern Hemisphere marine-terminating glaciers from 2000–2020. *Nature Communications*, *13*(1), p.5835.

Koppes, M., Conway, H., Rasmussen, L.A. and Chernos, M., 2011. Deriving mass balance and calving variations from reanalysis data and sparse observations, Glaciar San Rafael, northern Patagonia, 1950–2005. *The Cryosphere*, *5*(3), pp.791-808.

Koppes, M., Sylwester, R., Rivera, A. and Hallet, B., 2010. Variations in sediment yield over the advance and retreat of a calving glacier, Laguna San Rafael, North Patagonian Icefield. *Quaternary Research*, *73*(1), pp.84-95.

Koppes, M.N., 2007. *Glacier erosion and response to climate: From alaska to patagonia* (Doctoral dissertation, University of Washington).

Larour, E., Morlighem, M., Seroussi, H., Schiermeier, J. and Rignot, E., 2012. Ice flow sensitivity to geothermal heat flux of Pine Island Glacier, Antarctica. *Journal of Geophysical Research: Earth Surface*, *117*(F4).

Larsen, C.F., Burgess, E., Arendt, A.A., O'neel, S., Johnson, A.J. and Kienholz, C., 2015. Surface melt dominates Alaska glacier mass balance. *Geophysical Research Letters*, *42*(14), pp.5902-5908.

Leclercq, P.W., Oerlemans, J. and Cogley, J.G., 2011. Estimating the glacier contribution to sea-level rise for the period 1800–2005. *Surveys in Geophysics*, *32*, pp.519-535.

Lenaerts, J.T., van den Broeke, M.R., van Wessem, J.M., van de Berg, W.J., van Meijgaard, E., van Ulft, L.H. and Schaefer, M., 2014. Extreme precipitation and climate gradients in

Patagonia revealed by high-resolution regional atmospheric climate modeling. *Journal of climate*, *27*(12), pp.4607-4621.

Li, J., Chen, J., Ni, S., Tang, L. and Hu, X., 2019. Long-term and inter-annual mass changes of Patagonia Ice Field from GRACE. *Geodesy and Geodynamics*, *10*(2), pp.100-109.

Lodolo, E., Donda, F., Lozano, J., Baradello, L., Romeo, R., Bran, D.M. and Tassone, A., 2020. The submerged footprint of Perito Moreno glacier. *Scientific Reports*, *10*(1), p.16437.

Lopez, P., Chevallier, P., Favier, V., Pouyaud, B., Ordenes, F. and Oerlemans, J., 2010. A regional view of fluctuations in glacier length in southern South America. *Global and Planetary Change*, *71*(1-2), pp.85-108.

Loriaux, T. and Casassa, G., 2013. Evolution of glacial lakes from the Northern Patagonia Icefield and terrestrial water storage in a sea-level rise context. *Global and Planetary Change*, *102*, pp.33-40.

Malz, P., Meier, W., Casassa, G., Jaña, R., Skvarca, P. and Braun, M.H., 2018. Elevation and mass changes of the Southern Patagonia Icefield derived from TanDEM-X and SRTM data. *Remote Sensing*, *10*(2), p.188.

Mankoff, K.D., Solgaard, A., Colgan, W., Ahlstrøm, A.P., Khan, S.A. and Fausto, R.S., 2020. Greenland Ice Sheet solid ice discharge from 1986 through March 2020. *Earth System Science Data*, *12*(2), pp.1367-1383.

Marshall, G.J., 2003. Trends in the Southern Annular Mode from observations and reanalyses. *Journal of climate*, *16*(24), pp.4134-4143.

Marzeion, B., Hock, R., Anderson, B., Bliss, A., Champollion, N., Fujita, K., Huss, M., Immerzeel, W.W., Kraaijenbrink, P., Malles, J.H. and Maussion, F., 2020. Partitioning the uncertainty of ensemble projections of global glacier mass change. *Earth's Future*, *8*(7), p.e2019EF001470.

Marzeion, B., Jarosch, A.H. and Hofer, M., 2012. Past and future sea-level change from the surface mass balance of glaciers. *The Cryosphere*, *6*(6), pp.1295-1322.

Maussion, F., Butenko, A., Eis, J., Fourteau, K., Jarosch, A.H., Landmann, J., Oesterle, F., Recinos, B., Rothenpieler, T., Vlug, A. and Wild, C.T., 2018. The open global glacier model (OGGM) v1. 0. *Geoscientific Model Development Discussions*, pp.1-33.

McDonnell, M., Rupper, S. and Forster, R., 2022. Quantifying geodetic mass balance of the northern and Southern Patagonian Icefields since 1976. *Frontiers in Earth Science*, *10*, p.813574.

McNabb, R.W. and Hock, R., 2014. Alaska tidewater glacier terminus positions, 1948–2012. *Journal of Geophysical Research: Earth Surface*, *119*(2), pp.153-167.

McNabb, R.W., Hock, R. and Huss, M., 2015. Variations in Alaska tidewater glacier frontal ablation, 1985–2013. *Journal of Geophysical Research: Earth Surface*, *120*(1), pp.120-136.

Meerhoff, E., Castro, L.R., Tapia, F.J. and Pérez-Santos, I., 2019. Hydrographic and biological impacts of a Glacial Lake Outburst Flood (GLOF) in a Patagonian Fjord. *Estuaries and Coasts*, *42*, pp.132-143.

Meier, M.F., Dyurgerov, M.B., Rick, U.K., O'neel, S., Pfeffer, W.T., Anderson, R.S., Anderson, S.P. and Glazovsky, A.F., 2007. Glaciers dominate eustatic sea-level rise in the 21st century. *Science*, *317*(5841), pp.1064-1067.

Meier, W.J.H., Grießinger, J., Hochreuther, P. and Braun, M.H., 2018. An updated multi-temporal glacier inventory for the Patagonian Andes with changes between the Little Ice Age and 2016. *Frontiers in Earth Science*, *6*, p.62.

Mercer, J.H., 1961. The estimation of the regimen and former firn limit of a glacier. *Journal of Glaciology*, *3*(30), pp.1053-1062.

Mernild, S.H., Beckerman, A.P., Yde, J.C., Hanna, E., Malmros, J.K., Wilson, R. and Zemp, M., 2015. Mass loss and imbalance of glaciers along the Andes Cordillera to the sub-Antarctic islands. *Global and Planetary Change*, *133*, pp.109-119.

Mernild, S.H., Liston, G.E., Hiemstra, C. and Wilson, R., 2017. The Andes Cordillera. Part III: glacier surface mass balance and contribution to sea level rise (1979–2014). *International Journal of Climatology*, *37*(7), pp.3154-3174.

Michel, R. and Rignot, E., 1999. Flow of Glaciar Moreno, Argentina, from repeat-pass Shuttle Imaging Radar images: comparison of the phase correlation method with radar interferometry. *Journal of Glaciology*, *45*(149), pp.93-100.

Millan, R., Mouginot, J., Rabatel, A. and Morlighem, M., 2022. Ice velocity and thickness of the world's glaciers. *Nature Geoscience*, *15*(2), pp.124-129.

Millan, R., Rignot, E., Rivera, A., Martineau, V., Mouginot, J., Zamora, R., Uribe, J., Lenzano, G., De Fleurian, B., Li, X. and Gim, Y., 2019. Ice thickness and bed elevation of the Northern and Southern Patagonian Icefields. *Geophysical Research Letters*, *46*(12), pp.6626-6635.

Minowa, M., Schaefer, M. and Skvarca, P., 2023. Effects of topography on dynamics and mass loss of lake-terminating glaciers in southern Patagonia. *Journal of Glaciology*, pp.1-18.

Minowa, M., Schaefer, M., Sugiyama, S., Sakakibara, D. and Skvarca, P., 2021. Frontal ablation and mass loss of the Patagonian icefields. *Earth and Planetary Science Letters*, *561*, p.116811.

Minowa, M., Sugiyama, S., Sakakibara, D. and Skvarca, P., 2017. Seasonal variations in ice-front position controlled by frontal ablation at Glaciar Perito Moreno, the Southern Patagonia Icefield. *Frontiers in earth science*, *5*, p.1.

Moffat, C., Tapia, F.J., Nittrouer, C.A., Hallet, B., Bown, F., Boldt Love, K. and Iturra, C., 2018. Seasonal evolution of ocean heat supply and freshwater discharge from a rapidly retreating tidewater glacier: Jorge Montt, Patagonia. *Journal of Geophysical Research: Oceans*, *123*(6), pp.4200-4223.

Moon, T. and Joughin, I., 2008. Changes in ice front position on Greenland's outlet glaciers from 1992 to 2007. *Journal of Geophysical Research: Earth Surface*, *113*(F2).

Moon, T., Joughin, I., Smith, B. and Howat, I., 2012. 21st-century evolution of Greenland outlet glacier velocities. *Science*, *336*(6081), pp.576-578.

Motoki, A., Orihashi, Y., Naranjo, J.A., Hirata, D., Hosono, T., Cario, F.D. and Anma, R., 2003. Geologic occurrence and recent eruptive materials of the Lautaro Volcano, Chilean Patagonia. *The Journal of the Geological Society of Japan*, *109*(5), pp.IX-X.

Motyka, R.J., Hunter, L., Echelmeyer, K.A. and Connor, C., 2003. Submarine melting at the terminus of a temperate tidewater glacier, LeConte Glacier, Alaska, USA. *Annals of Glaciology*, *36*, pp.57-65.

Motyka, R.J., Truffer, M., Fahnestock, M., Mortensen, J., Rysgaard, S. and Howat, I., 2011. Submarine melting of the 1985 Jakobshavn Isbræ floating tongue and the triggering of the current retreat. *Journal of Geophysical Research: Earth Surface*, *116*(F1).

Mouginot, J. and Rignot, E., 2015. Ice motion of the Patagonian icefields of South America: 1984–2014. *Geophysical Research Letters*, *42*(5), pp.1441-1449.

Mouginot, J., Rignot, E., Bjørk, A.A., Van den Broeke, M., Millan, R., Morlighem, M., Noël, B., Scheuchl, B. and Wood, M., 2019. Forty-six years of Greenland Ice Sheet mass balance from 1972 to 2018. *Proceedings of the national academy of sciences*, *116*(19), pp.9239-9244.

Mouginot, J., Scheuchl, B. and Rignot, E., 2012. Mapping of ice motion in Antarctica using synthetic-aperture radar data. *Remote Sensing*, *4*(9), pp.2753-2767.

Muto, M. and Furuya, M., 2013. Surface velocities and ice-front positions of eight major glaciers in the Southern Patagonian Ice Field, South America, from 2002 to 2011. *Remote sensing of environment*, *139*, pp.50-59.

Nakajima, C. ed., 1985. Glaciological Studies in Patagonia Northern Icefield.

Nakawo, M. and Rana, B., 1999. Estimate of ablation rate of glacier ice under a supraglacial debris layer. *Geografiska Annaler: Series A, Physical Geography*, *81*(4), pp.695-701.

Naruse, R. and Skvarca, P., 2000. Dynamic features of thinning and retreating Glaciar Upsala, a lacustrine calving glacier in southern Patagonia. *Arctic, Antarctic, and Alpine Research*, *32*(4), pp.485-491.

Näslund, J.O., Jansson, P., Fastook, J.L., Johnson, J. and Andersson, L., 2005. Detailed spatially distributed geothermal heat-flow data for modeling of basal temperatures and meltwater production beneath the Fennoscandian ice sheet. *Annals of Glaciology*, *40*, pp.95-101.

Nick, F.M., Van der Veen, C.J., Vieli, A. and Benn, D.I., 2010. A physically based calving model applied to marine outlet glaciers and implications for the glacier dynamics. *Journal of Glaciology*, *56*(199), pp.781-794.

Nishimura, D., Sugiyama, S., Bauder, A. and Funk, M., 2013. Changes in ice-flow velocity and surface elevation from 1874 to 2006 in Rhonegletscher, Switzerland. *Arctic, antarctic, and alpine research*, *45*(4), pp.552-562.

Nye, J.F., 1952. The mechanics of glacier flow. *Journal of Glaciology*, *2*(12), pp.82-93.

O'Neel, S., Echelmeyer, K.A. and Motyka, R.J., 2003. Short-term variations in calving of a tidewater glacier: LeConte Glacier, Alaska, USA. *Journal of Glaciology*, *49*(167), pp.587-598.

Oerlemans, J., Anderson, B., Hubbard, A., Huybrechts, P., Johannesson, T., Knap, W.H., Schmeits, M., Stroeven, A.P., Van de Wal, R.S.W., Wallinga, J. and Zuo, Z., 1998. Modelling the response of glaciers to climate warming. *Climate dynamics*, *14*, pp.267-274.

Oppenheimer, M., Glavovic, B., Hinkel, J., Van de Wal, R., Magnan, A.K., Abd-Elgawad, A., Cai, R., Cifuentes-Jara, M., Deconto, R.M., Ghosh, T. and Hay, J., 2019. Sea level rise and implications for low lying islands, coasts and communities.

Orihashi, Y., Naranjo, J.A., Motoki, A., Sumino, H., Hirata, D., Anma, R. and Nagao, K., 2004. Quaternary volcanic activity of Hudson and Lautaro volcanoes, Chilean Patagonia: New constraints from K-Ar ages. *Revista geológica de Chile*, *31*(2), pp.207-224.

Osmanoğlu, B., Braun, M., Hock, R. and Navarro, F.J., 2013. Surface velocity and ice discharge of the ice cap on King George Island, Antarctica. *Annals of Glaciology*, *54*(63), pp.111-119.

Osmanoglu, B., Navarro, F.J., Hock, R., Braun, M. and Corcuera, M.I., 2014. Surface velocity and mass balance of Livingston Island ice cap, Antarctica. *The Cryosphere*, *8*(5), pp.1807-1823.

Östrem, G., 1959. Ice melting under a thin layer of moraine, and the existence of ice cores in moraine ridges. *Geografiska Annaler*, *41*(4), pp.228-230.

Pasquini, A.I., Lecomte, K.L. and Depetris, P.J., 2008. Climate change and recent water level variability in Patagonian proglacial lakes, Argentina. *Global and Planetary Change*, *63*(4), pp.290-298.

Pattyn, F., 2017. Sea-level response to melting of Antarctic ice shelves on multi-centennial timescales with the fast Elementary Thermomechanical Ice Sheet model (f. ETISh v1. 0). *The Cryosphere*, *11*(4), pp.1851-1878.

Pelletier, J.D., Comeau, D. and Kargel, J., 2010. Controls of glacial valley spacing on Earth and Mars. *Geomorphology*, *116*(1-2), pp.189-201.

Pętlicki, M., Rivera, A., Oberreuter, J., Uribe, J., Reinthaler, J. and Bown, F., 2023. Frontal collapse of San Quintín glacier (Northern Patagonia Icefield), the last piedmont glacier lobe in the Andes. *The Cryosphere Discussions*, pp.1-25.

Pfeffer, W.T., 2007. A simple mechanism for irreversible tidewater glacier retreat. *Journal of Geophysical Research: Earth Surface*, *112*(F3).

Pfeffer, W.T., Harper, J.T. and O'Neel, S., 2008. Kinematic constraints on glacier contributions to 21st-century sea-level rise. *Science*, *321*(5894), pp.1340-1343.

Podrasky, D., Truffer, M., Lüthi, M. and Fahnestock, M., 2014. Quantifying velocity response to ocean tides and calving near the terminus of Jakobshavn Isbræ, Greenland. *Journal of Glaciology*, *60*(222), pp.609-621.

Polyakov, I.V., Pnyushkov, A.V., Alkire, M.B., Ashik, I.M., Baumann, T.M., Carmack, E.C., Goszczko, I., Guthrie, J., Ivanov, V.V., Kanzow, T. and Krishfield, R., 2017. Greater role for Atlantic inflows on sea-ice loss in the Eurasian Basin of the Arctic Ocean. *Science*, *356*(6335), pp.285-291.

Ponce, R.D., Vásquez, F., Stehr, A., Debels, P. and Orihuela, C., 2011. Estimating the economic value of landscape losses due to flooding by hydropower plants in the Chilean Patagonia. *Water Resources Management*, *25*, pp.2449-2466.

Post, A., O'Neel, S., Motyka, R.J. and Streveler, G., 2011. A complex relationship between calving glaciers and climate. *Eos, Transactions American Geophysical Union*, *92*(37), pp.305-306.

Radić, V. and Hock, R., 2011. Regionally differentiated contribution of mountain glaciers and ice caps to future sea-level rise. *Nature Geoscience*, *4*(2), pp.91-94.

Radić, V., Bliss, A., Beedlow, A.C., Hock, R., Miles, E. and Cogley, J.G., 2014. Regional and global projections of twenty-first century glacier mass changes in response to climate scenarios from global climate models. *Climate Dynamics*, *42*, pp.37-58.

Ramsankaran, R.A.A.J., Pandit, A. and Azam, M.F., 2018. Spatially distributed ice-thickness modelling for Chhota Shigri Glacier in western Himalayas, India. *International Journal of Remote Sensing*, *39*(10), pp.3320-3343.

Rasmussen, L.A., Conway, H. and Raymond, C.F., 2007. Influence of upper air conditions on the Patagonia icefields. *Global and Planetary Change*, *59*(1-4), pp.203-216.

Recinos, B., Maussion, F. and Marzeion, B., 2023. Advances in data availability to constrain and evaluate frontal ablation of ice-dynamical models of Greenland's tidewater peripheral glaciers. *Annals of Glaciology*, pp.1-7.

Richter, A., Groh, A., Horwath, M., Ivins, E., Marderwald, E., Hormaechea, J.L., Perdomo, R. and Dietrich, R., 2019. The rapid and steady mass loss of the patagonian icefields throughout the GRACE era: 2002–2017. *Remote Sensing*, *11*(8), p.909.

Rignot, E., Box, J.E., Burgess, E. and Hanna, E., 2008. Mass balance of the Greenland ice sheet from 1958 to 2007. *Geophysical Research Letters*, *35*(20).

Rignot, E., Fenty, I., Xu, Y., Cai, C. and Kemp, C., 2015. Undercutting of marine-terminating glaciers in West Greenland. *Geophysical Research Letters*, *42*(14), pp.5909-5917.

Rignot, E., Jezek, K.C. and Sohn, H.G., 1995. Ice flow dynamics of the Greenland ice sheet from SAR interferometry. *Geophysical Research Letters*, *22*(5), pp.575-578.

Rignot, E., Rivera, A. and Casassa, G., 2003. Contribution of the Patagonia Icefields of South America to sea level rise. *Science*, *302*(5644), pp.434-437.

Rignot, E., Velicogna, I., van den Broeke, M.R., Monaghan, A. and Lenaerts, J.T., 2011. Acceleration of the contribution of the Greenland and Antarctic ice sheets to sea level rise. *Geophysical Research Letters*, *38*(5).

Rivera, A., Benham, T., Casassa, G., Bamber, J. and Dowdeswell, J.A., 2007. Ice elevation and areal changes of glaciers from the Northern Patagonia Icefield, Chile. *Global and Planetary Change*, *59*(1-4), pp.126-137.

Rivera, A., Corripio, J., Bravo, C. and Cisternas, S., 2012. Glaciar Jorge Montt (Chilean Patagonia) dynamics derived from photos obtained by fixed cameras and satellite image feature tracking. *Annals of Glaciology*, *53*(60), pp.147-155.

Rivera, A., Koppes, M., Bravo, C. and Aravena, J.C., 2012. Little ice age advance and retreat of Glaciar Jorge Montt, Chilean Patagonia. *Climate of the Past*, *8*(2), pp.403-414.

Rivera, A., Lange, H., Aravena, J.C. and Casassa, G., 1997. The 20th-century advance of Glaciar Pio XI, Chilean Patagonia. *Annals of Glaciology*, *24*, pp.66-71.

Robertson, C.M., Benn, D.I., Brook, M.S. and Holt, K.A., 2012. Subaqueous calving margin morphology at Mueller, Hooker and Tasman glaciers in Aoraki/Mount Cook National Park, New Zealand. *Journal of Glaciology*, *58*(212), pp.1037-1046.

Rosenblüth, B., Fuenzalida, H.A. and Aceituno, P., 1997. Recent temperature variations in southern South America. *International Journal of Climatology: A Journal of the Royal Meteorological Society*, *17*(1), pp.67-85.

Rounce, D.R., Hock, R., Maussion, F., Hugonnet, R., Kochtitzky, W., Huss, M., Berthier, E., Brinkerhoff, D., Compagno, L., Copland, L. and Farinotti, D., 2023. Global glacier change in the 21st century: Every increase in temperature matters. *Science*, *379*(6627), pp.78-83.

Rowan, A.V., Quincey, D.J., Gibson, M.J., Glasser, N.F., Westoby, M.J., Irvine-Fynn, T.D., Porter, P.R. and Hambrey, M.J., 2018. The sustainability of water resources in High Mountain Asia in the context of recent and future glacier change. *Geological Society, London, Special Publications*, *462*(1), pp.189-204.

Rückamp, M., Kleiner, T. and Humbert, A., 2022. Comparison of ice dynamics using full-Stokes and Blatter–Pattyn approximation: application to the Northeast Greenland Ice Stream. *The Cryosphere*, *16*(5), pp.1675-1696.

Sakai, A., Nishimura, K., Kadota, T. and Takeuchi, N., 2009. Onset of calving at supraglacial lakes on debris-covered glaciers of the Nepal Himalaya. *Journal of Glaciology*, *55*(193), pp.909-917.

Sakakibara, D. and Sugiyama, S., 2014. Ice-front variations and speed changes of calving glaciers in the Southern Patagonia Icefield from 1984 to 2011. *Journal of Geophysical Research: earth surface*, *119*(11), pp.2541-2554.

Sakakibara, D., Sugiyama, S., Sawagaki, T., Marinsek, S. and Skvarca, P., 2013. Rapid retreat, acceleration and thinning of Glaciar Upsala, Southern Patagonia Icefield, initiated in 2008. *Annals of Glaciology*, *54*(63), pp.131-138.

Schaefer, M., Machguth, H., Falvey, M. and Casassa, G., 2013. Modeling past and future surface mass balance of the Northern Patagonia Icefield. *Journal of Geophysical Research: Earth Surface*, *118*(2), pp.571-588.

Schaefer, M., Machguth, H., Falvey, M., Casassa, G. and Rignot, E., 2015. Quantifying mass balance processes on the Southern Patagonia Icefield. *The Cryosphere*, *9*(1), pp.25-35.

Schild, K.M. and Hamilton, G.S., 2013. Seasonal variations of outlet glacier terminus position in Greenland. *Journal of Glaciology*, *59*(216), pp.759-770.

Sciascia, R., Straneo, F., Cenedese, C. and Heimbach, P., 2013. Seasonal variability of submarine melt rate and circulation in an East Greenland fjord. *Journal of Geophysical Research: Oceans*, *118*(5), pp.2492-2506.

Shepherd, A., Ivins, E.R., Barletta, V.R., Bentley, M.J., Bettadpur, S., Briggs, K.H., Bromwich, D.H., Forsberg, R., Galin, N., Horwath, M. and Jacobs, S., 2012. A reconciled estimate of ice-sheet mass balance. *Science*, *338*(6111), pp.1183-1189.

Shugar, D.H., Burr, A., Haritashya, U.K., Kargel, J.S., Watson, C.S., Kennedy, M.C., Bevington, A.R., Betts, R.A., Harrison, S. and Strattman, K., 2020. Rapid worldwide growth of glacial lakes since 1990. *Nature Climate Change*, *10*(10), pp.939-945.

Skvarca, P. and Naruse, R., 1997. Dynamic behavior of Glaciar Perito Moreno, southern Patagonia. *Annals of Glaciology*, *24*, pp.268-271.

Skvarca, P., De Angelis, H., Naruse, R., Warren, C.R. and Aniya, M., 2002. Calving rates in fresh water: new data from southern Patagonia. *Annals of Glaciology*, *34*, pp.379-384.

Skvarca, P., Raup, B. and De Angelis, H., 2003. Recent behaviour of Glaciar Upsala, a fast-flowing calving glacier in Lago Argentino, southern Patagonia. *Annals of Glaciology*, *36*, pp.184-188.

Skvarca, P., Satow, K., Naruse, R. and Leiva, J.C., 1995. Recent thinning, retreat and flow of Upsala Glacier, Patagonia. *Bulletin of Glacier Research*, *13*, pp.11-20.

Slater, T., Hogg, A.E. and Mottram, R., 2020. Ice-sheet losses track high-end sea-level rise projections. *Nature Climate Change*, *10*(10), pp.879-881.

Smith, R.B. and Evans, J.P., 2007. Orographic precipitation and water vapor fractionation over the southern Andes. *Journal of Hydrometeorology*, *8*(1), pp.3-19.

Sommaruga, R., 2015. When glaciers and ice sheets melt: consequences for planktonic organisms. *Journal of plankton research*, *37*(3), pp.509-518.

Soncini, A., Bocchiola, D., Confortola, G., Minora, U., Vuillermoz, E., Salerno, F., Viviano, G., Shrestha, D., Senese, A., Smiraglia, C. and Diolaiuti, G., 2016. Future hydrological regimes and glacier cover in the Everest region: The case study of the upper Dudh Koshi basin. *Science of the Total Environment*, *565*, pp.1084-1101.

Sugiyama, S., Minowa, M., Sakakibara, D., Skvarca, P., Sawagaki, T., Ohashi, Y., Naito, N. and Chikita, K., 2016. Thermal structure of proglacial lakes in Patagonia. *Journal of Geophysical Research: Earth Surface*, *121*(12), pp.2270-2286.

Sugiyama, S., Skvarca, P., Naito, N., Enomoto, H., Tsutaki, S., Tone, K., Marinsek, S. and Aniya, M., 2011. Ice speed of a calving glacier modulated by small fluctuations in basal water pressure. *Nature Geoscience*, *4*(9), pp.597-600.

Sutherland, J.L., Carrivick, J.L., Gandy, N., Shulmeister, J., Quincey, D.J. and Cornford, S.L., 2020. Proglacial lakes control glacier geometry and behavior during recession. *Geophysical Research Letters*, *47*(19), p.e2020GL088865.

Swart, N.C. and Fyfe, J.C., 2012. Observed and simulated changes in the Southern Hemisphere surface westerly wind-stress. *Geophysical Research Letters*, *39*(16).

Tiberti, R., Buscaglia, F., Callieri, C., Rogora, M., Tartari, G. and Sommaruga, R., 2020. Food web complexity of high mountain lakes is largely affected by glacial retreat. *Ecosystems*, *23*, pp.1093-1106.

Truffer, M. and Motyka, R.J., 2016. Where glaciers meet water: Subaqueous melt and its relevance to glaciers in various settings. *Reviews of Geophysics*, *54*(1), pp.220-239.

Trüssel, B.L., Motyka, R.J., Truffer, M. and Larsen, C.F., 2013. Rapid thinning of lake-calving Yakutat Glacier and the collapse of the Yakutat Icefield, southeast Alaska, USA. *Journal of Glaciology*, *59*(213), pp.149-161.

Trüssel, B.L., Truffer, M., Hock, R., Motyka, R.J., Huss, M. and Zhang, J., 2015. Runaway thinning of the low-elevation Yakutat Glacier, Alaska, and its sensitivity to climate change. *Journal of Glaciology*, *61*(225), pp.65-75.

Tsutaki, S., Nishimura, D., Yoshizawa, T. and Sugiyama, S., 2011. Changes in glacier dynamics under the influence of proglacial lake formation in Rhonegletscher, Switzerland. *Annals of Glaciology*, *52*(58), pp.31-36.

Van der Veen, C.J., 2002. Calving glaciers. *Progress in Physical Geography*, *26*(1), pp.96-122.

Vaughan, D.G., Comiso, J.C., Allison, I., Carrasco, J., Kaser, G., Kwok, R., Mote, P., Murray, T., Paul, F., Ren, J. and Rignot, E., 2013. Observations: cryosphere. *Climate change*, *2103*, pp.317-382.

Vecchio, A.L., Lenzano, M.G., Durand, M., Lannutti, E., Bruce, R. and Lenzano, L., 2018. Estimation of surface flow speed and ice surface temperature from optical satellite imagery at Viedma glacier, Argentina. *Global and planetary change*, *169*, pp.202-213.

Vieli, A., Funk, M. and Blatter, H., 2000. Tidewater glaciers: frontal flow acceleration and basal sliding. *Annals of Glaciology*, *31*, pp.217-221.

Walker, C.C. and Gardner, A.S., 2017. Rapid drawdown of Antarctica's Wordie Ice Shelf glaciers in response to ENSO/Southern Annular Mode-driven warming in the Southern Ocean. *Earth and Planetary Science Letters*, *476*, pp.100-110.

Warren, C. and Aniya, M., 1999. The calving glaciers of southern South America. *Global and Planetary Change*, *22*(1-4), pp.59-77.

Warren, C., Benn, D., Winchester, V. and Harrison, S., 2001. Buoyancy-driven lacustrine calving, glaciar nef, chilean patagonia. *Journal of Glaciology*, *47*(156), pp.135-146.

Warren, C.R. and Kirkbride, M.P., 2003. Calving speed and climatic sensitivity of New Zealand lake-calving glaciers. *Annals of Glaciology*, *36*, pp.173-178.

Warren, C.R., 1991. Terminal environment, topographic control and fluctuations of West Greenland glaciers. *Boreas*, *20*(1), pp.1-15.

Warren, C.R., Glasser, N.F., Harrison, S., Winchester, V., Kerr, A.R. and Rivera, A., 1995. Characteristics of tide-water calving at Glaciar San Rafael, Chile. *Journal of glaciology*, *41*(138), pp.273-289.

Warren, C.R., Rivera, A. and Post, A., 1997. Greatest Holocene advance of glaciar Pío XI, Chilean Patagonia: possible causes. *Annals of Glaciology*, *24*, pp.11-15.

Watson, C.S., Kargel, J.S., Shugar, D.H., Haritashya, U.K., Schiassi, E. and Furfaro, R., 2020. Mass loss from calving in Himalayan proglacial lakes. *Frontiers in Earth Science*, *7*, p.342.

Weidemann, S.S., Sauter, T., Malz, P., Jaña, R., Arigony-Neto, J., Casassa, G. and Schneider, C., 2018. Glacier mass changes of lake-terminating grey and tyndall glaciers at the southern patagonia icefield derived from geodetic observations and energy and mass balance modeling. *Frontiers in Earth Science*, *6*, p.81.

Willis, M.J., Melkonian, A.K., Pritchard, M.E. and Ramage, J.M., 2012. Ice loss rates at the Northern Patagonian Icefield derived using a decade of satellite remote sensing. *Remote Sensing of Environment*, *117*, pp.184-198.

Willis, M.J., Melkonian, A.K., Pritchard, M.E. and Rivera, A., 2012. Ice loss from the Southern Patagonian ice field, South America, between 2000 and 2012. *Geophysical Research Letters*, *39*(17).

Wilson, R., Carrión, D. and Rivera, A., 2016. Detailed dynamic, geometric and supraglacial moraine data for Glaciar Pio XI, the only surge-type glacier of the Southern Patagonia Icefield. *Annals of Glaciology*, *57*(73), pp.119-130.

Wilson, R., Glasser, N.F., Reynolds, J.M., Harrison, S., Anacona, P.I., Schaefer, M. and Shannon, S., 2018. Glacial lakes of the Central and Patagonian Andes. *Global and Planetary Change*, *162*, pp.275-291.

Wood, M., Rignot, E., Fenty, I., Menemenlis, D., Millan, R., Morlighem, M., Mouginot, J. and Seroussi, H., 2018. Ocean-induced melt triggers glacier retreat in Northwest Greenland. *Geophysical Research Letters*, *45*(16), pp.8334-8342.

Wouters, B., Gardner, A.S. and Moholdt, G., 2019. Global glacier mass loss during the GRACE satellite mission (2002-2016). *Frontiers in earth science*, *7*, p.96.

Xu, Y., Rignot, E., Fenty, I., Menemenlis, D. and Flexas, M.M., 2013. Subaqueous melting of Store Glacier, west Greenland from three-dimensional, high-resolution numerical modeling and ocean observations. *Geophysical Research Letters*, *40*(17), pp.4648-4653.

Zalazar, L.V., Ferri Hidalgo, L., Castro, M.A., Gargantini, H., Giménez, M.M., Pitte, P.M., Ruiz, L.E. and Villalba, R., 2017. Glaciares de Argentina: resultados preliminares del Inventario Nacional de Glaciares.

Zemp, M., Huss, M., Thibert, E., Eckert, N., McNabb, R., Huber, J., Barandun, M., Machguth, H., Nussbaumer, S.U., Gärtner-Roer, I. and Thomson, L., 2019. Global glacier mass changes and their contributions to sea-level rise from 1961 to 2016. *Nature*, *568*(7752), pp.382-386.

Zuo, Z. and Oerlemans, J., 1997. Contribution of glacier melt to sea-level rise since AD 1865: a regionally differentiated calculation. *Climate Dynamics*, *13*, pp.835-845.

8.0 Appendices

A. Glacier Discharge and Margin Length Values

Table A. 1 - Northern Patagonian Icefield

Glacier	Termini Environment	Margin Length (km) (2004)	Margin Length (km) (2017)	Ice Discharge (Gt yr^{-1}) (2004)	Ice Discharge (Gt yr^{-1}) (2017)	Ice Discharge Difference (Gt yr^{-1})
Acodado	Lake	2.04	2.06	0.032	0.055	+ 0.023
Andree	Land	1.39	0.93	0.003	0.007	+ 0.004
Arco	Land	0.47	0.23	0.0006	0.0003	- 0.003
Bayo	Land	1.08	1.13	0.0004	0.002	+ 0.0016
Benito	Lake	1.59	1.41	0.035	0.052	+ 0.017
Cachet	Lake	0.86	0.53	0.029	0.011	- 0.018
Cachet Norte	Land	0.87	0.78	0.002	0.002	N/A
Colonia	Lake	3.47	1.85	0.143	0.037	- 0.106
Cristal	Land to Lake	0.53	0.48	0.00006	0.0016	+ 0.00154
Exploradores	Lake	3.83	7.41	0.057	0.179	+ 0.122
Fiero	Land to Lake	1.58	1.96	0.063	0.150	+ 0.087
Fraenkel	Lake	0.54	0.36	0.0003	0.001	+ 0.0007
Grosse	Land to Lake	1.29	1.18	0.002	0.001	- 0.001
Gualas	Lake	4.29	2.39	0.122	0.026	- 0.096
HPN1	Lake	1.14	1.34	0.0005	0.105	+ 0.1045
HPN4	Land	0.82	0.50	0.003	0.003	N/A
Hyades	Land to Lake	0.93	0.44	0.009	0.025	+ 0.016
Leones	Lake	2.26	2.24	0.088	0.089	+ 0.001
Mormex	Lake to Land	0.74	1.04	0.0002	0.005	+ 0.0048
Nef	Lake	1.62	2.20	0.025	0.047	+ 0.022
Pared Norte	Lake	0.98	0.58	0.0002	0.00009	- 0.00011
Pared Sur	Land	1.02	1.14	0	0.0006	+ 0.0006
Piscis	Lake	0.87	0.81	0.004	0.007	+ 0.003
Reicher	Lake	7.84	3.42	0.3	0.197	- 0.103
San Quintin	Lake	18.76	10.40	4.213	2.288	- 1.925
San Rafael	Marine	1.77	3.15	1.738	1.378	- 0.36
Soler	Lake	1.30	3.75	0.010	0.176	+ 0.166
Steffen	Lake	2.48	2.53	0.177	0.221	+ 0.044
Strindberg	Land	0.74	1.44	0.00009	0.009	+ 0.0089
U2	Land	0.93	1.43	0.004	0.005	+ 0.001
U3	Lake	0.58	0.55	0.002	0.006	+ 0.004
U4	Land	0.33	0.36	0.0001	0.0006	+ 0.0005
U6	Land	0.40	1.27	0.00002	0.0014	+ 0.00138
U7	Lake to Land	0.77	1.71	0.0004	0.016	+ 0.0156
Verde	Lake	0.65	0.77	0.0004	0.0006	+ 0.0002
Total		70.79	63.78	7.07	5.02	- 2.05

Table A. 2 - Southern Patagonian Icefield

Glacier	Termini Environment	Margin Length (km) (2004)	Margin Length (km) (2017)	Ice Discharge (Gt yr^{-1}) (2004)	Ice Discharge (Gt yr^{-1}) (2017)	Ice Discharge Difference (Gt yr^{-1})
Agassiz Bolados	Lake	3.48	3.80	0.086	0.062	- 0.024
Aguilera	Lake	0.55	0.68	0.004	0.006	+ 0.002
Amalia	Marine	3.27	3.04	0.417	0.476	+ 0.059
Ameghino	Lake	1.02	1.37	0.035	0.067	+ 0.032
Ante Cumbre Bertrand Sur	Lake	0.74	0.94	0.006	0.009	+ 0.003
Asia	Marine	1.94	2.01	0.153	0.139	- 0.014
Balmaceda	Lake	1.87	1.76	0.046	0.070	+ 0.024
Bernardo	Lake	1.77	2.80	0.100	0.285	+ 0.185
Bravo	Lake	0.77	1.55	0.015	0.073	+ 0.058
Calvo	Marine	2.33	2.59	0.136	0.344	+ 0.208
Cerro De Mayo Norte	Land	0.92	0.53	0.002	0.009	+ 0.007
Chico	Land to Lake	2.10	1.80	0.082	0.069	- 0.013
Dickson	Lake	3.86	2.67	0.187	0.182	- 0.005
Europa	Marine	1.66	1.70	1.464	0.999	- 0.465
Grande	Land to Lake	2.38	1.70	0.040	0.193	+ 0.153
Greve	Lake	6.71	5.15	0.865	0.934	+ 0.069
Grey	Lake	4.99	7.54	0.183	0.505	+ 0.322
Guilardi	Lake	1.45	1.58	0.015	0.041	+ 0.026
Heim	Land	0.75	0.60	0.004	0.007	+ 0.003
HPS10	Land to Lake	1.81	1.68	0.043	0.042	- 0.001
HPS11	Land to Lake	0.54	0.40	0.001	0.006	+ 0.005
HPS12	Marine	1.07	0.79	0.066	0.133	+ 0.067
HPS13	Marine	1.36	2.47	1.205	1.551	+ 0.346
HPS14	Marine	0.65	0.54	0.0001	0.0214	+ 0.0213
HPS15	Marine	2.72	2.98	0.424	0.177	- 0.247
HPS16	Lake to Land	0.15	2.05	0	0.014	+ 0.014
HPS17	Marine	0.97	0.97	0.0009	0.147	+ 0.1461
HPS18	Marine	1.65	1.73	0.0001	0.0735	+ 0.0734
HPS19	Marine	0.59	0.60	0.005	0.113	+ 0.108
HPS20	Land	0.21	0.38	0	0.001	+ 0.001
HPS22	Lake	1.12	1.09	0.010	0.038	+ 0.028
HPS24	Land	1.29	1.15	0.002	0.009	+ 0.007
HPS25	Lake	0.60	0.53	0.001	0.006	+ 0.005
HPS27	Marine	0.94	1.10	0.003	0.095	+ 0.092
HPS28	Marine	1.32	3.13	0.269	0.793	+ 0.524
HPS29	Marine	1.38	3.68	0.132	1.410	+ 1.278
HPS30	Lake	0.74	0.65	0.003	0.011	+ 0.008
HPS30(2)	Marine	0.61	0.58	0.0003	0.017	+ 0.0167
HPS31	Marine	1.03	1.68	0.001	0.213	+ 0.212
HPS33	Marine	1.49	1.43	0.005	0.120	+ 0.115

HPS34	Marine	3.15	3.36	0.126	0.638	+ 0.512
HPS35	Marine	0.60	0.34	0.0003	0.006	+ 0.0057
HPS38	Land to Lake	1.26	1.42	0.001	0.034	+ 0.033
HPS39	Land	1.08	0.69	0.0008	0.002	+ 0.0012
HPS41	Land to Lake	1.81	1.40	0.033	0.084	+ 0.051
HPS9	Lake	4.98	4.35	0.159	0.123	- 0.036
Jorge Montt	Marine	2.46	3.48	4.145	0.439	- 3.706
Lucia	Lake	1.52	1.98	0.040	0.143	+ 0.103
Marconi	Lake to Land	0.18	0.67	0.0001	0.001	+ 0.0009
Mayo	Lake	3.29	3.05	0.079	0.155	+ 0.076
Mellizo Sur	Lake	0.70	0.87	0.004	0.016	+ 0.012
Occidental	Lake	3.19	3.10	0.202	0.224	+ 0.022
Ofhidro	Lake	2.40	2.26	0.022	0.083	+ 0.061
O'Higgins	Lake	3.72	3.41	0.397	1.433	+ 1.036
Onelli	Land to Lake	1.77	1.64	0.055	0.052	- 0.003
Oriental	Lake	1.85	1.87	0.024	0.029	+ 0.005
Pascua	Land to Lake	1.02	1.14	0.005	0.005	N/A
Penguin	Marine	1.30	1.37	1.330	1.332	+ 0.002
Perito Moreno	Lake	2.77	2.75	0.489	0.484	- 0.005
Piedras Blancas	Lake	0.60	0.66	0.0003	0.005	+ 0.0047
Pingo	Lake	2.79	2.37	0.011	0.178	+ 0.167
Pio Xi	Marine	11.06	12.11	2.015	1.378	- 0.637
Snowy	Land to Lake	1.44	1.57	0.003	0.006	+ 0.003
Spegazzini	Lake	1.58	1.66	0.140	0.116	- 0.024
Tempano	Marine	3.75	3.24	0.258	0.117	- 0.141
Torre Adela Grande	Lake	0.98	0.86	0.002	0.006	+ 0.004
Tunel	Land	1.32	1.41	0.009	0.009	N/A
Tyndall	Lake	2.40	2.15	0.224	0.226	+ 0.002
UN1	Lake	0.55	0.59	0.0001	0.012	+ 0.0119
UN10	Lake	0.28	0.63	0.0008	0.004	+ 0.0032
UN11	Land	0.67	0.51	0.0006	0.003	+ 0.0024
UN12	Land	0.39	0.45	0.0003	0.001	+ 0.0007
UN13	Land	0.31	0.41	0.0001	0.001	+ 0.0009
UN14	Land	0.25	0.29	0.00001	0.001	+ 0.00099
UN15	Lake	0.31	0.18	0.0001	0.001	+ 0.0009
UN16	Land	1.59	1.35	0.004	0.002	- 0.002
UN17	Lake	1.26	0.57	0.004	0.007	+ 0.003
UN18	Lake	0.58	0.42	0.0001	0.01	+ 0.0099
UN19	Lake	1.52	0.70	0.0005	0.042	+ 0.0415
UN2	Land	1.07	1.13	0.009	0.019	+ 0.01
UN20	Lake	0.51	0.50	0.00006	0.0003	+ 0.00024
UN3	Land to Lake	0.15	0.68	0.0008	0.005	+ 0.0042
UN5	Land to Lake	3.28	3.66	0.059	0.050	- 0.009
UN6	Land to Lake	0.66	0.55	0.0009	0.007	+ 0.0061
UN7	Marine	0.59	0.66	0.0001	0.031	+ 0.0309
UN8	Lake	0.29	1.24	0.0006	0.005	+ 0.0044
UN9	Land	0.49	0.44	0.0005	0.003	+ 0.0025
Upsala	Lake	3.09	3.72	1.291	1.269	- 0.022
Viedma	Lake	2.35	2.86	0.349	0.644	+ 0.295
Total		149.96	215.24	17.52	18.92	+ 1.40

B. Average Velocity and Thickness Values Across the Flux Gate

Table B. 1 - Northern Patagonian Icefield

Glacier	Average Velocity (m/yr) (2004)	Average Velocity (m/yr) (2017)	Average Thickness (m) (2004)	Average Thickness (m) (2017)
Acodado	73.50	138.52	248.34	223.42
Andree	9.81	60.49	185.37	136.86
Arco	8.35	9.89	164.61	116.13
Bayo	2.82	10.15	168.52	189.98
Benito	52.33	117.58	424.28	331.98
Cachet	212.44	134.36	143.66	148.75
Cachet Norte	15.78	21.97	148.02	141.18
Colonia	100.73	58.42	451.74	347.40
Cristal	1.02	37.61	123.64	87.52
Exploradores	40.62	61.71	397.49	463.84
Fiero	117.21	311.54	350.76	256.46
Fraenkel	6.27	40.41	128.79	113.85
Grosse	9.45	11.77	144.23	100.49
Gualas	139.79	62.90	224.85	207.72
HPN1	3.86	47.26	138.50	180.93
HPN4	18.02	37.36	199.09	162.48
Hyades	129.04	489.44	105.86	129.46
Leones	209.80	228.36	183.97	172.43
Mormex	2.79	69.83	127.82	78.19
Nef	48.22	74.18	374.58	307.36
Pared Norte	22.18	47.58	45.87	20.88
Pared Sur	1.89	8.52	74.90	86.26
Piscis	25.14	50.49	171.42	162.54
Reicher	264.98	231.18	191.21	269.78
San Quintin	428.49	439.25	652.27	555.73
San Rafael	3623.13	1859.37	282.57	265.80
Soler	24.51	135.47	253.97	415.85
Steffen	185.76	235.08	411.60	373.49
Strindberg	1.82	54.32	73.02	128.25
U2	20.31	20.91	221.61	180.43
U3	27.45	168.59	172.35	139.20
U4	2.71	26.32	202.82	73.04
U6	0.88	11.97	99.26	111.97
U7	9.63	110.26	56.42	83.77
Verde	9.51	21.80	100.20	36.48

Table B. 2 - Southern Patagonian Icefield

Glacier	Average Velocity (m/yr) (2004)	Average Velocity (m/yr) (2017)	Average Thickness (m) (2004)	Average Thickness (m) (2017)
Agassiz Bolados	122.65	127.22	220.16	210.08
Aguilera	29.99	75.01	220.61	138.52
Amalia	447.04	657.06	284.75	240.12
Ameghino	130.88	198.20	309.10	249.54
Ante Cumbre Bertrand Sur	60.27	77.56	159.83	126.88
Asia	460.39	622.75	177.93	167.56
Balmaceda	235.53	181.31	263.64	205.75
Bernardo	132.22	368.20	437.07	431.08
Bravo	32.31	187.09	583.55	276.97
Calvo	5.83	534.12	130.88	135.82
Cerro De Mayo Norte	23.65	158.54	129.40	119.56
Chico	134.96	174.23	308.05	234.36
Dickson	203.72	625.33	261.18	210.96
Europa	7208.91	296.23	192.40	160.31
Grande	72.27	419.47	272.91	296.32
Greve	417.59	708.71	304.63	262.57
Grey	165.22	290.80	237.12	244.81
Guilardi	44.85	100.13	221.93	272.97
Heim	47.58	95.99	141.10	128.27
HPS10	86.46	103.20	275.43	242.77
HPS11	16.66	176.79	172.65	90.21
HPS12	3.51	336.70	87.28	122.78
HPS13	11.02	178.04	88.35	105.50
HPS14	5.69	311.90	141.85	130.43
HPS15	6.39	467.89	142.75	123.07
HPS16	3.19	46.15	146.72	162.1
HPS17	19.52	868.84	200.84	171.63
HPS18	9	339.28	86.82	110.31
HPS19	84.40	3779.12	205.23	149.20
HPS20	2.98	24.35	94.6	118.71
HPS22	39.55	150.75	251.07	230.66
HPS24	10.41	65.62	152.67	137.20
HPS25	17.33	101.01	133.99	125.37
HPS27	31.03	670.84	137.87	122.60
HPS28	1118.18	483.53	204.57	206.69
HPS29	469.01	1510.80	213.63	267.84
HPS30	21.47	109.75	175.68	153.91
HPS30(2)	3.37	192.36	151.30	157.95
HPS31	7.65	2285.23	183.11	161.18
HPS33	23.7	686.53	120.7	126.99
HPS34	259.05	1207.72	181.62	186.79
HPS35	5.44	154.43	123.07	118.39
HPS38	5.72	122.63	169.04	183.53
HPS39	3.27	21.97	230.41	161.26
HPS41	63.64	259.15	270.90	238.11

HPS9	87.86	79.46	394.04	379.96
Jorge Montt	1946.32	1230.68	650.99	240.18
Lucia	104.94	264.33	270.98	268.26
Marconi	2.74	16.58	226.97	132.22
Mayo	80.04	171.89	321.85	328.16
Mellizo Sur	32.70	159.67	184.91	128.55
Occidental	170.33	196.27	399.40	381.03
Ofhidro	39.86	183.08	266.99	198.12
O'Higgins	651.94	1460.33	274.20	358
Onelli	134.15	140.36	248.47	193.58
Oriental	48.73	48.74	299.95	357.22
Pascua	9.88	28.94	466.44	173.95
Penguin	106.09	397.58	197.39	192.66
Perito Moreno	498.34	490.39	390.29	379.43
Piedras Blancas	13.51	95.87	55.88	70.30
Pingo	19.73	463.30	228.11	186.63
Pio Xi	307.82	295.52	761.90	426.32
Snowy	25.18	30.12	260.26	136.45
Spegazzini	363.43	328.90	258.30	236.36
Tempano	310.21	197.53	229.16	180.25
Torre Adela Grande	10.95	48.89	214.73	174.77
Tunel	28.06	32.88	257.05	220.82
Tyndall	217.63	275.70	470.97	389.99
UN1	2.37	157.47	145.11	131.82
UN10	19.26	63.93	170.38	102.37
UN11	9.98	49.57	106.11	128.93
UN12	5.28	31.22	153.21	72.85
UN13	5.61	22.84	71.15	129.48
UN14	1.48	47.13	47.08	82.61
UN15	5.41	67.29	83.65	85.35
UN16	49.87	111.58	98.95	88.59
UN17	19.29	110.21	168.90	127.47
UN18	6.5	237	80.07	110.36
UN19	4.11	432.86	167.55	138.63
UN2	36.91	70.02	280.12	249.79
UN20	5.77	24.16	58.26	29.91
UN3	46.12	59.21	203.09	123.60
UN5	76.08	62.56	258.35	225.62
UN6	6.25	85.59	225.55	172.82
UN7	1.96	496.08	153.03	151.31
UN8	21.86	36.82	119.41	34.20
UN9	12.07	60.13	108.65	105.51
Upsala	1204.43	1146.03	455.89	324.85
Viedma	498.57	688.87	301.74	346.52

C. Pearson Correlation Test Results for Velocity Values

Table C. 1 - Lake-terminating glaciers that observed an increase in discharge comparing 2004 and 2017 (*represents statistically significant values)

Glacier	Region	P - value	Increase/Decrease
Acodado	NPI	> 0.05 *	Increase
Benito	NPI	> 0.05 *	Increase
Exploradores	NPI	> 0.05 *	Increase
Fraenkel	NPI	> 0.05 *	Increase
HPN1	NPI	> 0.05 *	Increase
Leones	NPI	0.657	Increase
Nef	NPI	> 0.05 *	Increase
Soler	NPI	> 0.05 *	Increase
Steffen	NPI	0.055	Increase
Verde	NPI	> 0.05 *	Increase
U3	NPI	> 0.05 *	Increase
Aguilera	SPI	> 0.05 *	Increase
Ameghino	SPI	> 0.05 *	Increase
Balmaceda	SPI	0.106	Decrease
Grey	SPI	> 0.05 *	Increase
Guilardi	SPI	> 0.05 *	Increase
HPS22	SPI	> 0.05 *	Increase
HPS25	SPI	> 0.05 *	Increase
HPS30	SPI	> 0.05 *	Increase
Lucia	SPI	> 0.05 *	Increase
Mayo	SPI	> 0.05 *	Increase
Occidental	SPI	0.135	Increase
Ofhidro	SPI	> 0.05 *	Increase
Oriental	SPI	0.99	Equal
Pingo	SPI	> 0.05 *	Increase
Tyndall	SPI	0.056	Increase
UN10	SPI	> 0.05 *	Increase
UN15	SPI	> 0.05 *	Increase
UN17	SPI	> 0.05 *	Increase
UN18	SPI	> 0.05 *	Increase
UN19	SPI	> 0.05 *	Increase
UN20	SPI	> 0.05 *	Increase
UN8	SPI	> 0.05 *	Increase
Ante Cumbre Bertrand Sur	SPI	0.181	Increase
Bernardo	SPI	> 0.05 *	Increase
Bravo	SPI	> 0.05 *	Increase
Mellizo Sur	SPI	> 0.05 *	Increase
O'Higgins	SPI	> 0.05 *	Increase
Piedras Blancas	SPI	> 0.05 *	Increase
Torre Adela Grande	SPI	> 0.05 *	Increase
UN1	SPI	> 0.05 *	Increase
Greve	SPI	> 0.05 *	Increase
Viedma	SPI	> 0.05 *	Increase

Table C. 2 - Marine-terminating glaciers that observed an increase in discharge comparing 2004 to 2017 (*represents statistically significant values)

Glacier	Region	P - value	Increase/Decrease
Amalia	SPI	> 0.05 *	Increase
Calvo	SPI	> 0.05 *	Increase
HPS12	SPI	0.112	Increase
HPS13	SPI	> 0.05 *	Increase
HPS14	SPI	> 0.05 *	Increase
HPS17	SPI	> 0.05 *	Increase
HPS18	SPI	> 0.05 *	Increase
HPS19	SPI	> 0.05 *	Increase
HPS27	SPI	> 0.05 *	Increase
HPS28	SPI	0.139	Decrease
HPS29	SPI	> 0.05 *	Increase
HPS30(2)	SPI	> 0.05 *	Increase
HPS31	SPI	> 0.05 *	Increase
HPS33	SPI	> 0.05 *	Increase
HPS34	SPI	> 0.05 *	Increase
HPS35	SPI	> 0.05 *	Increase
Penguin	SPI	> 0.05 *	Increase
UN7	SPI	> 0.05 *	Increase